Title
Antiphage immune system failure in P. aeruginosa

Author
Mendoza, Senen Dario

Publication Date
2021

Peer reviewed|Thesis/dissertation

Antiphage immune system failure in P. aeruginosa

by
Senen Mendoza

DISSERTATION
Submitted in partial satisfaction of the requirements for degree of
DOCTOR OF PHILOSOPHY

in

Biochemistry and Molecular Biology

in the

GRADUATE DIVISION
of the
UNIVERSITY OF CALIFORNIA, SAN FRANCISCO

Approved:

Alexander Johnson
Alexander Johnson
Chair

DocuSigned by:
Joseph Bondy-Denomy
Joseph Bondy-Denomy

DocuSigned by:
Carol Gross
Carol Gross
F2413DA7F84F46A...

Committee Members

Acknowledgements

I would like to thank my thesis advisor, Dr. Joseph Bondy-Denomy for his guidance of my work through two fascinating, yet challenging projects. Not only has he been an excellent advisor on experimental and conceptual matters, but he has also been a wonderful mentor in matters of scientific development, empowerment of my career, and personal growth. The training I received from Dr. Joseph Bondy-Denomy is of the highest possible metric and has enabled many achievements. I would like to thank my committee, including Drs. Carol Gross and Alexander Johnson. Dr. Carol Gross has been a dear mentor for most of my scientific career and has been a person that I can reliably count on to look out for my best interests and guide to meet the promise of my potential. Dr. Alexander Johnson has served as an excellent chair of my committee and his quick understanding of my data and sharp questions have revealed to me the most pressing questions to work on. I would like to give a special thank you to all the wonderful colleagues I have worked with at UCSF and especially in the Bondy-Denomy lab that have made my life in science such an exquisite pleasure.

Contributions

Chapter 2 contains work previously submitted for publication:

Mendoza SD, Nieweglowska ES, Govindarajan S, Leon LM, Berry JD, Tiwari A, Chaikeeratisak V, Pogliano J, Agard D, Bondy-Denomy J: **A bacteriophage nucleus-like compartment shields DNA from CRISPR nucleases.** *Nature.* 2020 Jan;**577**(7789):244-248. doi: 10.1038/s41586-019-1786-y

Antiphage immune system failure in *P. aeruginosa*

Senén D. Mendoza

Abstract

Cells coexist with and are often outnumbered by a long and diverse list of molecular parasites that utilize cellular resources to replicate. Viruses are particularly deleterious, as their replicative cycle often culminates in cellular lysis. To prevent resource-costly and potentially lethal infection by bacterial viruses (bacteriophages, phages), bacteria contain many different anti-phage immune systems. In this thesis, I discuss two examples of bacterial immune system failure in *Pseudomonas aeruginosa*. First, I discuss the mechanism by which ΦKZ, a jumbophage, resists all tested DNA-targeting immune systems. ΦKZ resisted 4 different CRISPR-Cas and 2 different restriction-modification (R-M) DNA-targeting systems *in vivo* but succumbed to the RNA-targeting CRISPR-Cas13. Fluorescently-labeled DNA nucleases were excluded from accessing ΦKZ's DNA, because the phage assembles a nucleus-like compartment. A fusion of EcoRI to a phage-encoded recombinase trafficked the restriction enzyme into the DNA compartment and enabled immune activity. ΦKZ is the most immune evasive phage studied to date and our work revealed the mechanism, DNA segregation. Second, I discuss an epigenetic state in which an R-M system is inactivated for greater than 60 generations after cellular replication at 43 °C. Though first discovered more than 50 years ago, this phenomenon has not been further investigated and its molecular mechanism remains unknown. I determined that inactivation of restriction occurs post-translationally and requires bacterial replication in liquid culture at greater than 42 °C. Preliminary results suggest that protein aggregation may be involved in inactivation of the restriction enzyme. Together, the studies in this thesis explain 2 interesting cases of bacterial immune system failure, which occur by fascinating mechanisms.

Table of Contents

Chapter 1: Introduction 1

References 8

Chapter 2: A bacteriophage nucleus-like compartment shields DNA from CRISPR nucleases . 14

References 21

Chapter 3: Heat-induced inactivation of immunity across bacteria 55

References 73

List of Figures:

Chapter 1:

Figure 1.1: Restriction-Modification and CRISPR-Cas cleave phage nucleic acids but differ in self vs. non-self recognition 13

Chapter 2:

2.1. Identification of a phage that resists targeting by diverse CRISPR-Cas and restriction-modification systems 33

2.2. CRISPR-Cas and restriction proteins are excluded from ΦKZ's nucleus-like structure 34

2.3. ΦKZ genomic DNA can be cleaved by immune enzymes 35

2.4. Phage ΦKZ DNA is sensitive to RNA-targeting Cas13..... 36

2.5. Jumbo phage ΦPA3 resists targeting by CRISPR Cas and a restriction-modification system 37

2.6. Phage ΦKZ resists *P. aeruginosa* Type I-C and Type I-F CRISPR-Cas immunity..... 38

2.7. Phage ΦKZ resists targeting by heterologous Type II-A and V-A CRISPR-Cas systems ... 39

2.8. Quantification of Cas9 localization during phage ΦKZ infection of *P. aeruginosa*..... 40

2.9. Phage ΦKZ genomic DNA is susceptible *in vitro* to cleavage by Restriction Endonucleases 41

2.10. Cas9 fusion to ORF152 localizes to periphery of shell, but does not enable immune activity against ΦKZ..... 42

2.11. Fusion of EcoRI restriction enzymes to ORF152 enables immune activity 43

2.12. Phage ΦKZ DNA is sensitive to RNA-targeting Cas13..... 44

2.13. Phage ΦKZ escaper mutants are selected by Cas13-mediated RNA targeting 45

2.14. Observation of DAPI-stained phage DNA adjacent to a Cherry-TopA nascent shell 46

Chapter 3:

3.1. PAO1's restriction against phage JBD30 is ablated after growth at 43 °C 85

3.2. PAO1's HsdM's methylation activity is partially inhibited after bacterial growth at 43 °C 86

3.3. iREN is inherited for > 60 generations, while inactivation of methylation recovers much more quickly 87

3.4. Restriction is inactivated during early log-phase at 43 °C 88

3.5. Incubation at 43 °C during mid-log is insufficient for full inactivation of restriction 89

3.6. Restriction activity is inactivated partially at 40.5 °C and fully at 42 °C 90

3.7. *P. aeruginosa* strain PA14 has temperature-insensitive restriction while PAK's restriction is inactivated at 43 °C 91

3.8. PAO1's electrocompetence improves after incubation at 43 °C independent of *hsdR*, but this improvement is not inherited 93

3.9. PAO1's *hsdSMR* locus and mutants used in this study 94

3.10. PAO1 Δ*hsdR*'s loss of restriction can be complemented by overexpression of HsdR from a plasmid, but this is toxic during iREN 95

3.11. hsdSM and hsdR transcripts are present during iREN 96

3.12. RNA-Seq does not identify any statistically significant changes to PAO1's transcriptome during iREN 97

3.13. Western blots using custom antibodies reveal that HsdR is lowly expressed and insoluble in its native context 98

3.14. PAO1 sfCherry2-*hsdR* grown at 43 °C retains fluorescence despite losing restriction activity 100

3.15. sfCherry2-HsdR forms red puncta during iREN but is diffuse in naïve cells 101

3.16. *P.aeruginosa's* restriction activity is inhibited post-translationally 102

List of Tables:

Chapter 2:

Table 2.1. ΦKZ and ΦKZ-like phages have no natural spacers matching their genomes from a natural collection of >4000 *P. aeruginosa* spacers 47

Table 2.2. Phage and Strains 48

Table 2.3. Plasmids 49

Table 2.4. Oligonucleotides, g-blocks, crRNAs 50

Table 2.5. Spacer sequences 53

Chapter 3:

Table 3.1. iREN in *P. aeruginosa* 103

Table 3.2. RNA-Seq Hits 104

Table 3.3. Phages and Strains 105

Table 3.4. Plasmids 106

Table 3.5. Oligonucleotides 107

Table 3.6. Antigens 110

Chapter 1: Introduction

Bacterial immune systems

In order to prevent lethal predation by viruses and other mobile genetic elements, cells often maintain immunity systems. Prokaryotes boast a long and diverse list of immune systems[1]. These immune systems have immense diversity in the means by which they detect viruses, the stage at which they inactivate viral replication and the mechanism by which they do so, and whether or not immune activity is lethal to the infected cell.

Restriction-Modification

The earliest discovered bacterial immune systems are classified as restriction-modification systems[2]. These immune systems were discovered through the observation that the host range of a bacterial virus (bacteriophage, phage) could be expanded by first propagating the phage on other bacterial strains. The host range of the phage could then be restricted again after viral replication on a different bacterial strain. The cause of this nongenetic inheritance was determined to be genes encoded in the bacterial hosts which were named “host specificity determination”, or *hsd* genes. These *hsd* genes are now known to comprise the type I restriction-modification (R-M) system, which cleaves foreign DNA unless it has been protectively methylated by its cognate methyltransferase[3]. Other types of R-M systems were later discovered, including type II through type IV R-M systems[2,4]. Each type of R-M immune system features different gene organization and gene functions as well as using somewhat different molecular mechanisms. The commonality of all R-M immune systems is that they recognize specific dsDNA sequences called restriction sites and depending on whether the DNA is methylated or not they may introduce a double-stranded break (DSB) in the DNA molecule. Due to their revolutionary utility for genetic engineering, type II R-M systems are the most studied and best understood[5]. However, type I R-M systems are the most common R-M systems and they feature fascinating molecular

mechanisms in their own right and boast interesting regulatory schemes throughout the central dogma[6–10].

Type I R-M systems are best understood through different model systems from *E. coli*: EcoKI, EcoAI, and EcoR124I[3,11–13]. Type I R-M systems encode 3 different genes: *hsdS*, *hsdM,* and *hsdR*. *hsdS* encodes a sequence-specific DNA-binding protein that recognizes a restriction site, which is bipartite and asymmetric, such as EcoKI's $AACN_6GTGC$. *hsdM* encodes an S-adenosylmethionine (SAM)-dependent methyltransferase (MTase) that binds HsdS protein in a 2:1 ratio. S_1M_2 protein complexes comprise an MTase that methylates the N^6 position of adenosine residues on both strands of the restriction site. *hsdR* encodes a helicase and endonuclease protein subunit that assembles with the S_1M_2 MTase in a 2:1 ratio to form an endonuclease holoenzyme. The $S_1M_2R_2$ endonuclease is a SAM-dependent MTase and an ATP- and Mg^{2+}-dependent helicase and endonuclease. Upon binding a hemi-methylated substrate, the MTase activity prevails and methylates the unmodified strand. However, when the substrate is fully unmethylated, both HsdR subunits translocate DNA through the HsdR subunit, forming DNA loops on both sides. HsdR subunits translocate long distances until translocation is stalled, such as by encountering another HsdR subunit on the DNA. At this point, the protein introduces a DSB in the DNA molecule. Because these enzymes introduce DSBs at varied loci on a particular substrate, they did not find much utility in technology. Still, type I R-M systems feature intricate and interesting molecular mechanisms worthy of study in their own right. They have yielded numerous examples of unique regulatory mechanisms.

Nuclease-based immune systems, such as type I R-M, offer strong protection to their bacterial hosts against phages but they also pose a serious risk of autoimmunity. DSBs are highly toxic to bacterial cells and any nuclease encoded by a bacterial genome must be strongly regulated to make these events as rare as possible. Despite the fact that *hsdS* and *hsdM* genes

are encoded on the same transcript, which is distinct from the *hsdR* transcript, there is no evidence of differential transcriptional regulation[14]. Additionally, because nucleolytic activity requires formation of the MTase, cells with nuclease activity must also have MTase activity[12]. The holoenzyme's ability to methylate hemimethylated restriction sites further makes autoimmunity less likely, especially in moments of rapid DNA replication.

An interesting challenge for cells expressing type I R-M is the creation of unmethylated restriction sites. Most often, this occurs during DNA damage and subsequent homologous recombination, which can generate fully unmethylated restriction sites. In a fascinating process known as restriction alleviation (RA), type I R-M nucleases translocating on the bacterial chromosome have their HsdR subunits proteolytically degraded by ClpXP, after DNA damage[6,15]. This leads to an increase in the concentration of S_1M_2 complexes relative to $S_1M_2R_2$ complexes in the cell, which favors protective methylation of any unmethylated chromosomal restriction sites.

CRISPR-Cas

Another bacterial immune system that revolutionized gene editing and genome engineering is clustered regularly interspaced short palindromic repeats (CRISPR-Cas), which is a large set of bacterial immune systems with unique properties that are useful for different applications. In addition to their technological benefits, CRISPR-Cas systems represent extremely potent antiphage immune systems[16–19]. Though they must first acquire a spacer that targets a particular sequence before they can cleave that sequence, CRISPR-Cas systems allow strong targeting against target sequences. CRISPR-Cas features broad diversity of mechanisms and gene structures. Class 1 CRISPR-Cas systems, including type II, type V, and type VI feature single protein effectors that process their own crRNAs and complete nucleolytic cleavage on their own[20]. Meanwhile, Class 2 CRISPR-Cas systems, including type I, type III, and type IV utilize protein complexes composed of multiple Cas protein subunits to process their crRNAs and mediate

nucleolytic cleavage[21]. In addition to this diversity of gene organization, the substrate requirements of CRISPR-Cas systems vary in the protospacer adjacent motif (PAM) that is required for cleavage and in the type of molecule that is targeted. For example, the type V CRISPR-Cas12 system is able to target ssDNA in addition to dsDNA[22,23], type III CRISPR-Cas is able to target both dsDNA and its transcribed mRNA molecules[24], and type VI CRISPR-Cas exclusively targets RNA[25–29]. This diversity of molecules CRISPR-Cas systems can target suggests different strategies for what molecular pathogens are targeted by these immune systems or the stages of replication at which this targeting happens.

Novel antiphage immune systems

Recent efforts to consolidate an inventory of all bacterial immune systems have taken bioinformatic approaches to predict bacterial genes involved in antiphage immunity[30]. These approaches have utilized defense islands, which are syntenic regions with high numbers of known bacterial immune genes. Defense islands are typically enriched for type I R-M genes, as well as type III transposase systems and are typically found proximal to bacterial tRNAs. These features suggest acquisition of immune genes by horizontal transfer. Training of hidden Markov models (HMMs) on defense islands has led to the prediction of candidate immune genes throughout the bacterial metagenome. Recently, this has resulted in the identification of many different and novel bacterial immune systems which protect bacteria from lethal phage predation. The existence and diversity of so many different antiphage immune systems suggests a necessity for varied strategies to effectively inhibit phages. This may also suggest that phages have evolved means to evade existing bacterial antiphage immune systems, necessitating the evolution of new ones.

Viral immune system inhibitors

In spite of these varied and potent antiphage immune systems, phages continue to replicate efficiently and even outnumber their bacterial hosts[31]. Phages have two means of evading

bacterial immunity: 1) mutation of the molecular targets of bacterial immune systems and 2) evolution of molecular inhibitors of bacterial immune systems[32–36].

In the case of R-M, phages can, at high multiplicities of infection (MOIs), overwhelm bacterial immunity and become methylated by the restriction endonuclease's cognate MTase. In this case, the phage is able to replicate without inhibition and can fulfill their life cycle. Any progeny phage will then have acquired the protective methylation of the particular R-M system and will then be able to infect cells encoding this R-M system to full efficiency. In addition to overwhelming their host and acquiring the protective modification, phages can also encode small protein inhibitors of restriction endonucleases. One example that functions against type I R-M systems is the ArdB/KlcA family of proteins, which are hypothesized to function by binding HsdR during its translocation on unmodified DNA[35,37]. Another example is the Ocr protein, which functions as a DNA mimic to bind type I R-M complexes[36].

Anti-CRISPRs were discovered by the observation that certain lysogens failed to target any phages, even when provided with the adequate spacers[38]. This was only true for lysogens of certain phages, leading to the identification of anti-CRISPR (acr) genes in these prophage's genomes. These first discovered anti-CRISPRs (acrs) were type I-F inhibitors. Since then, inhibitors have been discovered for many known CRISPR-Cas types and subtypes including I-C, I-E, I-F, II-A, II-C, III, V-A, and VI-A[38–44]. These inhibitors are small proteins with a large diversity of molecular mechanisms. Most anti-CRISPRs inhibit binding of Cas proteins to their crRNA's protospacer target[45]. Additionally, anti-CRISPRs have been found that inhibit their target by degradation of the target Cas protein or by enzymatic activities[39].

All known phage-encoded inhibitors of bacterial immune systems have very specific molecular targets. Though some examples exist of inhibitors that are capable of inhibiting distinct

immune systems[39], inhibitors generally inhibit only a particular subclass of immune systems (e.g. type I-C CRISPR-Cas, or Type I-B R-M).

Jumbophages and the ΦKZ-like family of bacteriophages

Historically, isolated and tractable bacteriophages have been known to have genomes ranging in size from ~30 kb - ~150 kb. However, phages with extremely large genome sizes (>200 kb) exist and some have been known about for several decades[46]. Jumbophages are classified as phages whose genome size exceeds 200 kb. As techniques for isolating phages or for cataloging all genomes in environmental isolates have improved, jumbophages are being understood to be a prevalent and important members of microbial communities[47]. The large genomes of jumbophages encode many genes with no known function, suggesting a wellspring of novel biology. Jumbophages feature bizarre characteristics such as encoding metabolic genes. The genus of jumbophages described by ΦKZ (ΦKZ-like viruses) feature unique traits, such as formation of a proteinaceous nucleus-like compartment (shell) during viral replication[48,49]. The shell contains the viral genomic DNA, while the host bacterium's chromosome is degraded by early-expressed phage nucleases. These DNA compartments are selectively permeable and allow entry of phage-encoded DNA polymerases, RNA polymerases, and recombinases and some host proteins such as topoisomerase. Because translation occurs outside this compartment, viral mRNAs are thought to be exported to the cytoplasm. The viral capsid is assembled in the cytoplasm and the phage head docks on the surface of the shell, where it is loaded with the viral chromosome across the shell. The viral particle then completes its maturation in the cytoplasm, including assembly of the phage tail. Phage-encoded metabolic genes such as thymidylate synthase are localized to the cytoplasm. The phage compartment is centered in the middle of the cell body by the tubulin homolog PhuZ. Most recently, it was discovered that phage heads bind the PhuZ filaments and traffic on them towards the shell for DNA loading[50]. All of these unique

features make ΦKZ an interesting subject of study and its long list of uncharacterized genes represents a mostly unexplored source of novel genes and pathways.

References:

1. Koonin, E. V., Makarova, K. S. & Wolf, Y. I. Evolutionary Genomics of Defense Systems in Archaea and Bacteria. *Annu. Rev. Microbiol.* **71**, 233–261 (2017).
2. Roberts, R. J. & Murray, K. Restriction Endonuclease. *CRC Crit. Rev. Biochem.* **4**, 123–164 (1976).
3. Loenen, W. A. M., Dryden, D. T. F., Raleigh, E. A. & Wilson, G. G. Type I restriction enzymes and their relatives. *Nucleic Acids Res.* **42**, 20–44 (2014).
4. Roberts, R. J. A nomenclature for restriction enzymes, DNA methyltransferases, homing endonucleases and their genes. *Nucleic Acids Res.* **31**, 1805–1812 (2003).
5. Pingoud, A. Structure and function of type II restriction endonucleases. *Nucleic Acids Res.* **29**, 3705–3727 (2001).
6. Bickle, T. A. Restricting restriction: Restriction alleviation. *Mol. Microbiol.* **51**, 3–5 (2003).
7. Mruk, I., Kaczorowski, T. & Witczak, A. Natural tuning of restriction endonuclease synthesis by cluster of rare arginine codons. *Sci. Rep.* **9**, 5808 (2019).
8. Dybvig, K., Sitaraman, R. & French, C. T. A family of phase-variable restriction enzymes with differing specificities generated by high-frequency gene rearrangements. *Proc. Natl. Acad. Sci.* **95**, 13923–13928 (1998).
9. Li, J. *et al.* Epigenetic Switch Driven by DNA Inversions Dictates Phase Variation in Streptococcus pneumoniae. *PLOS Pathog.* **12**, e1005762 (2016).
10. Zamora, M., Ziegler, C. A., Freddolino, P. L. & Wolfe, A. J. A Thermosensitive, Phase-Variable Epigenetic Switch: *pap* Revisited. *Microbiol. Mol. Biol. Rev.* **84**, e00030-17, /mmbr/84/3/MMBR.00030-17.atom (2020).
11. Davies, G. P. *et al.* On the structure and operation of type I DNA restriction enzymes. *J. Mol. Biol.* **290**, 565–579 (1999).
12. Murray, N. E. Type I Restriction Systems: Sophisticated Molecular Machines (a Legacy of Bertani and Weigle). *Microbiol. Mol. Biol. Rev.* **64**, 412–434 (2000).

13. Powell, L. M., Dryden, D. T. F. & Murray, N. E. Sequence-specific DNA binding by EcoKI, a type IA DNA restriction enzyme. *J. Mol. Biol.* **283**, 963–976 (1998).

14. Loenen, W. A. M., Daniel, A. S., Braymer, H. D. & Murray, N. E. Organization and sequence of the hsd genes of Escherichia coli K-12. *J. Mol. Biol.* **198**, 159–170 (1987).

15. Simons, M., Diffin, F. M. & Szczelkun, M. D. ClpXP protease targets long-lived DNA translocation states of a helicase-like motor to cause restriction alleviation. *Nucleic Acids Res.* **42**, 12082–12091 (2014).

16. Mojica, F. J. M., Díez-Villaseñor, C., García-Martínez, J. & Soria, E. Intervening Sequences of Regularly Spaced Prokaryotic Repeats Derive from Foreign Genetic Elements. *J. Mol. Evol.* **60**, 174–182 (2005).

17. Pourcel, C., Salvignol, G. & Vergnaud, G. CRISPR elements in Yersinia pestis acquire new repeats by preferential uptake of bacteriophage DNA, and provide additional tools for evolutionary studies. *Microbiology* **151**, 653–663 (2005).

18. Datsenko, K. A. *et al.* Molecular memory of prior infections activates the CRISPR/Cas adaptive bacterial immunity system. *Nat. Commun.* **3**, 945 (2012).

19. Bolotin, A., Quinquis, B., Sorokin, A. & Ehrlich, S. D. Clustered regularly interspaced short palindrome repeats (CRISPRs) have spacers of extrachromosomal origin. *Microbiology* **151**, 2551–2561 (2005).

20. Ofir, G. & Sorek, R. Contemporary Phage Biology: From Classic Models to New Insights. *Cell* **172**, 1260–1270 (2018).

21. Makarova, K. S. *et al.* Evolutionary classification of CRISPR–Cas systems: a burst of class 2 and derived variants. *Nat. Rev. Microbiol.* **18**, 67–83 (2020).

22. Parameshwaran, H. P. *et al.* The bridge helix of Cas12a imparts selectivity in *cis* -DNA cleavage and regulates *trans* -DNA cleavage. *FEBS Lett.* **595**, 892–912 (2021).

23. Chen, J. S. *et al.* CRISPR-Cas12a target binding unleashes indiscriminate single-stranded DNase activity. *Science* **360**, 436–439 (2018).

24. Pyenson, N. C. & Marraffini, L. A. Type III CRISPR-Cas systems: when DNA cleavage just isn't enough. *Curr. Opin. Microbiol.* **37**, 150–154 (2017).

25. Liu, L. *et al.* The Molecular Architecture for RNA-Guided RNA Cleavage by Cas13a. *Cell* **170**, 714-726.e10 (2017).

26. Smargon, A. A. *et al.* Cas13b Is a Type VI-B CRISPR-Associated RNA-Guided RNase Differentially Regulated by Accessory Proteins Csx27 and Csx28. *Mol. Cell* **65**, 618-630.e7 (2017).

27. Yan, W. X. *et al.* Cas13d Is a Compact RNA-Targeting Type VI CRISPR Effector Positively Modulated by a WYL-Domain-Containing Accessory Protein. *Mol. Cell* **70**, 327-339.e5 (2018).

28. Mendoza, S. D. & Bondy-Denomy, J. Cas13 Helps Bacteria Play Dead when the Enemy Strikes. *Cell Host Microbe* **26**, 1–2 (2019).

29. Meeske, A. J., Nakandakari-Higa, S. & Marraffini, L. A. Cas13-induced cellular dormancy prevents the rise of CRISPR-resistant bacteriophage. *Nature* **570**, 241–245 (2019).

30. Doron, S. *et al.* Systematic discovery of antiphage defense systems in the microbial pangenome. *Science* **359**, eaar4120 (2018).

31. Cobián Güemes, A. G. *et al.* Viruses as Winners in the Game of Life. *Annu. Rev. Virol.* **3**, 197–214 (2016).

32. Borges, A. L., Davidson, A. R. & Bondy-Denomy, J. The Discovery, Mechanisms, and Evolutionary Impact of Anti-CRISPRs. *Annu. Rev. Virol.* **4**, 37–59 (2017).

33. Davidson, A. R. *et al.* Anti-CRISPRs: Protein Inhibitors of CRISPR-Cas Systems. *Annu. Rev. Biochem.* **89**, 309–332 (2020).

34. Li, Y. & Bondy-Denomy, J. Anti-CRISPRs go viral: The infection biology of CRISPR-Cas inhibitors. *Cell Host Microbe* **29**, 704–714 (2021).

35. Balabanov, V. P. *et al.* ArdB Protective Activity for Unmodified λ Phage Against EcoKI Restriction Decreases in UV-Treated Escherichia coli. *Curr. Microbiol.* **76**, 1374–1378 (2019).

36. Walkinshaw, M. D. *et al.* Structure of Ocr from Bacteriophage T7, a Protein that Mimics B-Form DNA. *Mol. Cell* **9**, 187–194 (2002).

37. Kudryavtseva, A. A., Okhrimenko, I. S., Didina, V. S., Zavilgelsky, G. B. & Manukhov, I. V. Antirestriction Protein ArdB (R64) Interacts with DNA. *Biochem. Mosc.* **85**, 318–325 (2020).

38. Bondy-Denomy, J., Pawluk, A., Maxwell, K. L. & Davidson, A. R. Bacteriophage genes that inactivate the CRISPR/Cas bacterial immune system. *Nature* **493**, 429–432 (2013).

39. Marino, N. D. *et al.* Discovery of widespread type I and type V CRISPR-Cas inhibitors. *Science* **362**, 240–242 (2018).

40. Pawluk, A., Bondy-Denomy, J., Cheung, V. H. W., Maxwell, K. L. & Davidson, A. R. A New Group of Phage Anti-CRISPR Genes Inhibits the Type I-E CRISPR-Cas System of Pseudomonas aeruginosa. *mBio* **5**, (2014).

41. Rauch, B. J. *et al.* Inhibition of CRISPR-Cas9 with Bacteriophage Proteins. *Cell* **168**, 150-158.e10 (2017).

42. Pawluk, A. *et al.* Naturally Occurring Off-Switches for CRISPR-Cas9. *Cell* **167**, 1829-1838.e9 (2016).

43. Athukoralage, J. S. *et al.* The dynamic interplay of host and viral enzymes in type III CRISPR-mediated cyclic nucleotide signalling. *eLife* **9**, e55852 (2020).

44. Meeske, A. J. *et al.* A phage-encoded anti-CRISPR enables complete evasion of type VI-A CRISPR-Cas immunity. *Science* **369**, 54–59 (2020).

45. Kim, I. *et al.* Structural and mechanistic insights into the CRISPR inhibition of AcrIF7. *Nucleic Acids Res.* **48**, 9959–9968 (2020).

46. Krylov, V. *et al.* Phage phiKZ—The First of Giants. *Viruses* **13**, 149 (2021).

47. Al-Shayeb, B. *et al.* Clades of huge phages from across Earth's ecosystems. *Nature* **578**, 425–431 (2020).

48. Chaikeeratisak, V. *et al.* Assembly of a nucleus-like structure during viral replication in bacteria. *Science* **355**, 194–197 (2017).

49. Chaikeeratisak, V. *et al.* The Phage Nucleus and Tubulin Spindle Are Conserved among Large Pseudomonas Phages. *Cell Rep.* **20**, 1563–1571 (2017).

50. Chaikeeratisak, V. *et al.* Viral Capsid Trafficking along Treadmilling Tubulin Filaments in Bacteria. *Cell* **177**, 1771-1780.e12 (2019).

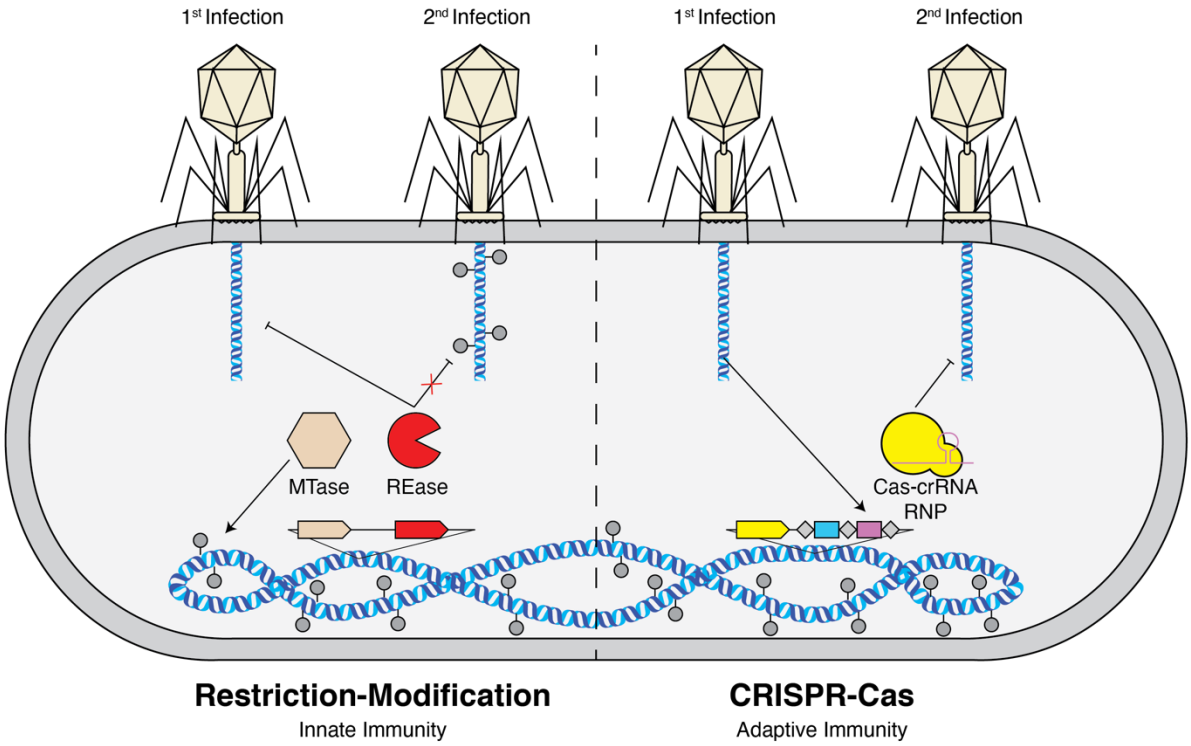

Figure 1.1: Restriction-Modification and CRISPR-Cas cleave phage nucleic acids but differ in self vs. non-self recognition. a, Restriction-Modification systems encode MTase and Restriction Endonuclease (REase) activities. The REase activity cleaves DNA at specific restriction sites. The MTase activity protects host DNA from nucleolytic cleavage. At high MOIs, phage DNA can overwhelm the REase and its progeny phage become methylated, protecting them from restriction in future infections. **b,** CRISPR-Cas systems encode a CRISPR array, which stores acquired sequences from infecting phages. The CRISPR array is transcribed and processed into crRNAs, which assemble with Cas proteins to form Cas-crRNA ribonucleoproteins (RNPs), which target sequences complementary to the crRNA.

Chapter 2: A bacteriophage nucleus-like compartment shields DNA from CRISPR nucleases

Abstract

All viruses require strategies to inhibit or evade the immunity pathways of cells they infect. The viruses that infect bacteria, bacteriophages (phages), must avoid nucleic-acid targeting immune pathways such as CRISPR-Cas (clustered regularly interspaced short palindromic repeats and CRISPR-associated genes) and restriction-modification (R-M) systems to replicate efficiently. Here, we show that jumbo phage ΦKZ, infecting *Pseudomonas aeruginosa,* segregates its DNA from immunity nucleases by constructing a proteinaceous nucleus-like compartment. ΦKZ resists many DNA-targeting immune systems *in vivo*, including two CRISPR-Cas3 subtypes, Cas9, Cas12a, and the restriction enzymes HsdRMS and EcoRI. Cas and restriction enzymes are unable to access the phage DNA throughout the infection, but engineered re-localization of EcoRI inside the compartment enables phage targeting and cell protection. Moreover, ΦKZ is sensitive to the RNA targeting CRISPR-Cas enzyme, Cas13a, likely due to phage mRNA localizing to the cytoplasm. Collectively, we propose that *Pseudomonas* jumbo phages evade a broad spectrum of DNA-targeting nucleases through the assembly of a protein barrier around their genome.

Jumbo phage ΦKZ Resists CRISPR-Cas targeting

Phages that infect *Pseudomonas aeruginosa* can avoid CRISPR-mediated destruction by encoding “anti-CRISPR" (Acr) proteins that inhibit the Type I-E and I-F CRISPR-Cas systems[2-4]. To determine whether any *P. aeruginosa* phages are resistant to the *P. aeruginosa* Type I-C CRISPR-Cas system[5], a common and understudied variant[6], a strain engineered to express Type I-C *cas3, cas5, cas8, cas7*[7] was provided with a panel of crRNAs targeting phages from five taxonomic groups: JBD30, D3, and JBD68 (distinct temperate siphophages), F8 and ΦKZ (distinct lytic myophages). All phages succumbed to targeting, except ΦKZ (Fig. 2.1) and a related phage

ΦPA3 (Fig. 2.5). ΦKZ titer did not decrease when challenged using 11 different Type I-C crRNAs (Fig. 2.1, Fig. 2.6) nor when exposed to the type I-F CRISPR-Cas system of *P. aeruginosa*[8] (Fig. 2.6).

The ΦKZ genome possesses no homologs of known *acr*[2-4,9,10] or anti-CRISPR associated (*aca*) genes that have previously enabled identification of *acr* genes[4,9,10]. Moreover, gene knockout approaches have not been previously established for ΦKZ. To determine the mechanism for CRISPR evasion, we attempted to utilize the Type II-A CRISPR-Cas9 (SpyCas9) as a genetic tool. SpyCas9 and sgRNAs robustly targeted control phage JBD30 but ΦKZ replication and associated cell lysis was unaffected (Fig. 2.1). An additional six sgRNA sequences also failed to target ΦKZ (Fig. 2.7), as did four against ΦPA3 (Fig. 2.5). Given the ability of this phage to evade unrelated CRISPR systems (Type I and II), including one from a microbe that this phage does not infect (*Streptococcus pyogenes*), we considered that ΦKZ may be generally resistant to CRISPR-Cas immunity, as opposed to relying on specific inhibitor proteins. Type V-A Cas12a (Cpf1) CRISPR-Cas system from *Moraxella bovoculi* was expressed in *P. aeruginosa* and sucessfully targeted the control phage, but not ΦKZ with any of the nine crRNAs tested (Fig. 2.1, Fig. 2.7). The ability of this phage to resist CRISPR systems found in its natural host, *Pseudomonas* (Type I-C and I-F), and those not naturally present (Type II-A and V-A) suggests that this phage possesses a mechanism enabling “pan-CRISPR” resistance.

Restriction-modification systems are the most common form of bacterial immunity in nature and pose a significant impediment to phage replication[1]. Type I R-M (HsdRMS from *P. aeruginosa*) and Type II R-M (EcoRI from *E. coli*) were next tested, possessing 24 and 92 cut sites in the ΦKZ genome, respectively. ΦKZ was propagated on strain PAK, an isolate that generates phages susceptible to PAO1 HsdRMS restriction. When phage JBD30 (5 Type I R-M sites) was assayed in this manner, its titer was reduced by ~5 orders of magnitude, dependent

on *hsdR* (Fig. 2.1). In contrast, no restriction was observed for ΦKZ (Fig. 2.1) or ΦPA3 (Fig. 2.5). Similarly, the expression of EcoRI reduced JBD30 titer by 3 orders of magnitude (12 EcoRI sites) but had no impact on ΦKZ (92 EcoRI sites) (Fig. 2.1). Together, these experiments demonstrate that ΦKZ is refractory to the *six* selected CRISPR-Cas and restriction endonucleases *in vivo*.

Phage nucleus-like structure excludes immune enzymes

ΦKZ and ΦKZ-like phages infecting *P. aeruginosa* and *P. chlororaphis* were recently shown to construct an elaborate proteinaceous nucleus-like compartment where phage DNA replicates[11,12]. Additionally, a phage-encoded tubulin homologue, PhuZ, centers the compartment within the host cell[11-15]. Proteins involved in DNA replication, transcription, and recombination localize inside the shell, while mRNA and proteins mediating translation localize in the cytoplasmic space[11], akin to the eukaryotic nucleus. Given the apparent exclusion of select proteins, we considered whether this structure was responsible for the pan-resistance of ΦKZ to such distinct immune processes.

P. aeruginosa cells infected with ΦKZ were imaged with immunofluorescence to detect Cas9 (Fig. 2.2, Fig. 2.4); likewise, Cherry fusions with Cas9, two signature proteins from the Type I-C and I-F CRISPR-Cas systems (Cas8 and Cas3, Fig. 2.2), as well as the restriction enzyme HsdR (Fig. 2.2) were imaged using live cell imaging. These experiments revealed that the immune enzymes are excluded from the shell during phage infection. DAPI staining revealed the phage DNA inside the shell, while the host genome was degraded[14]. Proteins previously shown to be internalized in the shell, phage ORF152 (imaged with anti-myc immunofluorescence and Cherry fusion) and host Topoisomerase I (Cherry fusion) co-localized with the DAPI signal, while Cherry was excluded (Fig. 2.2). Although the rules for protein internalization in the shell are currently unknown, each protein of known function that localizes inside of the shell interacts with DNA[11,12] (i.e. DNA replication and transcription machinery), suggesting that the exclusion of DNA-binding Cas and restriction proteins is an adaptive function of the shell.

To confirm that the ΦKZ phage genome could be a substrate for DNA cleavage, if accessed, two enzymes that failed *in vivo*, EcoRI and Cas9, were assayed *in vitro*. ΦKZ DNA was extracted from virions and subjected to restriction digestion reactions with a panel of restriction enzymes. EcoRI, HindIII, KpnI, and NcoI each cleaved the DNA, while SacI lacks a sequence recognition motif in the ΦKZ genome and did not (Fig. 2.3, Fig. 2.9). Cas9's ability to cleave ΦKZ gDNA *in vitro* was next assessed. Due to the large size of the ΦKZ genome (280 kbp), we first subjected purified phage DNA to the restriction enzyme KasI to liberate a 6.98 kbp product and then cleaved that species with a dual crRNA:tracrRNA-loaded SpyCas9 nuclease *in vitro*. This reaction depleted the substrate, liberating the expected 4.9 kb and 2.1 kb fragments, confirming that the phage gDNA is sensitive to Cas9 cleavage (Fig. 2.3). Together these results demonstrate that immune enzymes are capable of cleaving ΦKZ gDNA when accessed and that immune evasion is likely not due to an intrinsic feature of the phage DNA, such as base modifications that can impede Cascade-Cas3, Cas9, and EcoRI[16-19].

Immune enzyme re-localization enables phage targeting

Due to a current inability to mutate, weaken, or knockout the shell structure, we next sought to enable an immunity enzyme to bypass the shell to access phage DNA *in vivo*. The single effector enzyme Cas9 was fused to ORF152, a phage-encoded RecA-like protein that is internalized within the shell[11,12]. Independent fusions to the N- or C- terminus did not affect ΦKZ replication, however (Fig. 2.10). Imaging of one fusion orientation (ORF152-Cas9) revealed peri-shell localization (Fig. 2.10), suggesting that the fusion redirected Cas9 from its previously diffuse state, but perhaps the large Cas9 protein (1,368 amino acids, 158 kDa) was unable to traverse the shell border.

Given the large size (e.g. Cas12a) and complexity (e.g. Cascade, HsdRMS) of each of the other immune systems, we next fused the small, single effector protein EcoRI (278 amino acids, 31.5 kDa) to Cherry-ORF152. This fusion resulted in a notable >2.5 order of magnitude reduction in ΦKZ phage titer and markedly reduced plaque sizes (Fig. 2.3), the first successful *in vivo* DNA targeting observed in this study. Liquid infections revealed that cells expressing EcoRI-Cherry-ORF152 were extremely well protected, gaining >5 orders of magnitude resistance to phage-induced lysis (Fig. 2.3). A catalytic mutant EcoRI(E111G) fused to Cherry-ORF152 displayed no immune activity against ΦKZ in either assay, nor did active EcoRI-Cherry without the ORF152 fusion (Fig. 2.3). Similar results were observed in the absence of the Cherry tag (i.e. EcoRI-ORF152), however ΦKZ targeting was more modest in that case, reducing titers by ~10-fold and protecting cells by a factor of ~10^4 (Fig. 2.11). Imaging of infected cells expressing EcoRI-Cherry or EcoRI(E111G)-Cherry demonstrated that these proteins are excluded from the shell, while EcoRI(E111G)-Cherry-ORF152 is successfully localized inside (Fig. 2.3). EcoRI-Cherry-ORF152 impaired the ability of infected cells to form full shells and proceed through the infection process, and the EcoRI fusion protein was often localized within or adjacent to the DAPI-stained puncta (Fig. 2.3). Some host DNA can be seen in these cells and infection does not proceed (Fig. 2.3, Fig. 2.11). By bypassing the physical barrier of the shell using rational engineering, we conclude that the shell is the cause of resistance to immunity displayed by jumbo phage ΦKZ.

Phage mRNA is sensitive to Cas13a

The nucleus-like structure produced by ΦKZ provides robust resistance to DNA-targeting immune systems, but natural immune systems may exist that can evade this mechanism. We envisaged that the mRNA exported for translation in the cytoplasm is likely susceptible to targeting and that a ribonuclease could provide anti-ΦKZ immunity. To test this, we adapted the Type VI-A CRISPR RNA-guided RNA nuclease LseCas13a[20,21] for phage targeting in *P. aeruginosa*. Three LseCas13a spacers (two targeting head gene *gp146* and one targeting the shell gene *gp054*)

decreased ΦKZ plaquing efficiency by >10^6-fold (Fig. 2.4, Fig. 2.12). Corroborating the plaquing results, LseCas13a was also effective at protecting *P. aeruginosa* in liquid cultures, with 1-2 orders of magnitude resistance to phage induced lysis (Fig. 2.4). We suspect that the previously demonstrated collateral damage caused by Cas13a[22] is detrimental to cell fitness, leading to a modest enhancement to the growth curves compared to EcoRI targeting. At a frequency of ~10^{-6}–10^{-7}, Cas13 escaper phages were identified (Fig. 2.13) and surprisingly contained genomic deletions at the site of targeting (Fig. 2.4). Notably, all deletions were in-frame and 5/6 escapers had clear microhomology regions ranging from 7-21 bp flanking the deletion. One guide targeting the 5' end of *orf146* selected for deletions where the upstream gene (*orf145*) became fused, in frame, to the targeted gene (Fig. 2.4). These data support the conclusion that sequence-specific CRISPR-Cas RNA targeting can inhibit this phage.

Prior to shell construction, it is unknown what the state of the phage DNA is. During Cas13a targeting of the shell mRNA, imaging revealed that infections arrested before the phage DNA proceeded from its injection site at the poles. Most cells had two polar puncta, even one hour after infection (Fig. 2.4). The absence of phage DNA diffusion or clearance (e.g. by the endogenous Type I R-M system) suggests that the injected phage genome may be protected by a yet unknown mechanism involving injected, rapidly synthesized, or pre-existing host factors, prior to shell assembly. This is additionally corroborated by observations in the absence of Cas13a arrest, where we have observed DAPI-stained phage DNA adjacent to: i) EcoRI-Cherry-ORF152 puncta (Fig. 2.3) or ii) to a nascent shell localizing TopA (Fig. 2.14). The molecular nature and mechanisms underlying this early protection event remain to be elucidated.

Discussion

The assembly of a proteinaceous compartment to house the replicating phage DNA creates a physical protective barrier resulting in the resistance of phage ΦKZ to DNA-cleaving enzymes

(Fig. 2.4). Evasion of endogenous *P. aeruginosa* Type I CRISPR-Cas systems by ΦKZ suggests that these jumbo phages are likely Type I CRISPR-Cas resistant in nature. Supporting this hypothesis, our analysis of >4,000 non-redundant *P. aeruginosa* spacers (Type I-C, I-E, and I-F) reported by van Belkum *et al*. (2015) found no spacers against ΦKZ or its jumbo phage relatives ΦPA3, PaBG, KTN4, and PA7 (Table 2.1). This is in contrast to the many spacer matches from each system matching diverse *P. aeruginosa* phages, such as those assayed in our screen (Fig. 2.1) and those encoding anti-CRISPR proteins. Additionally, given the efficacy of the RNA-targeting CRISPR-Cas13 system, we propose that Type VI CRISPR systems are well-suited to target the mRNA of DNA phages when the DNA is inaccessible (i.e. due to base modifications or physical segregation).

This phage compartment has only been documented among the jumbo phages of *Pseudomonas*[11,12], however, we consider that physical occlusion of phage genomic DNA through this and other mechanisms may comprise a novel route to immune system evasion by phages. Indeed, recently discovered “mega phages” were reported to encode homologues of phage tubulin, which centers this compartment during infection[23]. The pan-resistance of ΦKZ to DNA-targeting enzymes provides an explanation for the elaborate and impressive nucleus-like structure. Furthermore, the polar localization of the injected phage DNA during mRNA targeting suggests a poorly understood early protective mechanism. Considering the pronounced resistance to overexpressed immune enzymes and the previously observed docking of capsids at the shell periphery[11,24], we propose that the phage DNA is never exposed to the cytoplasm (Fig. 2.4). Other hypotheses to explain the importance of the shell remain to be addressed, including protection from phage-derived nucleases that degrade the bacterial genome and spatial organization of the large phage genome during replication and packaging. Regardless, we conclude that the phage-assembled nucleus-like structure provides a strong protective barrier to DNA-targeting immune pathways.

REFERENCES

1. Koonin, E. V., Makarova, K. S. & Wolf, Y. I. Evolutionary Genomics of Defense Systems in Archaea and Bacteria. *Annu Rev Microbiol* 71, annurev–micro–090816–093830 (2017).

2. Bondy-Denomy, J., Pawluk, A., Maxwell, K. L. & Davidson, A. R. Bacteriophage genes that inactivate the CRISPR/Cas bacterial immune system. *Nature* 493, 429–432 (2013).

3. Pawluk, A., Bondy-Denomy, J., Cheung, V. H. W., Maxwell, K. L. & Davidson, A. R. A new group of phage anti-CRISPR genes inhibits the type I-E CRISPR-Cas system of Pseudomonas aeruginosa. *mBio* 5, e00896–e00896–14 (2014).

4. Pawluk, A. *et al.* Inactivation of CRISPR-Cas systems by anti-CRISPR proteins in diverse bacterial species. *Nature Microbiology* 1, 1–6 (2016).

5. van Belkum, A. *et al.* Phylogenetic Distribution of CRISPR-Cas Systems in Antibiotic-Resistant Pseudomonas aeruginosa. *mBio* 6, e01796–15 (2015).

6. Makarova, K. S. *et al.* An updated evolutionary classification of CRISPR-Cas systems. *Nat Rev Micro* 13, 722–736 (2015).

7. Marino, N. D. *et al.* Discovery of widespread Type I and Type V CRISPR-Cas inhibitors. *Science* 362, eaau5174–242 (2018).

8. Cady, K. C., Bondy-Denomy, J., Heussler, G. E., Davidson, A. R. & O'Toole, G. A. The CRISPR/Cas adaptive immune system of Pseudomonas aeruginosa mediates resistance to naturally occurring and engineered phages. 194, 5728–5738 (2012).

9. Pawluk, A. *et al.* Naturally Occurring Off-Switches for CRISPR-Cas9. *Cell* 167, 1829–1838.e9 (2016).

10. Rauch, B. J. *et al.* Inhibition of CRISPR-Cas9 with Bacteriophage Proteins. *Cell* 168, 150–158.e10 (2017).

11. Chaikeeratisak, V. *et al.* Assembly of a nucleus-like structure during viral replication in bacteria. *Science* 355, 194–197 (2017).

12. Chaikeeratisak, V. *et al.* The Phage Nucleus and Tubulin Spindle Are Conserved among Large Pseudomonas Phages. *Cell Rep* 20, 1563–1571 (2017).

13. Kraemer, J. A. *et al.* A phage tubulin assembles dynamic filaments by an atypical mechanism to center viral DNA within the host cell. *Cell* 149, 1488–1499 (2012).

14. Erb, M. L. *et al.* A bacteriophage tubulin harnesses dynamic instability to center DNA in infected cells. *Elife* 3, e03197 (2014).

15. Zehr, E. A. *et al.* The structure and assembly mechanism of a novel three-stranded tubulin filament that centers phage DNA. *Structure* 22, 539–548 (2014).

16. Bryson, A. L. *et al.* Covalent Modification of Bacteriophage T4 DNA Inhibits CRISPR-Cas9. *mBio* 6, e00648–15–9 (2015).

17. Strotskaya, A. *et al.* The action of Escherichia coli CRISPR-Cas system on lytic bacteriophages with different lifestyles and development strategies. *Nucleic Acids Research* 45, 1946–1957 (2017).

18. Vlot, M. *et al.* Bacteriophage DNA glucosylation impairs target DNA binding by type I and II but not by type V CRISPR-Cas effector complexes. *Nucleic Acids Research* 46, 873–885 (2018).

19. Huang, L. H., Farnet, C. M., Ehrlich, K. C. & Ehrlich, M. Digestion of highly modified bacteriophage DNA by restriction endonucleases. *Nucleic Acids Research* 10, 1579–1591 (1982).

20. Abudayyeh, O. O. *et al.* C2c2 is a single-component programmable RNA-guided RNA-targeting CRISPR effector. *Science* 353, aaf5573 (2016).

21. Gootenberg, J. S. *et al.* Nucleic acid detection with CRISPR-Cas13a/C2c2. *Science* 356, eaam9321–442 (2017).

22. Meeske, A. J. & Marraffini, L. A. RNA Guide Complementarity Prevents Self-Targeting in Type VI CRISPR Systems. *Mol Cell* 71, 791–801.e3 (2018).

23. Al-Shayeb, B. *et al.* Clades of huge phage from across Earth's ecosystems. *bioRxiv* 3, 572362 (2019).

24. Chaikeeratisak, V. *et al.* Viral Capsid Trafficking along Treadmilling Tubulin Filaments in Bacteria. *Cell* 177, 1771–1780.e12 (2019).

25. Choi, K.-H. & Schweizer, H. P. mini-Tn7 insertion in bacteria with single attTn7 sites: example Pseudomonas aeruginosa. *Nat Protoc* 1, 153–161 (2006).

26. Jinek, M. *et al.* A Programmable Dual-RNA-Guided DNA Endonuclease in Adaptive Bacterial Immunity. *Science* 337, 86–821 (2012).

27. Cowles, K. N. *et al.* The putative Poc complex controls two distinct Pseudomonas aeruginosa polar motility mechanisms. *Molecular Microbiology* 90, 923–938 (2013).

28. Mesyanzhinov, V. V. *et al.* The genome of bacteriophage phi KZ of Pseudomonas aeruginosa. *Journal of Molecular Biology* 317, 1–19 (2002).

29. Bondy-Denomy, J. *et al.* Prophages mediate defense against phage infection through diverse mechanisms. *The ISME Journal* 10, 2854–2866 (2016).

30. Kropinski, A. M. Sequence of the genome of the temperate, serotype-converting, Pseudomonas aeruginosa bacteriophage D3. 182, 6066–6074 (2000).

31. Qiu, D., Damron, F. H., Mima, T., Schweizer, H. P. & Yu, H. D. PBAD-Based Shuttle Vectors for Functional Analysis of Toxic and Highly Regulated Genes in Pseudomonas and Burkholderia spp. and Other Bacteria. *Applied and Environmental Microbiology* 74, 7422–7426 (2008).

32. Choi, K.-H. & Schweizer, H. P. mini-Tn7 insertion in bacteria with single attTn7 sites: example Pseudomonas aeruginosa. *Nat Protoc* 1, 153–161 (2006).

33. Choi, K.-H. *et al.* Genetic tools for select-agent-compliant manipulation of Burkholderia pseudomallei. *Applied and Environmental Microbiology* 74, 1064–1075 (2008).

Methods

Bacterial growth and genetic manipulation

Strains, plasmids, phages, and spacer sequences used in this study are listed in Tables 2.2-2.5. *Pseudomonas aeruginosa* strain PAO1 was grown in LB at 37 °C with aeration at 225 RPM. When necessary, plating was performed on LB agar with carbenicillin (250 µg/ml) or gentamicin (50 µg/ml). Gene expression was induced by the addition of L-arabinose (0.1% final) and/or isopropyl β-D-1-thiogalactopyranoside (IPTG, 0.5 mM or 1 mM final). For chromosomal insertions at the attTn7 locus, *P. aeruginosa* cells were electroporated with the integrating vector pUC18T-lac and the transposase expressing helper plasmid pTNS3, and selected on gentamicin. Potential integrants were screened by colony PCR with primers PTn7R and PglmS-down. Electrocompetent cell preparations, transformations, integrations, selections, plasmid curing, and FLP recombinase mediated marker excision with pFLP were performed as described previously[25].

Phage growth and DNA extraction

Phage growth was conducted in LB at 37 °C with PAO1 as a host. Growth curves were conducted in a Biotek Synergy plate reader at 37 °C with orbital shaking set to maximum speed. Phage stocks were diluted and stored in SM buffer[8] and used for routine plaquing assays. Plaque assays were conducted at 37 °C with 20 mL of bottom agar containing 10 mM $MgSO_4$ and 0.35% or 0.7% top agar (often both concentrations were used in parallel) also containing 10 mM $MgSO_4$ and any inducer molecules. 3 µL spots were applied to the top agar after it had been poured and solidified. For high titer lysates to generate phage DNA, plates with a high number of plaques were flooded with SM buffer and collected[8]. The lysates were subsequently DNase treated. Phage DNA was extracted with the Wizard Genomic DNA Purification Kit (Promega). DNA restriction assays were

performed according to standard NEB protocols and restriction fragments were assessed by agarose gel electrophoresis.

Type I-C CRISPR-Cas system assay and expression in *P. aeruginosa* PAO1

Type I-C CRISPR-Cas function was tested by electroporating a strain that naturally contains I-C *cas* genes (strain: F11) with pHERD30T plasmids encoding crRNAs that target phages. To express this system heterologously in PAO1, the four effector *cas* genes (*cas3-5-8-7*) were cloned into pUC18T-lac and inserted in the PAO1 chromosome as described above. After removal of the gentamicin marker, this strain was electroporated with the same pHERD30T crRNA-encoding plasmids to confirm function upon IPTG/arabinose induction.

Type I-F CRISPR-Cas system expression in *P. aeruginosa* PAO1

To express the Type I-F system heterologously in PAO1, all I-F *cas* genes (*cas1, cas3, csy1-4*) were cloned into pMMBHE plasmid and transformed into PAO1. Subsequently, this strain was electroporated with the pHERD30T crRNA-encoding plasmids to confirm function upon IPTG/arabinose induction. To maintain pHERD30T and pMMBHE in the same strain of *P. aeruginosa*, double selection of 30 µg/mL gentamicin and 100 µg/mL carbenicillin was employed.

crRNA cloning and expression

All crRNAs used here, were cloned into established entry vectors in the pHERD30T background. After removing a pre-existing BsaI cut site in the vector by mutagenesis, a pseudo-CRISPR array (i.e. repeat-spacer-repeat for Type I, V, VI, or a sgRNA scaffold for Type II) was then cloned into the vector, where the spacing sequence possessed two inverted BsaI digest sites, to facilitate scarless cloning of new spacers. Desired spacer sequences were chosen randomly across the phage genome (with the correct PAM sequence for the cognate CRISPR-Cas system) and

ordered as two complementary oligonucleotides that generate sticky ends when annealed, to be cloned into the entry vector, which was BsaI digested. Spacer oligonucleotides were PNK treated, annealed, and ligated into the entry vector.

Streptococcus pyogenes (Spy) Cas9 and sgRNA expression in *P. aeruginosa*

The *S. pyogenes Cas9* gene was cloned into a pUC18T-Ara integration vector and then inserted into the attTn7 locus of PAO1. A single guide RNA scaffold was constructed based on a previous design[26] with internal BsaI cut sites to enable insertion of pre-annealed oligos for scarless sgRNA design. This sgRNA scaffold was amplified with primers p30T-gRNA_BsaI and p30T-gRNA_BsaI_rev. The resulting product was inserted into the pHERD30T vector via Gibson assembly following backbone (pJW1) amplification by inverse PCR with primers gRNA_BsaI-p30T and gRNA_BsaI-p30T-rev. The sgRNA scaffold was positioned into pJW1 so that following BsaI cleavage the spacer insert +1 position would conincide with the pBAD TSS +1 position. The resulting plasmid, pJB1, was BsaI digested (NEB) followed by ligation of indicated pre-annealed oligos. Table 2.5 contains a complete list of all target sequences. The sequence of the sgRNA construct with BsaI site locations is shown in Table 2.4.

Cas9 in vitro cleavage

Cas9-based phage genome cleavage *in vitro* was conducted with purified Cas9 protein (NEB #M0386S), and the Cas9-gRNA-tracrRNA based cleavage reaction was then performed according to the manufacturer's (NEB) instructions. Cas9 crRNAs (Table 2.4) were ordered as Alt-R CRISPR-Cas9 crRNAs from IDT and utilized without further modification. The tracrRNA was amplified using primers tracrRNA-FOR and tracrRNA-REV from a plasmid (pBR62). The tracrRNA was produced through a T7 RNAP reactions using dsDNA encoding the tracrRNA downstream of a T7 RNAP promoter. Cas9 protein (NEB) was combined with pre-annealed crRNA and tracRNA complex at a 1:1 molar ratio. For targeting KasI-liberated ΦKZ genomic DNA,

500 ng of ΦKZ DNA was co-incubated with Cas9 RNP, which would cleave at pos. 183,270, and KasI in NEB buffer 3.1 for 1 hour. After stopping the reaction by proteinase K treatment, products were assessed by agarose gel electrophoresis. For Cas9 digestion of whole DNA, the reaction was performed at 37 °C for 4 hrs with 300 ng of ΦKZ or DMS3 genomic DNA and the products were assessed by agarose gel electrophoresis. Two Cas9 guides were selected that would cleave at pos. 158,649 and 168,715 of the ΦKZ genome to liberate an ~10 kb fragment.

Cas12a and crRNA design for PA expression

The humanized allele of the *cpf1* gene of *Moraxella bovoculli* (MBO_03467, KDN25524.1) was sub-cloned from pTE4495 (Addgene) into pUC18T-lac using primers pUC_cpf1_F and pUC_cpf1_R and inserted in the PAO1 chromosome as described above. A Cpf1 repeat-spacer-repeat pseudo-CRISPR array was synthesized as oligonucleotides, annealed, and ligated into a pHERD30T vector, digested with NcoI and HindIII. Spacer sequences were cloned into the resulting vector (pJB2) following BsaI digestion and ligation of pre-annealed spacer oligonucleotide pairs.

Cas13a and crRNA design for PA expression

The wild type allele of the *cas13* gene of *Listeria seeligeri* and *Leptotrichia shahii* were sub-cloned from p2CT-His-MBP-Lse_C2c2_WT and p2CT-His-MBP-Lsh_C2c2_WT (Addgene) into pUC18T-lac. LseCas13 and Lsh Cas13 were inserted in the PAO1 chromosome as described above. An Lse and an Lsh Cas13a repeat-spacer-repeat pseudo-CRISPR array were synthesized as oligonucleotides, annealed, and ligated into a pHERD30T vector, digested with NcoI and EcoRI. Spacer sequences were cloned into the resulting vectors (pSDM057 and pSDM070, respectively) following BsaI digestion and ligation of pre-annealed spacer oligonucleotide pairs. crRNA expression vectors were introduced into PAO1 tn7::*cas13*^{Lse} and PAO1 tn7::*cas13*^{Lsh}. The resulting strains were were assayed for phage sensitivity under standard phage plaing conditions,

with induction of both Cas13 and the gRNAs (50 µg/mL gentamicin, 0.1% (L)-arabinose, 1 mM IPTG).

EcoRI expression in *P. aeruginosa*

The wild type allele of the M.*EcoRI* (Methyltransferase) and *R.EcoRI* (Endonuclease) genes were sub-cloned from pSB1A3 EcoRI Methylase-AmilCP and pSB1A3 EcoRI-RTX with EcoRI Methylase-AmilCP (Addgene plasmid # 85166, Addgene plasmid # 85165)p2CT-His-MBP-Lse_C2c2_WT and p2CT-His-MBP-Lsh_C2c2_WT (Addgene) into pHERD30T using Gibson assembly. The resulting plasmids, pSDM160 and pSDM161, were electroporated into PAOI Δ*hsdR* (SDM020). The resulting strains were were assayed for phage sensitivity under standard phage plaing conditions, with induction of both M.EcoRI (for genome protection) and R.EcoRI (50 µg/mL gentamicin, 0.1% (L)-arabinose).

Restriction-Modification Assay

PAO1, PAK, and PAO1 Δ*hsdR* were grown to saturation in LB at 37 °C. 4 mL of 0.7% agar, 10 mM $MgSO_4$ molten top agar were seeded with 100 µL saturated culture and spread on 20 mL 10 mM $MgSO_4$ LB agar plates. 2.5 µL 10-fold serial dilutions of bacteriophage JBD30 and ΦKZ propagated on strain PAO1 and PAK were spotted on plates. Plates were incubated at 37°C overnight and were imaged the following day.

Chromosomal Knockout of *hsdR*

To delete *hsdR* (NP_251422.1) from the PAO1 genome, a PAO1 strain expressing Cas9 from *S. pyogenes* was programmed to express a sgRNA against *hsdR*: GCCCTCATCGAAGAAACCAG. Additionally, the pHERD30T plasmid expressing this sgRNA was engineered to carry a repair template. This repair template consisted of the 500 bp upstream of *hsdR* and the 500 bp downstream of *hsdR* directly enjoined to one another. Induction of Cas9 and sgRNA led to cellular

toxicity, as measured by OD_{600} (data not shown). Survivors of Cas9-mediated targeting were isolated. The *hsdR* locus of survivors was then amplified by colony PCR with primers binding outside of the region encompassed by the repair template. Products were resolved by gel electrophoresis in a 1.0% agarose TAE gel at 100 V and visualized using SYBR safe DNA stain. Amplicons of a reduced size were then sequenced, confirming the chromosomal deletion of *hsdR*. A clone with the correct deletion, SDM020, was chosen for downstream experiments.

Construction of fusion proteins

Plasmids expressing cherry alone or cherry tagged with cas3, cas8 (of Type I-C and Type I-F system) and TopA were constructed by Gibson assembly in pHERD30T plasmid digested with SacI and PstI. These fusions have ggaggcggtggagcc (G-G-G-G-A) linker sequence in between them. Cherry was amplified from SF-pSFFV-sfCherryFL1M3_TagBFP (kindly provide by Bo Huang lab, UCSF). cas3, cas8 of the Type I-C and Type I-F systems were amplified from LL77 and PA14 respectively. topA was amplified from gDNA of PAO1. All the primers used for the construction of the plasmids are listed in Table 2.4.

Plasmids expressing cherry-Cas9 (pESN28) (primers: prESN74, prESN75, prESN76, prESN77) and Cherry-Cas9-ORF152 (pESN29) (prESN80, prESN81, prESN82, prESN83) were constructed using Gibson Assembly in the pHERD30T plasmid. Cherry-ORF152 (pESN32) (prESN91, prESN92) was constructed by PCR amplification to omit Cas9 and ligated using a KLD reaction. An sgaaaaggsqk linker connects Cherry to the other proteins. A ggggs linker connects Cas9 and ORF152. The plasmid expressing cMyc-ORF152 (prESN153, prESN154) was constructed. All plasmids were designed using SnapGene.

To make translational fusions of proteins, desired gene fragments including Cas9, M.EcoRI, R.EcoRI, ORF152 (NP_803718.1), and sfCherry2 were amplified by PCR from templates pHERD30T::Cas9, pSB1A3::M.EcoRI-AmilCP, pSB1A3::M.EcoRI-AmilCP;R.EcoRI-RTX, ΦKZ genomic DNA, and pHERD30T::sfCherry2, respectively. pHERD30T was linearized

by restriction digest with SacI-HF and PstI-HF or by PCR. PCR primers included 15-30 bp overhangs for Gibson assembly. Overhangs enjoining genes included linkers GGGGS or GGSGGS. PCRs were treated with DpnI to eliminate template DNA. All PCRs and restriction digests were purified using a PCR clean up kit (Zymo Research DNA Clean and Concentrator Kits). Linearized vector and gene fragments treated with Gibson assembly. Gibson assembly reactions were transformed into competent *E. coli*. Plasmid products were isolated by miniprep and submitted for sequencing. Correct assemblies were electroporated into appropriate *P. aeruginosa* strains.

Cas13 escaper isolation

For identifying escapers of Cas13a RNA-targeting, 3 µl of high concentration ϕKZ lysates were mixed with 150 µl of overnight cultures of SDM078, SDM109 or SDM107 (strains expressing Cas13a and a gRNA against ϕKZ) . After incubating at 37 °C for 10 minutes, samples were mixed with 4 mL of 0.7% agar, 10 mM MgSO4, 1 mM IPTG and 0.1% arabinose and plated in LB agar plates with Gentamicin (50 µg/ml). After overnight incubation, plates were examined for the presence of escaper plaques. Escapers were formed in SDM078 and SDM109 but not in SDM107. 10 phages that escaped targeting from SDM078 and SDM109 were purified and the protospacer locus was amplified using PCR and subsequently sequenced. Six unique outcomes were identified and shown in Figure 2.4.

Growth curve experiments

Growth curve experiments were carried out in a plate reader as in Borges AL *et al* 2018 *Cell*. Briefly, cells were diluted 1:100 from a saturated overnight culture with 10 mM MgSO4 and antibiotics and inducers, as appropriate. 140 µL of diluted culture was added, together with 10 µL of phage to wells in a 96-well plate. This plate was cultured with maximum double orbital rotation at 37 °C for 24 hours with OD600 measurements every 5 minutes

Immunofluorescence

Sample Growth

5 mL overnight cultures of a strain expressing Cas9 and an sgRNA targeting ΦKZ (SDM065) and a strain expressing cMyc-ORF152 (bESN27) were grown at 30 °C in LB media with gentamicin. A 1:30 back-dilution of the overnight culture into LB was grown at 30 °C for 1 h. Protein and guide expression was induced with 0.1% arabinose and 0.5 mM IPTG, respectively. After 1 h of expression, an aliquot of uninfected cells was fixed while the remaining cultures were infected with ΦKZ using MOI 1.5. Infected cell aliquots were collected and fixed at 60 mpi.

Fixation

This protocol was adapted from ref. [27]. Samples were fixed with 5X Fix Solution (12.5% paraformaldehyde, 150 mM KPO4, pH 7.2) and incubating for 15 minutes at room temperature followed by 20 minutes on ice. Samples were then washed in PBS 3 times and finally resuspended in GTE (50 mM glucose, 10 mM EDTA, pH 8.0, 20 mM Tris-HCl, pH 7.65) with 10 ug/mL lysozyme. Resuspended cells were transferred to polylysinated coverslips and dried. Once dry, coverslips were incubated in cold methanol for 5 minutes followed by cold acetone for 5 minutes. Cells were rehydrated by a rinse in PBS followed by a 3-minute incubation in PBS + 2% BSA blocking solution. Cells were incubated with a 1:50 dilution of primary antibody (Cas9 (7A9-3A3): sc-517386 or cMyc (9E10): sc-40) in PBS + 2% BSA for 1 hr followed by 3, 7 minute washes in fresh PBS + 2% BSA. Coverslips were then incubated in the dark for 1 hr with secondary antibody (goat anti-mouse Alexa Fluor 555, Life Technologies A-21424) diluted 1:500 in PBS + 2% BSA. DAPI was added for the final 10 minutes of the incubation. Cells were washed in PBS 3 times for 7 minutes. Coverslips were then placed on slides using mounting media (v/v 90% glycerol, v/v 10%Tris pH 8.0 and w/v 0.5% propyl-gallate) and sealed with clear nail polish.

Microscopy and Analysis

Images were collected using a Zeiss Axiovert 200M microscope. Images were later processed using NIS Analysis software at the UCSF NIC. Compartments and cells were manually selected using the Simple ROI Editor. Background subtractions were conducted for each cell and compartment separately. The corrected intensities for the cytoplasmic and compartment regions were averaged over the area of each cell and compartment using Matlab and plotted using Prism 6. Data from two pooled replicates was fitted with a line, showing 95% confidence intervals with dashed lines. The slope is as reported in the plots.

Live cell imaging

For live cell imaging of ϕKZ infection, freshly grown cells from LB plates were picked and resuspended in 100 µl of LB media. 5-10 µL of samples are spotted on 0.85% agarose pads with 1:5 diluted LB. Arabinose (0.01% to 0.05%) and DAPI (2 µg/ml). Samples were then incubated in a humidified chamber and allowed to grow for 3 hours at 30 °C. 5 µL ϕKZ lysate was spotted on top of the agar pad and the samples were grown for an additional 1 hour. Cells were visualized in the microscope after covering them with a cover slip. Nikon Ti2-E inverted microscope equipped with Perfect Focus System (PFS) and Photometrics Prime 95B-25mm camera were used for live cell imaging. Images were processed using NIS Elements-AR software.

Figures:

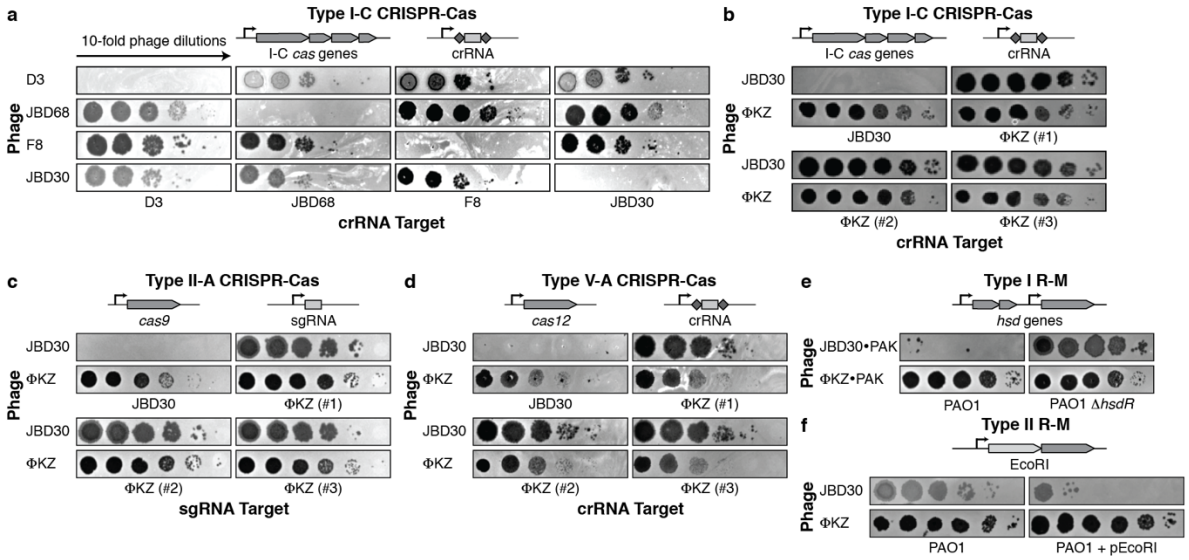

Figure 2.1: Identification of a phage that resists targeting by diverse CRISPR-Cas and restriction-modification systems. Plaque assay with the indicated phage spotted in ten-fold serial diluations on a lawn of *P. aeruginosa*, dark clearings in the lawn represent phage replication. Strain PAO1 expressing: **a,** Type I-C *cas* genes (*cas3-5-8-7*) and crRNAs targeting the indicated phages. **b,** Type I-C *cas* genes and crRNAs targeting phage JBD30 or distinct phage ΦKZ-targeting crRNAs (#1-#3). **c,** Type II-A *cas9* and distinct single guide RNAs (sgRNAs) targeting the indicated phage. **d,** Type V-A *cas12a* and distinct crRNAs against the indicated phage. **e,** Endogenous Type I R-M system (*hsdRSM*) in strain PAO1 was assayed using phages propagated on PAK (e.g. JBD30•PAK was first propagated on strain PAK). Together with an isogenic PAO1Δ*hsdR* knockout. **f,** Type II EcoRI R-M system. Restriction activity was assayed using phages JBD30 and ΦKZ. All plaque assays replicated ≥ 2 times with similar results.

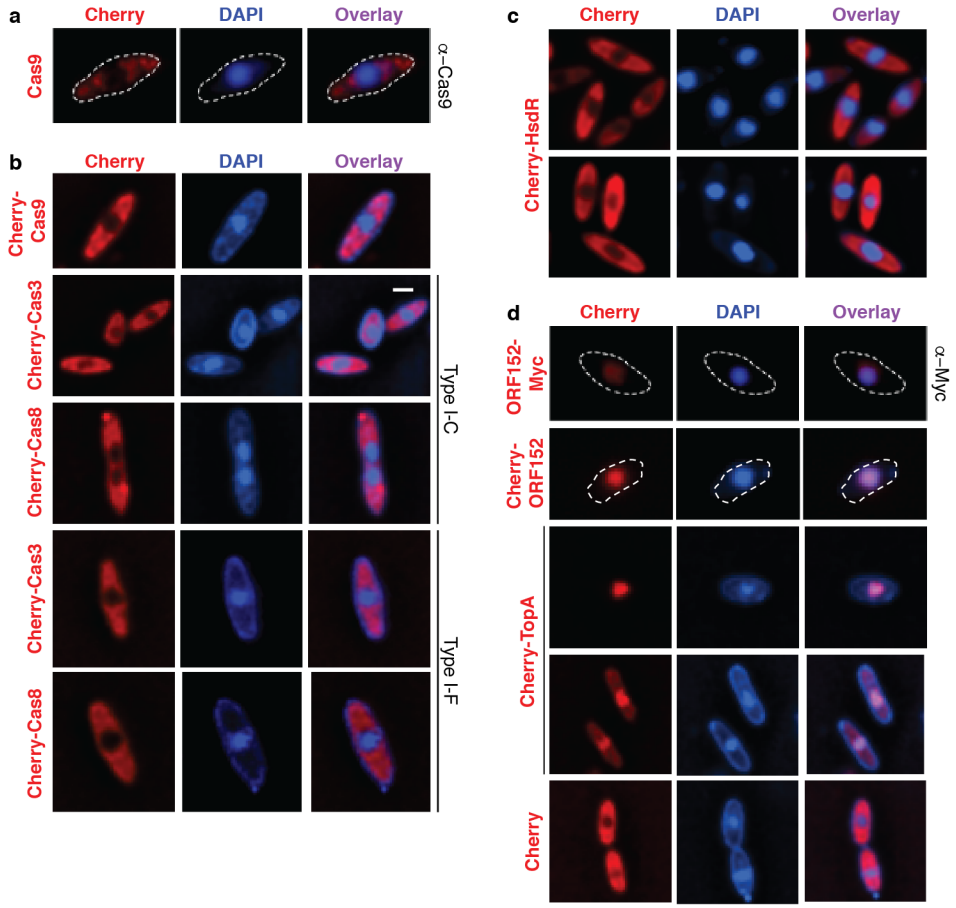

Figure 2.2: CRISPR-Cas and restriction proteins are excluded from ΦKZ's nucleus-like structure. a, Fluorescence microscopy of *P. aeruginosa* immunostained for Cas9, DAPI stain shows the phage DNA within the nucleus-like structure. Live fluorescence microscopy of *P. aeruginosa* strains engineered to express **b,** II-A Cas9 or I-C or I-F Cas8 or Cas3 proteins fused to Cherry, **c,** a Cherry-HsdR fusion, **d,** Immunostained for Myc-ORF152 (top panels), or live imaging of ORF152 and TopA proteins fused to Cherry, or Cherry alone. All experiments were replicated ≥ 2 times with similar results.

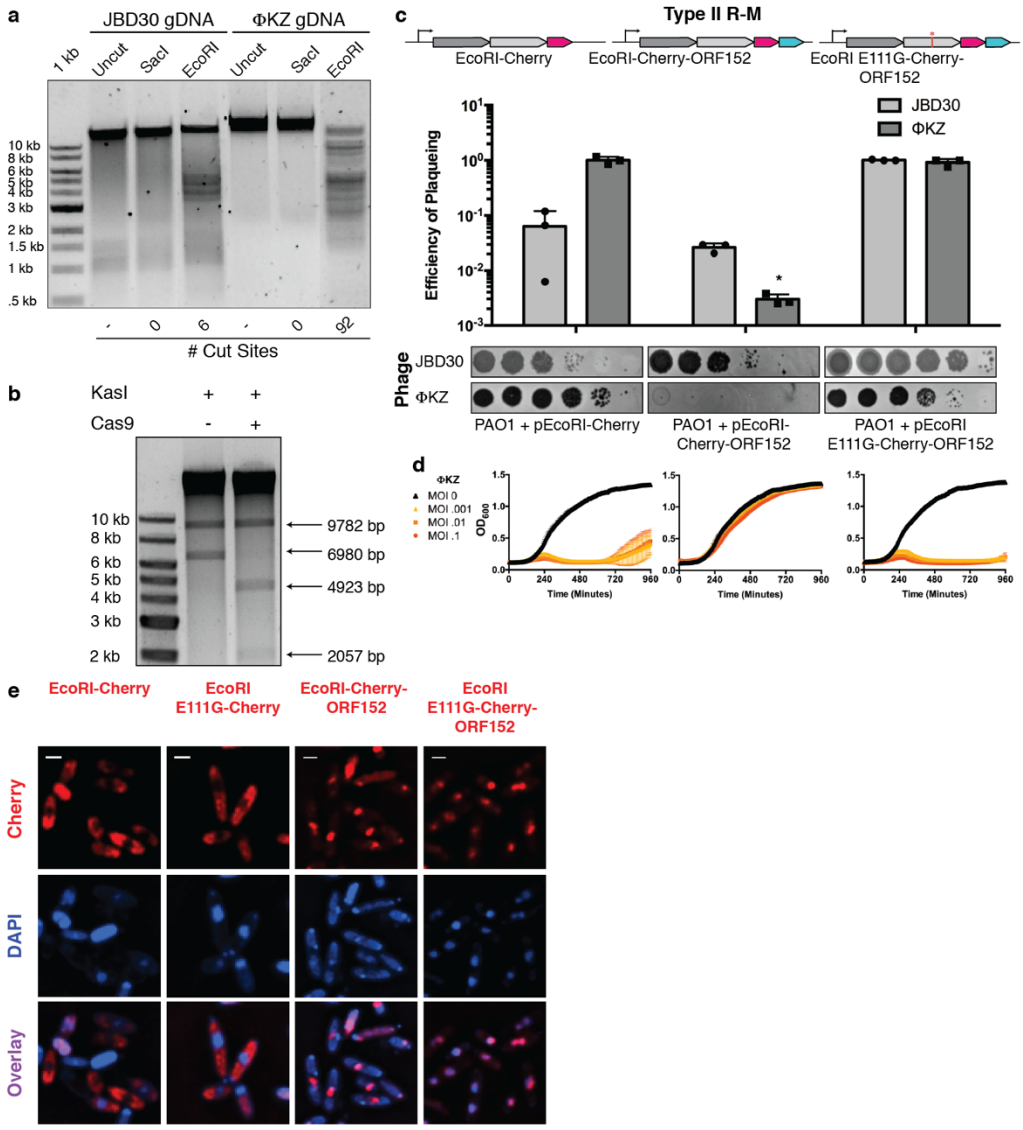

Figure 2.3: ΦKZ genomic DNA can be cleaved by immune enzymes. a, ΦKZ and JBD30 genomic DNA digested with the indicated restriction enzymes *in vitro*. The first lane contains a 1 kb DNA ladder. The number of cut sites for each enzyme is shown at the bottom of the gels. Products were visualized on a 0.7% agarose gel, visualized with SYBR Safe nucleic acid stain. **b,** ΦKZ phage genomic DNA digested *in vitro* using KasI, and incubated with and without Cas9 loaded with crRNA:tracrRNA targeting the fragment liberated by KasI. Products were visualized on a 0.7% agarose gel, visualized with SYBR Safe nucleic acid stain. **c,** Strain PAO1 expressing EcoRI-Cherry, EcoRI-Cherry-ORF152, or EcoRI E111G-Cherry-ORF152 fusion protein. Plaque assays were conducted as in Fig. 2.1 and quantified (n=3). Mean values are plotted as bars with error bars representing standard deviation. A t-test comparing ΦKZ EOP on PAO1 pEcoRI-Cherry to PAO1 pEcoRI-Cherry-ORF152 yielded a p-value of 2.88×10^{-4}. **d,** Growth curves monitoring the OD_{600} of PAO1 cells infected with the indicated ΦKZ multiplicity of infection (MOI). **e,** Live fluorescence imaging of infected *P. aeruginosa* strains engineered to express EcoRI-Cherry, EcoRI E111G-Cherry, EcoRI-Cherry-ORF152 or EcoRI E111G-Cherry-ORF152. DAPI stain shows the phage DNA. Cherry shows EcoRI fusion protein. *In vitro* digestion experiments **a** and **b** replicated twice with similar results. Plaque assays I, growth curves (**d**), and microscopy (**e**) were replicated ≥ 3 times.

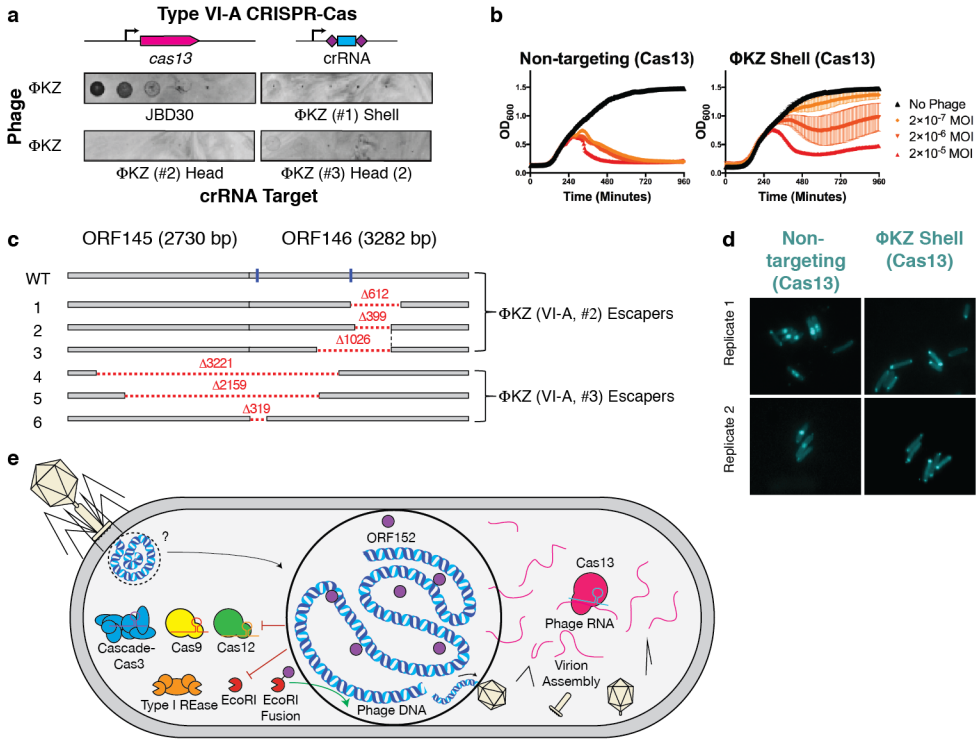

Figure 2.4: Phage ΦKZ DNA is sensitive to RNA-targeting Cas13. a, PAO1 expressing LseCas13a and a crRNA targeting phage ΦKZ. Plaque assays were conducted as in Fig. 2.1. **b,** Growth curves measuring the OD_{600} of PAO1 infected with the indicated ΦKZ MOI. **c,** Cas13 escaper ΦKZ phage mutant deletions (red dashed lines) with target sites indicated (blue line). **d,** Live fluorescence imaging of *P. aeruginosa* strains engineered to express LseCas13a and crRNAs targeting ΦKZ. Cyan stain shows the phage DNA. **e**, Model summarizing the ΦKZ nucleus-like structure excluding (flat arrow) Cas9, Cas12, Cascade-Cas3 (Type I-C, Type I-F) and Type I restriction endonucleases (REase) and Type II REase, while the mRNA (red) is exported and can be targeted by Cas13. The nucleus-like structure is resistant to the indicated nucleases, but EcoRI fusion (to internal protein ORF152) enables targeting. Cas13 plaque assays **a** were replicated >3 times with similar results. Growth curve experiments **b** were replicated twice with similar results. Escaper mutants **c** were isolated once and verified by PCR, sequencing, and plaque assays. Microscopy **d** was replicated twice with similar results.

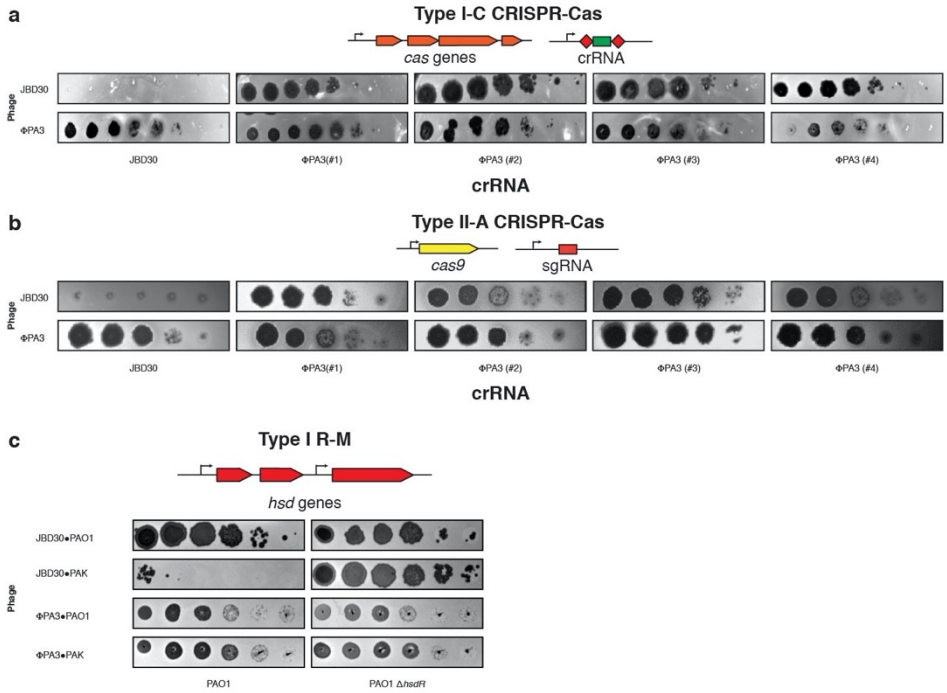

Figure 2.5: Jumbo phage ΦPA3 resists targeting by CRISPR Cas and a restriction-modification system. a, Strain PAO1 was engineered to express the I-C *cas* genes and distinct crRNAs targeting the indicated phages, and plaque assays were conducted as in Fig. 2.1. **b,** Strain PAO1 was engineered to express the Type II-A Cas9 protein and distinct single guide RNAs (sgRNAs) targeting the indicated phage. Plaque assays were conducted as in Figure 2.1. **c,** The endogenous Type I R-M system (*hsdRSM*) in strain PAO1 was assayed using phages propagated on PAO1 or PAK as indicated (e.g. JBD30•PAO1 was first propagated on strain PAO1). Together with an isogenic PAO1Δ*hsdR* knockout, all strains were subjected to a plaque assay as in Figure 2.1. All plaque assays were replicated twice with similar results.

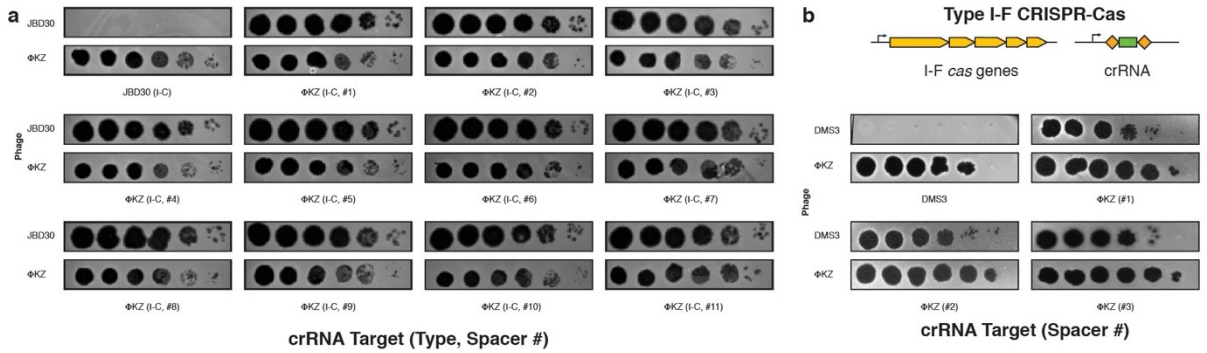

Figure 2.6: Phage ΦKZ resists *P. aeruginosa* Type I-C and Type I-F CRISPR-Cas immunity. **a,** Strain PAO1 was engineered to express the I-C *cas* genes and distinct crRNAs targeting phage JBD30 and phage ΦKZ, and plaque assays were conducted as in Fig. 2.1. **b,** Strain PAO1 was engineered to express the I-F *cas* genes and distinct crRNAs targeting phage JBD30 and phage ΦKZ, and plaque assays were conducted as in Fig. 2.1. All plaque assays replicated ≥ 2 times with similar results.

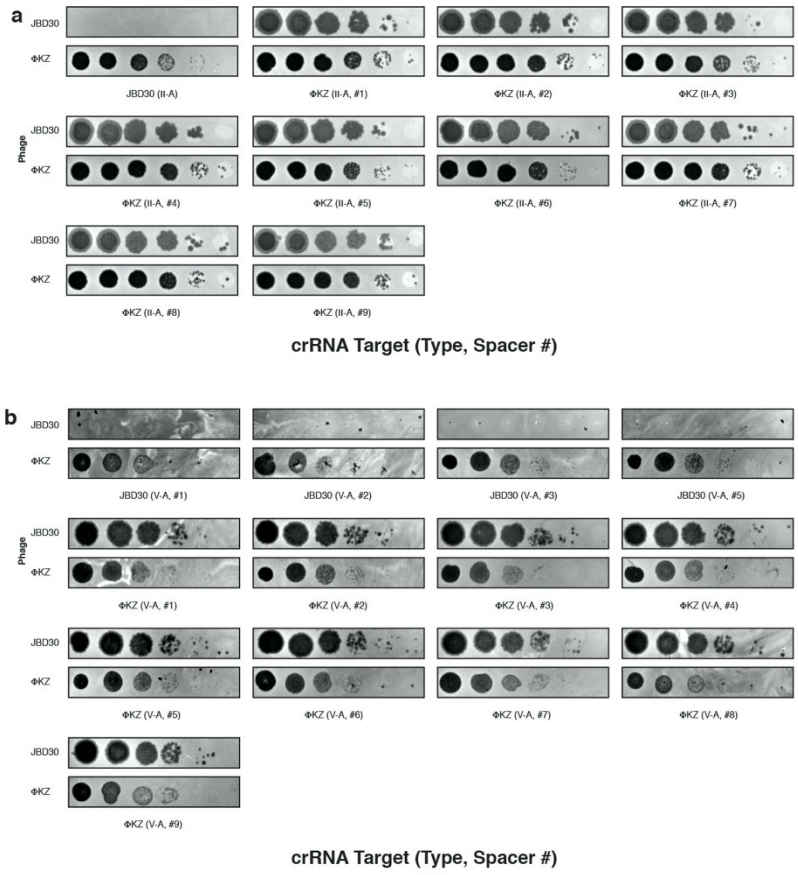

Figure 2.7: Phage ΦKZ resists targeting by heterologous Type II-A and V-A CRISPR-Cas systems. a, Strain PAO1 was engineered to express the Type II-A Cas9 protein and distinct single guide RNAs (sgRNAs) targeting the indicated phage. Plaque assays were conducted as in Figure 2.1. **b,** Strain PAO1 was engineered to express the Type V-A Cas12a protein and distinct crRNAs against the indicated phage. Plaque assays were conducted as in Figure 2.1. All plaque assays replicated ≥ 2 times with similar results.

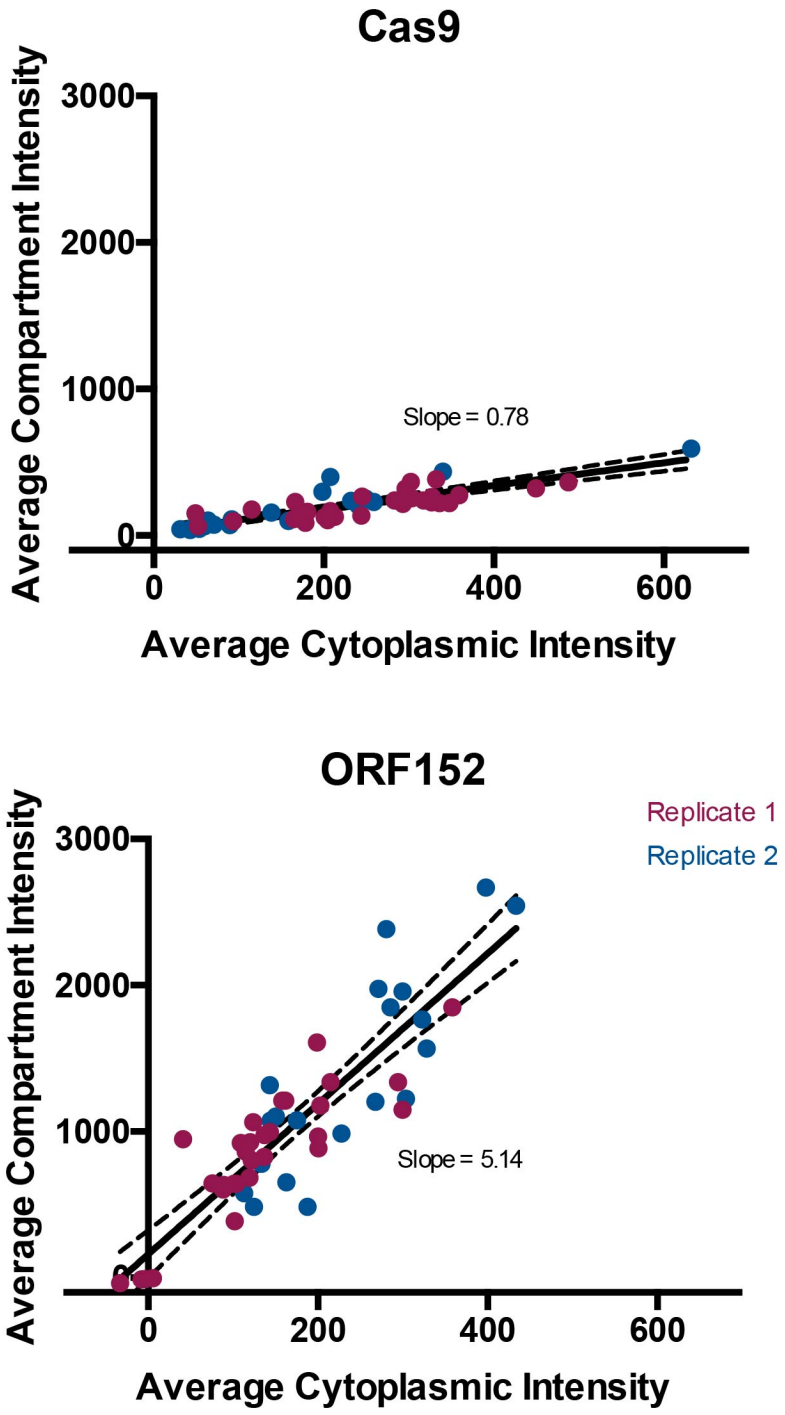

Figure 2.8: Quantification of Cas9 localization during phage ΦKZ infection of *P. aeruginosa*. Localization of Cas9 and ORF152 in the cytoplasm and shell during ΦKZ infection were quantified. Data points (individual cells) from two pooled replicate experiments were fitted with a line, showing 95% confidence intervals with dashed lines. The slope is as reported in the plots.

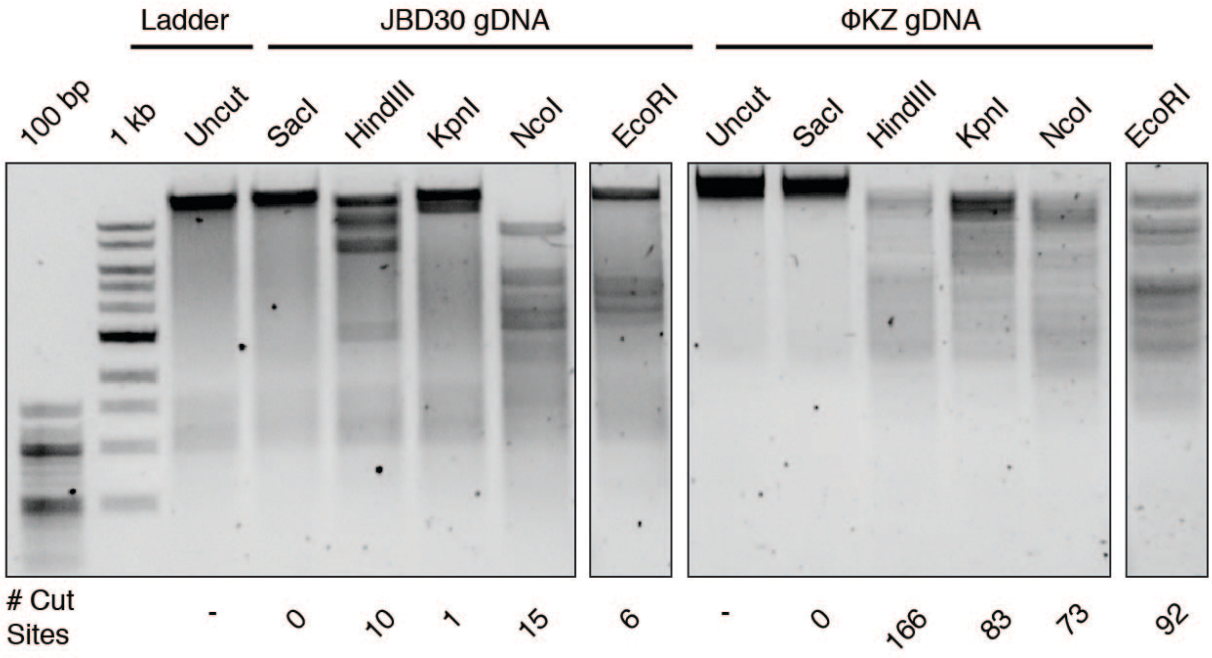

Figure 2.9: Phage ΦKZ genomic DNA is susceptible *in vitro* to cleavage by Restriction Endonucleases. Genomic DNA was isolated from phages ΦKZ and JBD30 and was subjected to digestion with the indicated restriction enzymes *in vitro*. The number of cut sites for each enzyme is shown at the bottom of the gels. Products were visualized on a 0.7 % agarose gel, visualized with SYBR Safe nucleic acid stain. *In vitro* digestion experiment was replicated twice with similar results.

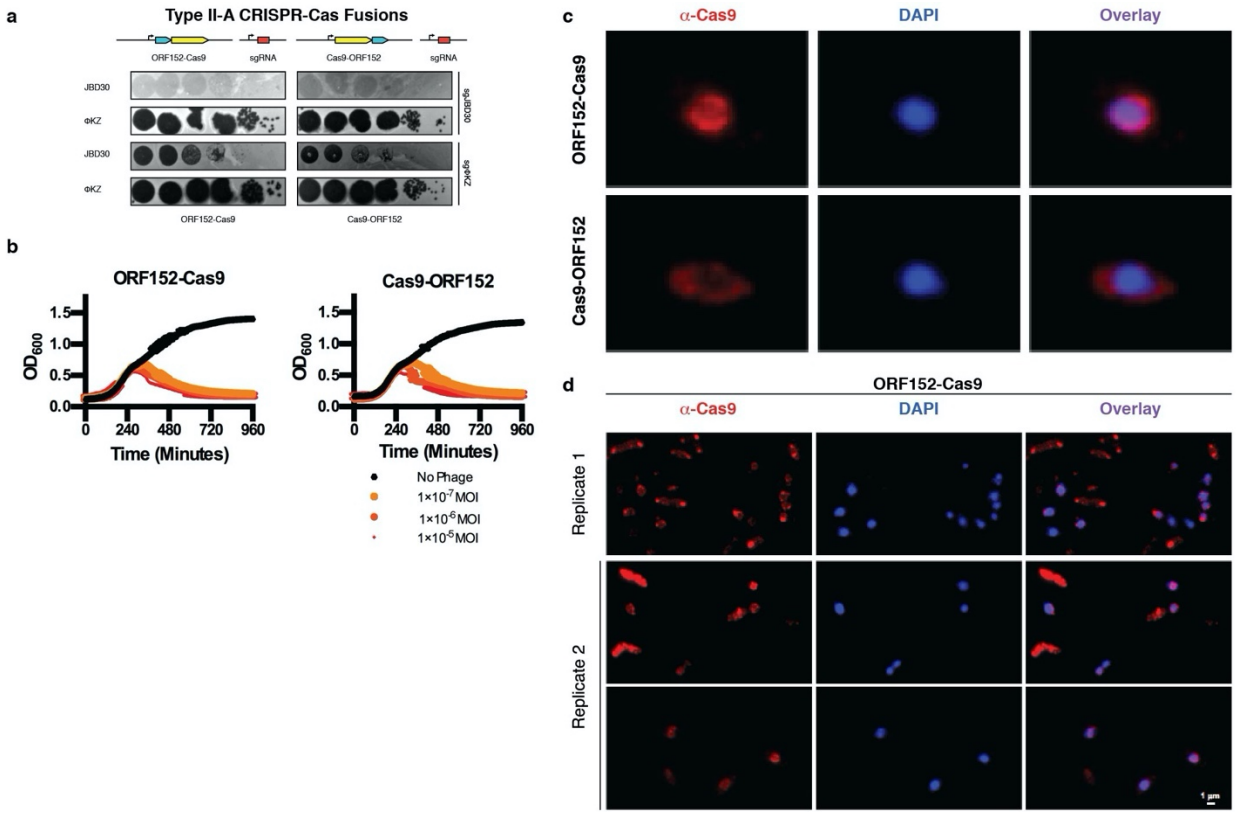

Figure 2.10: Cas9 fusion to ORF152 localizes to periphery of shell, but does not enable immune activity against ΦKZ. a, Strain PAO1 was engineered to express Cas9 fused to ORF152 at either the N- or C-terminus, with single guide RNAs (sgRNAs) targeting the indicated phage. Plaque assays were conducted as in Fig. 2.1, **b,** growth curves were conducted, monitoring the OD_{600} of PAO1 cells infected with the indicated ΦKZ multiplicity of infection (MOI). **c,** Fluorescence microscopy of PAO1 fusion strains, immunostained for Cas9, in cells expressing ORF152-Cas9 or Cas9-ORF152. DAPI stain shows the phage DNA within the shell. **d,** Fluorescence microscopy of *P. aeruginosa*, immunostained for Cas9, in cells expressing ORF152-Cas9. DAPI stain shows the phage DNA within the shell. All plaque assays were replicated 4 times with similar results. Growth curve experiments were replicated three times with similar results. Microscopy was replicated twice with similar results.

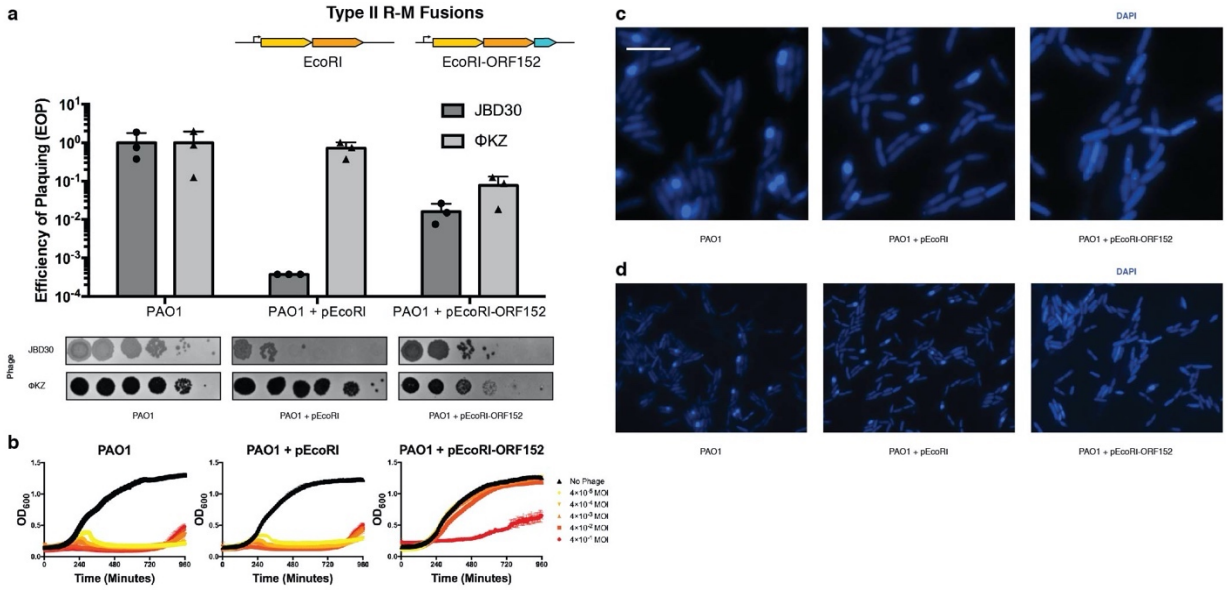

Figure 2.11: Fusion of EcoRI restriction enzymes to ORF152 enables immune activity. a, Strain PAO1 was engineered to express EcoRI or EcoRI-ORF152 fusion protein. Plaque assays were conducted as in Fig. 2.1 and quantified (n=3). **b,** Growth curves were conducted, monitoring the OD_{600} of PAO1 cells infected with the indicated ΦKZ multiplicity of infection (MOI). **c,** Live fluorescence imaging of *P. aeruginosa* strains engineered to express EcoRI or EcoRI-ORF152. DAPI stain shows the phage DNA. **d,** Live fluorescence imaging of *P. aeruginosa* strains engineered to express EcoRI, or EcoRI-ORF152. DAPI stain shows the phage DNA within the shell. Wide field of view. All plaque assays were replicated 3 times with similar results. Growth curve experiments were replicated twice with similar results. Microscopy was replicated twice with similar results.

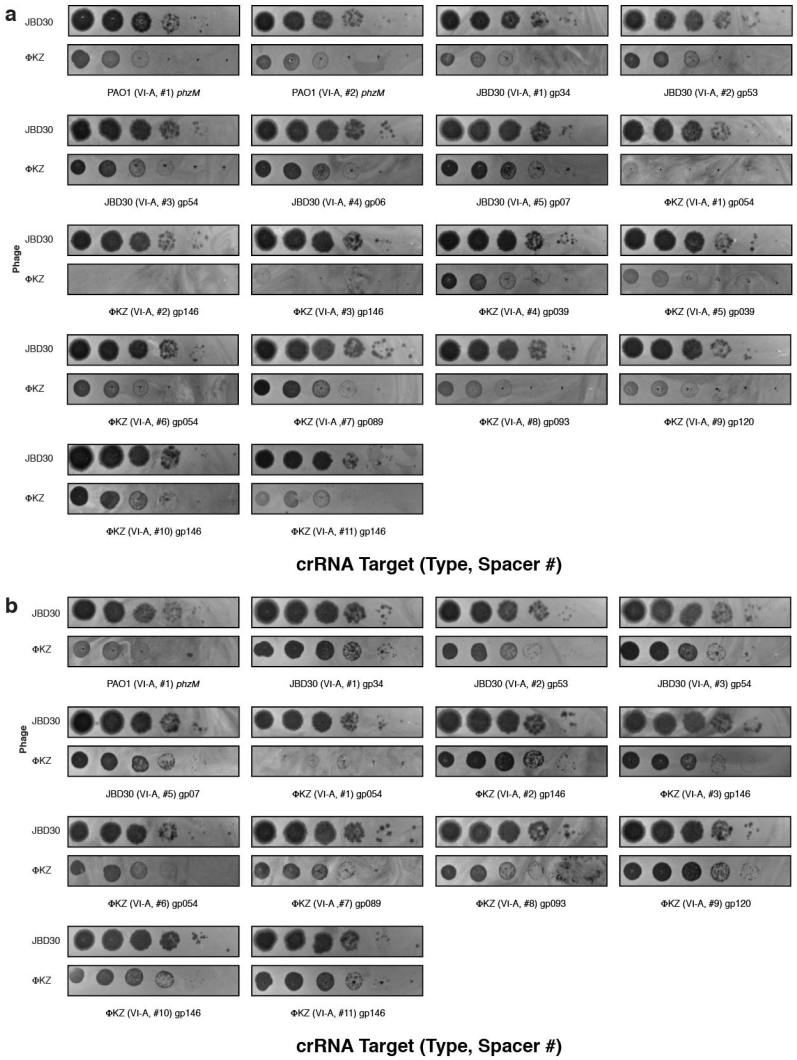

Figure 2.12: Phage ΦKZ DNA is sensitive to RNA-targeting Cas13. a, Strain PAO1 expressing LseCas13a and distinct crRNAs targeting the indicated gene. Plaque assays conducted as in Figure 2.1. **b,** Strain PAO1 expressing LshCas13a and distinct crRNAs targeting the indicated gene. Plaque assays conducted as in Figure 2.1. All plaque assays were replicated twice with similar results.

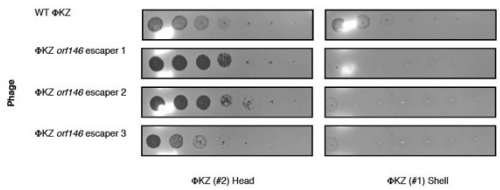

Figure 2.13: Phage ΦKZ escaper mutants are selected by Cas13-mediated RNA targeting. Strain PAO1 expressing LseCas13a and a crRNA targeting the indicated gene. Plaque assays conducted as in Figure 2.1 using wild type and escaper mutant ΦKZ. WT ΦKZ is targeted by both strains and the faint clearings observed here are not observed as plaques in a full-plate assay. All plaque assays were replicated twice with similar results.

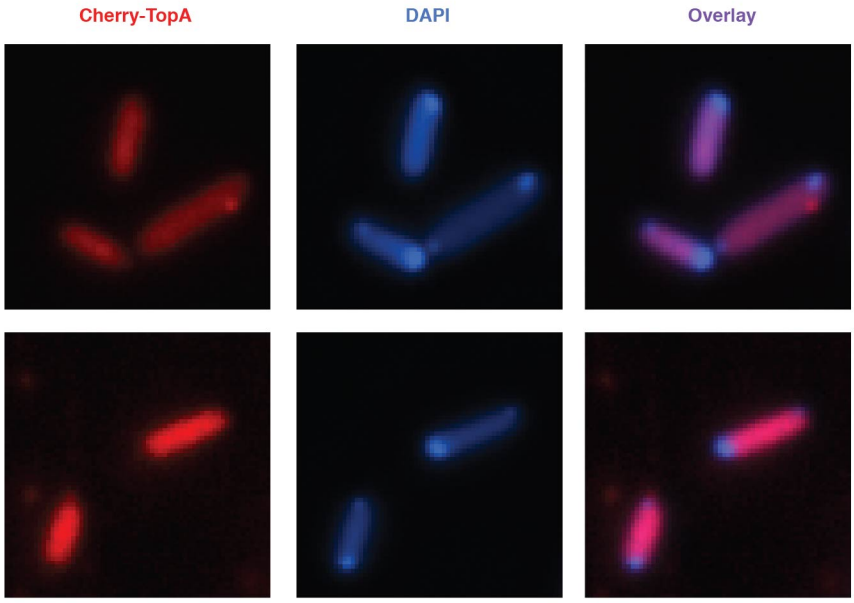

Figure 2.14: Observation of DAPI-stained phage DNA adjacent to a Cherry-TopA nascent shell. Live fluorescence imaging of *P. aeruginosa* strains engineered to express Cherry-TopA infected with ΦKZ. DAPI stain labels DNA. Microscopy was replicated three times with similar results.

Tables:

Table 2.1: ΦKZ and ΦKZ-like phages have no natural spacers matching their genomes from a natural collection of >4000 *P. aeruginosa* spacers.
The total number of Type I CRISPR spacers with a perfect match to the indicated P. aeruginosa phages assayed in this study and previous CRISPR-Cas studies. The experimental sensitivity of each phage to the indicated subtypes are shown. AcrIE3 and AcrIF1 are I-E and I-F anti-CRISPR proteins, respectively. * indicates that all spacers have mismatches (≤4) to the F8 genome.

Phage	# spacers	Type I CRISPR sensitivity	Reference
DMS3m	75	I-C: sensitive I-E: resistant (AcrIE3) I-F: sensitive	This study, ref. 3,8
JBD30	51	I-C: sensitive I-E: sensitive I-F: resistant (AcrIF1)	This study, ref. 2,3
JBD18	51	I-F: sensitive	Ref. 8
JBD25	46	I-F: sensitive	Ref. 8
JBD68	28	I-C: sensitive	This study
D3	49	I-C: sensitive	This study
F8	3*	I-C: sensitive	This study
ΦKZ	0	I-C: resistant I-F: resistant	This study
phiPA3	0	I-C: resistant	This study
PaBG	0	not assayed	
KTN4	0	not assayed	
PA7	0	not assayed	

Table 2.2. Phage and Strains

Name	Source	Reference
ΦKZ	Davidson Lab	[28]
ΦPA3	Agard Lab	[12]
DMS3m	O'Toole Lab	[8]
JBD30	Davidson Lab	[29]
F8	Davidson Lab	Unpublished Accession: DQ163917
D3	Davidson Lab	[30]
JBD68	Davidson Lab	[29]
	Genotype	**Reference**
F11	Wild-type isolate (Native I-C system)	Unpublished (Davidson Lab)
JW31	PAO1 tn7::I-C/Cas3^{PA}	This study
JB10	PAO1 tn7::cas9^{Spy}	This study
JB90	PAO1 tn7::cas12a^{Mb}	This study
SDM084	PAO1 tn7::cas13^{Lse}	This study
SDM020	PAO1 Δ*hsdR*	This study

Table 2.3. Plasmids

Name	Information	Ref.
pHERD30T	Arabinose inducible, gentamicin resistant shuttle vector	[31]
pUC18T-Lac	IPTG inducible, Amp^R/$Gent^R$, Tn7 integrative plasmid with FRT sites flanking gentamicin cassette	[32]
pTNS3	Expresses tnsABCD for flipping out cassette flanked by FRT sites	[33]
pBR62	Contains Spy Cas9 tracrRNA sequence	This study
pJW1	pHERD30T with BsaI site at pos. 235 GAGACC mutated to GTGACC	This study
pJW13	pJW1 with Type I-C pseudo-CRISPR array for spacer cloning	This study
pJB1	pJW1 with Type II-A sgRNA backbone at the +1 TSS of pBAD	This study
pJB2	pJW1 with Type V-A pseudo-CRISPR array for spacer cloning	This study
pSDM057	pJW1 with Type VI-A (LseCas13a) pseudo-CRISPR array for spacer cloning	This study
pSDM070	pJW1 with Type VI-A (LshCas13a) pseudo-CRISPR array for spacer cloning	This study
pSDM046	pHERD30T with ORF152-Cas9 Fusion	This study
pSDM051	pHERD30T with Cas9-ORF152	This study
pSDM160	pHERD30T with M.EcoRI-AmilCP	This study
pSDM161	pHERD30T with M.EcoRI-AmilCP;R.EcoRI	This study
pSDM164	pHERD30T with M.EcoRI-AmilCP;R.EcoRI-ORF152	This study
pSDM166	pHERD30T with M.EcoRI-AmilCP;R.EcoRI-sfCherry2-ORF152	This study
pSDM168	pHERD30T with M.EcoRI-AmilCP;R.EcoRI E111G-ORF152	This study
pSDM169	pHERD30T with M.EcoRI-AmilCP;R.EcoRI E111G-sfCherry-ORF152	This study
pSDM170	pHERD30T with M.EcoRI-AmilCP;R.EcoRI E111G-sfCherry2	This study
pSDM171	pHERD30T with M.EcoRI-AmilCP;R.EcoRI-sfCherry2	This study
pSG-IF-cas	IPTG inducible, $Carb^R$ pMMBHE plasmid with all Type I-F cas genes (cas1,cas3,csy1-4)	This study
pAB04	pHERD30T with Type I-F pseudo-CRISPR array for spacer cloning	This study
pSG30T-cherry	Expresses cherry from arabinose inducible pHERD30T vector	This study
pSG30T-cherry-cas3(IC)	Expresses cherry-tagged Cas3 (Type I-C) from arabinose inducible pHERD30T vector	This study
pSG30T-cherry-cas8(IC)	Expresses cherry-tagged Cas8 (Type I-C) from arabinose inducible pHERD30T vector	This study
pSG30T-cherry-cas3(IF)	Expresses cherry-tagged Cas3 (Type I-F) from arabinose inducible pHERD30T vector	This study
pSG30T-cherry-cas8(IF)	Expresses cherry-tagged Cas8 (Type I-C) from arabinose inducible pHERD30T vector	This study
pSG30T-cherry-TopA	Expresses cherry-tagged TopA (PA01) from arabinose inducible pHERD30T vector	This study
pESN28	Expresses cherry-Cas9	This study
pESN29	Expresses Cherry-Cas9-ORF152	This study
pESN32	Expresses Cherry-ORF152	This study
pESN34	Expresses cMyc-ORF152	This study

Table 2.4. Oligonucleotides, g-blocks, crRNAs

Name	Sequence	Notes
I-C_BsaI_for	gatccGTCGCGCCCCGCACGGGCGCGTGGATTGAAACgagac c*TCTCTGGACAAA*ggtctc GTCGCGCCCCGCACGGGCGCGTGGATTGAAACa	Underlined regions indicate location of BsaI sites
I-C_BsaI_rev	agcttGTTTCAATCCACGCGCCCGTGCGGGGCGCGACgagacc *TTTGTCCAGAGA*ggtctcGTTTCAATCCACGCGCCCGTGCGG GGCGCGACg	Underlined regions indicate location of BsaI sites
sgRNA scaffold sequence	ccatagagaccACGTACGTACggtctcAGTTTTAGAGCTAGAAATA GCAAGTTAAAATAAGGCTAGTCCGTTATCAACTTGAAAAAG TGGCACCGAGTCGGTGCTTTTTTT	Underlined regions indicate location of BsaI sites
p30T-gRNA_BsaI	ctctactgtttctccatccatagagaccacgtacgtacg	
p30T-gRNA_BsaI_rev	gcccaaaaaaacgggtccgggcaggataggtgaag	
gRNA_BsaI-p30T	atggagaaacagtagagagttgc	
gRNA_BsaI-p30T-rev	acccgttttttgggctag	
Cpf1_crRNA_top	catgaaatttctactgtttgtagatGgagaccTCTCTGGACAAAggtctcGaaat ttctactgtttgtagat	Underlined regions indicate location of BsaI sites
Cpf1_crRNA_bottom	agctatctacaaacagtagaaatttCgagaccTTTGTCCAGAGAggtctcCat ctacaaacagtagaaatt	Underlined regions indicate location of BsaI sites
tracrRNA-FOR	gaaattaatacgactcaactatagaaaacagcatagcaagttaaaata	For T7 RNAP in vitro rxn
tracrRNA-REV	aaaaaaagcacccgactcggtgccac	For T7 RNAP in vitro rxn
PTn7R	cacagcataactggactgaatttc	Ref. [32]
PglmS-down	gcacatcgggcgacgtgctctc	Ref. [32]
LseCas13a crRNA Top	catggggtaagagactacctctatatgaaagaggactaaaaccgagaccacgtacgt acggtctccggtaagagactacctctatatgaaagaggactaaaacg	Underlined regions indicate location of BsaI sites
LseCas13a crRNA Bottom	aattcgttttagtcctctttcatatagaggtagtctcttaccggagaccgtacgtacgtggtct ccggttttagtcctctttcatatagaggtagtctcttaccc	Underlined regions indicate location of BsaI sites
LshCas13a crRNA Top	catggggatttagaccaccccaatatcgaaggggactaaaaccgagaccacgtacgt acggtctccggatttagaccaccccaatatcgaaggggactaaaacg	Underlined regions indicate location of BsaI sites
LshCas13a crRNA Bottom	aattcgttttagtccccttcgatattggggtggtctaaatccggagaccgtacgtacgtggt ctcggttttagtccccttcgatattggggtggtctaaatccc	Underlined regions indicate location of BsaI sites
Alt-R CRISPR-Cas9 crRNA		
KZ (IV) – KasI	rArUrC rUrUrG rCrGrC rCrArG rArUrC rArCrG rUrGrG rUrUrU rUrArG rArGrC rUrArU rGrCrU	Pos. 183,270
KZ (IV) – 1	rGrArArUrCrUrGrCrUrArArUrArArGrGrU rUrCrArGrUrUrUrUrArGrArGrCrUrArUrGrC rU	Pos. 158,649
KZ (IV) – 2	rUrCrArCrCrArCrGrCrArUrUrArCrArUr rCrArGrGrUrUrUrUrArGrArGrCrUrArUrGrC rU	Pos. 168,715
DMS3m (IV) - 1	rGrCrC rGrArC rArUrU rUrUrC rCrArG rUrUrG rGrCrG rUrUrU rUrArG rArGrC rUrArU rGrCrU	Pos. 17,751
DMS3m (IV) - 2	rUrCrA rCrGrA rCrGrA rCrCrC rArGrA rArGrC rGrUrG rUrUrU rUrArG rArGrC rUrArU rGrCrU	Pos. 28,033
Fusion primers		
prESN80	CTAAAGCAAAAGCTtaaAAGCTTGGCACTGGCCG	Cherry-Cas9-ORF152
prESN81	AGCCACCGCCACCgtcacctcctagctgactcaaatcaat	
prESN82	ctaggaggtgacGGTGGCGGTGGC	
prESN83	AGTGCCAAGCTTttaAGCTTTTGCTTTAGCTAGTTCAAGAG	
prESN74	tgagtcagctaggaggtgactaaAAGCTTGGCACTGGCC	Cherry-Cas9
prESN75	attgagtatttcttatccatTTTTTGGCTGCCTCCTGC	

Name	Sequence	Notes
prESN76	CTGCAGGAGGCAGCCAAAAAatggataagaaatactcaataggcttagatatcgg	
prESN77	CGGCCAGTGCCAAGCTTttagtcacctcctagctgactcaaatcaatgcgt	
prESN91	ATGTTTGGTAAACATTTCGAACGTCCA	
prESN92	TTTTTGGCTGCCTCCTGCAG	
prESN153	AGACCTGGGTGGCGGTGGCTCG	cMyc-ORF152
prESN154	TCTTCGCTAATCAGTTTCTGTTCCATAGAGCTCGAATTCTTATCAG	
F-30T-sfCh_P29	tacccatgggatctgataagaattcgagctATGGAGGAGGACAACATGGCC	pSG30T-cherry
R-csy1-link-sfCh(TAA-)_P30	GTAGGCGTTGGGAGGGGAGAGGTggctccaccgcctccGCCGCCGGTGCTGTGTCTGGC	
F-link-csy1 (ATG-)_P31	ggaggcggtggagccACCTCTCCCCTCCCAACGCCTAC	
R-30T-csy1_P32	gacggccagtgccaagcttgcatgcctgcaTCAGTCACGCTCATCTTCGAG	
F-30T-sfCh_P29	tacccatgggatctgataagaattcgagctATGGAGGAGGACAACATGGCC	pSG30T-cherry-cas3(IC)
R-Cas3(IC)-link-chry_P101	TGAGTATCGCTAGCCTCCGCGTCggctccaccgcctccGCCGCCGGTGCTGTGTCTGG	
F-link-Cas3(IC)_P102	ggaggcggtggagccGACGCGGAGGCTAGCGATACTCA	
R-30T-Cas3(IC)_P103	gacggccagtgccaagcttgcatgcctgcaCTACCAACATAGCCGCTCGC	
F-30T-sfCh_P29	tacccatgggatctgataagaattcgagctATGGAGGAGGACAACATGGCC	pSG30T-cherry-cas8(IC)
R-Cas8c-link-Cherry_P104	TAGTCATTGAGGGCCGAAAGGATggctccaccgcctccGCCGCCGGTGCTGTGTCTGG	
F-link-Cas8c_P105	ggaggcggtggagccATCCTTTCGGCCCTCAATGACTA	
R-30T-Cas8c_P106	gacggccagtgccaagcttgcatgcctgcaTTACTCGACGGAATCGGGGC	
F-30T-sfCh_P29	tacccatgggatctgataagaattcgagctATGGAGGAGGACAACATGGCC	pSG30T-cherry-cas3(IF)
R-csy1-link-sfCh(TAA-)_P30	GTAGGCGTTGGGAGGGGAGAGGTggctccaccgcctccGCCGCCGGTGCTGTGTCTGGC	
F-link-csy1 (ATG-)_P31	ggaggcggtggagccACCTCTCCCCTCCCAACGCCTAC	
R-30T-csy1_P32	gacggccagtgccaagcttgcatgcctgcaTCAGTCACGCTCATCTTCGAG	
F-30T-sfCh_P29	tacccatgggatctgataagaattcgagctATGGAGGAGGACAACATGGCC	pSG30T-cherry-cas8(IF)
R-cas3 (ATG-)-link-sfCh_P42	CATTGCGACACCAGCAGGATGTTggctccaccgcctccGCCGCCGGTGCTGTGTCTGG	
F-link-cas3_P43	ggaggcggtggagccAACATCCTGCTGGTGTCGCAATG	
R-30T-cas3_P44	gacggccagtgccaagcttgcatgcctgcaTCAGTTGTATTTCTTGAACC	
F-30T-sfCh_P29	tacccatgggatctgataagaattcgagctATGGAGGAGGACAACATGGCC	pSG30T-cherry-TopA
R-topA-link-ch_P107	TCCACGATGACCAGCGATTTACCggctccaccgcctccGCCGCCGGTGCTGTGTCTGG	
F-link-topA_P108	ggaggcggtggagccGGTAAATCGCTGGTCATCGTGGA	
R-30T-topA_P109	gacggccagtgccaagcttgcatgcctgcatcaGCGCTTGTCTTCGACCTTC	
M.EcoRI-AmilCP_fwd	CTGATAAGAGGAGGACAGCTATGGCCGGCGCACGCAAC	pSDM160
M.EcoRI-AmilCP_rev	TAA AAC GAC GGC CAG TGC CAT TAA CCG GTG GCG ACC ACA GG	
M.EcoRI-AmilCP;R.EcoRI-rev	TAAAACGACGGCCAGTGCCATTAACCGGTTTTGCTAGTCAGCTGCTC	pSDM161

Name	Sequence	Notes
M.EcoRI-AmilCP;R.EcoRI-rev	TAAAACGACGGCCAGTGCCATTAACCGGTTTTGCTAGTCAGCTGCTC	pSDM164
ORF152_fwd	GGTGGCGGTGGCTCGATGTTTGGTAAACATTTCGAAC	
ORF152_rev	TAAAACGACGGCCAGTGCCATTAAGCTTTTGCTTTAGCTAG	
GGS(2)-sfCherry2_fwd	GGCGGGTCGGGCGGCTCGATGGAGGAGGACAACATG	pSDM166
sfCherry2_rev	TGGGTTTCATGCCGCCGGTGCTGTGTCT	
EcoRI-mut Rev	ctggtgctttgctccggcaactaac	pSDM168, pSDM169, pSDM170
EcoRI-mut Fwd	gttagttgccggagcaaagcaccag	
GS-Cas9 F	GGTGGCGGTGGCTCGatggataagaaatactcaataggc	pSDM046
Cas9-p30T R2	ccagtgccaagcttgcatgcctgcaTTAGTCACCTCCTAGCTGACTC	
pHERD30T-ORF152 F	GGGATCTGATAAGAATTCGAGCTatgtttggtaaacatttcgaacg	
ORF152-GS R	CGAGCCACCGCCACCagcttttgctttagctagttc	
p30T-Cas9 F2	atgggatctgataagaattcgagctATGGATAAGAAATACTCAATAGGC	pSDM051
Cas9-p30T R2	ccagtgccaagcttgcatgcctgcaTTAGTCACCTCCTAGCTGACTC	

Table 2.5. Spacer sequences

Phage (Type, #)	Sequence
JBD30 (I-C)	AACCTCGCGGCATCCGCAACAACAACCCCGGCAA
D3 (I-C)	ACGATTGCGGACATGGCAGGCTGCCGCTGCTGGA
F8 (I-C)	GCCAATCGGCCGATAGATGAAGCTGTGGAGGGTC
JBD68 (I-C)	AGCGGCGTGAGGTTGGACCTTGCTGCCGACCATT
ΦKZ (I-C, #1)	TGGACTAACAAATACGCCTATATATTCCGATCCT
ΦKZ (I-C, #2)	GAACTTGTATTTAACCCAAAGGTTTTTAAATGGT
ΦKZ (I-C, #3)	CCCATTTATTATTTTCTTTATTTATCCAACCGTA
ΦKZ (I-C, #4)	TAAAAAGAAAATTATATAAATAGTATATTATGTG
ΦKZ (I-C, #5)	TTTACATTCTTCTAAACTAATATTTAATTCATCT
ΦKZ (I-C, #6)	CATTATCATCTACCTCTTTTAATTTATCTTTAAT
ΦKZ (I-C, #7)	CAAAAGGATTATTTGATGTTGTGGTGAAAGAAAA
ΦKZ (I-C, #8)	GCCATTTTCTTTCACCACAACATCAAATAATCCT
ΦKZ (I-C, #9)	AGATAATGGGGATATTTTGTATTTTGATAACAAG
ΦKZ (I-C, #10)	TACTGGTACCCATAGAAGTTATATTTTACCAGCT
ΦKZ (I-C, #11)	ATTGAAATCAAGTAAAATCTCAAATGGAATCTGT
JBD30 (II-A)	GGCATCCGCAACAACAACCC
ΦKZ (II-A, #1)	GAATCTGCTAATAAGGTTCA
ΦKZ (II-A, #2)	TCACCACGCATTACATCAGG
ΦKZ (II-A, #3)	AAATTATATTAATCACAATG
ΦKZ (II-A, #4)	ATATATTCCGATCCTTATCC
ΦKZ (II-A, #5)	AAACATCCTCATGATAACCA
ΦKZ (II-A, #6)	AGCAGTAGCTTGAGTTTGAA
ΦKZ (II-A, #7)	TTTTAGATGAAGTAAAAAAG
ΦKZ (II-A, #8)	CTATTACCATTTTCGTCAAT
ΦKZ (II-A, #9)	CTCATTTTTTATTCCTACGT
ΦKZ (II-A, #10)	AGAGAACTGTTTAAACACAA
JBD30 (V-A, #1)	CGTTTTACCCACTGAGCGAACGC
JBD30 (V-A, #2)	GCCCGTTTCGATACCGCACATA
JBD30 (V-A, #3)	TACCGCGCCGCCCTTCTGGAGGA
JBD30 (V-A, #4)	AAGGTGCCGCACGGTGTCCCAGT
JBD30 (V-A, #5)	CGCATGACTCTCTATATGGGGCC
ΦKZ (V-A, #1)	GAATCTGCTAATAAGGTTCATGG
ΦKZ (V-A, #2)	AATAGGAATATAGCTATGCTAAT
ΦKZ (V-A, #3)	TGTGTCTCTTTTCCAAATGCTTT
ΦKZ (V-A, #4)	GGGATTCAACTATTGGAAAAGCA
ΦKZ (V-A, #5)	GCTAGTTGTTCATCAAATGATGA
ΦKZ (V-A, #6)	CTCATTAATAACAGATACTTTGT
ΦKZ (V-A, #7)	CTGGGCATTAATGACGATATATC
ΦKZ (V-A, #8)	TTACAGCCTCGTCAGACAGGTAA
ΦKZ (V-A, #9)	CCTAATGCATTCCATTTAAATAC
PAO1 (VI-A, #1)	TCAAATTACGCGCAGCAGCAAGAT
PAO1 (VI-A, #2)	CGGCCTGCAGGATGGCCTTGGTCA
JBD30 (VI-A, #1)	GCGGCCAGCCCGGCCCCTCGTCCA
JBD30 (VI-A, #2)	GGCGCGTTGATGCGGACCTGGCCA
JBD30 (VI-A, #3)	AATGCCCTTCTCCCGGCAAACCGT
JBD30 (VI-A, #4)	TACCCGCAAGTTGTTGAGGGCTGA
JBD30 (VI-A, #5)	GGTGCCGGCCGGCTTGATGCCCAT
ΦKZ (VI-A, #1)	GCAGGAGCAGTAGCTTGAGTTTGA
ΦKZ (VI-A, #2)	TCATTAGTTTCAACCCAGTATGAA
ΦKZ (VI-A, #3)	ACATAATCTTCAAATGCAGAAGCC
ΦKZ (VI-A, #4)	AACCAGCACCACCACAAAAGTAAA
ΦKZ (VI-A, #5)	AGAATTACTAGTGCATTTAGTACT
ΦKZ (VI-A, #6)	AACGATGTAAGGAGTGAACTGCGG
ΦKZ (VI-A, #7)	TAACAGCTTGTAGATAATAACCAG
ΦKZ (VI-A, #8)	GTCTGCAATAGTCTTCGGATTATT
ΦKZ (VI-A, #9)	AGGTTAGCATTGGAGTTACCCATT
ΦKZ (VI-A, #10)	CAGCACCTTTGGAAACTACCCAAT

Phage (Type, #)	Sequence
ΦKZ (VI-A, #11)	GCTTCCATAGTAACTAAGTATGCT
ΦPA3 (II-A, #1)	TCGTATGTCTCGTGCATCTT
ΦPA3 (II-A, #2)	ATGTGTAAAGTTCTCTGATG
ΦPA3 (II-A, #3)	CTCCCACTTATTCCATCTCA
ΦPA3 (II-A, #4)	GCTGTACCAGTCCACTTGTC
ΦPA3 (II-A, #5)	CTCACTCATTAGACAAGTTT
DMS3 (I-F)	AACGGCCGACGCTTCTGGGTCGTCGTGAAAGT
ΦKZ (I-F, #1)	GGCATTATGAAGTGGACCTAATGTATCAATAA
ΦKZ (I-F, #2)	GATGGCTACCATCATTAATACTCTTAAGACTT
ΦKZ (I-F, #3)	AGGAATTGATGATGACATTAAAGTAATTGATT
ΦKZ (I-F, #4)	ATTCTACTAATAAATGCCGGTGACAGAAATTA
ΦKZ (I-F, #5)	TCGTGGATTAAGTGATAGTGGATATTTACAAT

Chapter 3: Heat-induced inactivation of immunity across bacteria

Introduction

Many examples of variation in restriction-modification activity in bacteria have been reported with some commonalities and differences between them. In 1965, Holloway BW reported that *Pseudomonas aeruginosa* strain PA1 grown at 43 °C (rather than 37 °C) becomes permissive of plaquing by bacteriophage B3, which is typically restricted by PA1. Interestingly, this induced ability of phage to replicate on PA1 was inherited for greater than 60 generations but decayed fully after ~70 generations[1]. This experiment also demonstrated that the susceptible state could again be induced after recovery by a subsequent incubation at 43 °C. During this time and since, similar phenotypes were reported in other bacterial species, including *E. coli*[2], *Salmonella spp.*[3,4], and *L. lactis*[5]. All of these examples concern loss of R-M immunity, as they acquire permissiveness to phages that are usually restricted. Despite their similarities, there are some important differences among these reports. In these other examples a relatively brief (1 min. – 60 min.) heat treatment (40 – 50 °C) is sufficient for inactivation of restriction, in contrast to *P. aeruginosa's* inactivation of restriction requires a comparatively long incubation during bacterial replication at ≥ 42 °C for full inactivation [Fig. 3.4, Fig. 3.6]. Additionally, all of these restriction-inactive states recover much more quickly than in *P. aeruginosa*, within 10 – 60 minutes. Despite these reports that bacteria become permissive to phages after exposure to heat, no investigation to my knowledge has studied the mechanism of these phenomena.

The inactivated antiphage immune system in *P. aeruginosa* was not identified, though Holloway's results are typical of an R-M system[1]. *P.* aeruginosa strain PAO1was recently shown to encode a functional type I R-M system[6]. This R-M system was shown by PacBio sequencing to methylate the N_6 position of the adenosine residues on both strands of the GATCN_6GTC sequence motif globally in the PAO1 genome[6]. This genomic modification was dependent on the putative *hsdS* and *hsdM* genes, which were bioinformatically predicted by their homology to

known *hsdS* and *hsdM* genes. The focus of this study was global methylation of PAO1's genome and methylation's effect on the transcriptome, so the restriction activity of the *hsdR* gene was not convincingly tested. Regardless, PAO1's type I R-M system is an attractive candidate for a target of heat-induced inactivation of antiphage immunity.

The best-characterized post-translational regulatory pathway for type I R-M is restriction alleviation (RA), which regulates *E. coli* K-12's EcoKI[7]. Following DNA damage, the restriction activity of *E. coli* is reduced but not eliminated. This decrease in restriction activity depends on HsdR's translocation along DNA[8]. After DNA damage, ClpXP is specifically recruited to HsdR subunits translocating on the bacterial chromosome. ClpXP then proteolytically degrades the EcoKI HsdR subunits, while sparing the HsdS and HsdM subunits. This process leads to an increase in the ratio of MTase complexes to endonuclease complexes, allowing the methylation of any chromosomal unmethylated restriction sites that were created during DNA damage and its repair. Stimuli that induce the RA phenotype include chemical and radiation-based means of DNA damage[7]. Importantly, EcoKI's decrease in restriction activity recovers within ~10 generations. The inducing stimuli, incomplete inactivation, and quick recovery distinguish RA from the inactivation of restriction in *P. aeruginosa* studied here.

The considerable list of stress-inactivated immune systems betrays the importance of tight regulation of nucleolytic enzymes. The best studied bacterial immune systems, including R-M and CRISPR-Cas, function via nucleolytic cleavage of nucleic acids, which poses a significant threat of creating double stranded-breaks (DSBs) in the host chromosome. DSBs are immensely toxic to bacterial cells and harboring nucleases that can cleave the chromosome represents a fitness cost that is balanced by their immune activities against phages and ameliorated by ways to prevent autoimmunity. As exemplified by RA, the principal concern of inactivating an immune pathway is the prevention of lethal autoimmunity. While DNA damage clearly is able to create unmethylated substrates for cleavage in the chromosome, it is less obvious how bacterial growth at high temperatures necessitates inactivation of immune systems.

Heat shock treatments are typically brief exposures to a high temperature, greater than 42 °C. During this time, many proteins are denatured by heat and to survive this stressful event, cells enact a heat shock response. The heat shock response is mediated by σ factors which transcriptionally activate specific genes, including proteases and chaperones, which clear or refold misfolded and denatured proteins[9].

An exciting and growing field of research is the existence and function of prions and other heritable protein aggregates in bacterial cells[10]. Though first reported in metazoans as the causative agent of spongiform encephalopathies, prions have since been discovered in yeast and more recently in bacteria[11–13]. Although prions were first associated with disease, they are now understood to often serve adaptive functions. For example, yeast acquire different traits after entering the prion trait that could enable survival in challenging environments[14,15]. Bacterial prions include the transcription terminator rho and single-stranded DNA binding-protein (SSB)[16]. These prions were discovered by HMMs trained on known prion forming domains (PrD). Their inheritance persists for ≥ 120 generations[10]. Functional impacts of prion formation in bacteria remain unclear.

Results

Inactivation of restriction

To determine whether Holloway's results hold true in our strains, some of his experiments have been replicated. First, I confirmed that our model *P. aeruginosa* strain, PAO1, loses its restriction activity against phage JBD30 after growth at 43 °C (Fig. 3.1). I also confirmed that PAO1 exhibited immunity against JBD30 grown on strain PA14 (JBD30·PA14) but not JBD30·PAO1, which is stereotypical of R-M systems (Fig 3.1). This phenomenon was named **i**nactivation of **R**estriction **EN**donuclease (iREN), as it inactivates restriction. To identify the genes inhibited by iREN, I listed the known immune systems in PAO1. PAO1 only encodes 1 R-M system, a type I R-M system which is encoded by genes PA2732, PA2734, and PA2735 (Fig. 3.9). These genes were excellent candidates for inhibition during iREN so I used CRISPR-Cas9 to knockout the *hsdR* gene, PA2732 (Fig. 3.9). The resulting strain lost restriction activity against JBD30·PA14, which had an identical efficiency of plating (EOP) as on iREN PAO1 (Fig. 3.1).

Loss of methylation

The effect of bacterial growth at 43 °C on HsdM's MTase activity was investigated by propagation of JBD30·PAO1 on naïve and iREN PAO1. I then performed a plaque assay using JBD30·PAO1(naïve) and JBD30·PAO1(iREN) on naïve PAO1. In this experiment, the ability of naïve PAO1 to restrict JBD30·PAO1(iREN) indicates the degree to which JBD30 was protectively methylated by iREN PAO1. This experiment showed a mild inhibition of methylation activity in iREN PAO1 relative to naïve PAO1 (Fig. 3.2). Interestingly, the degree of this effect is variable per experiment and ranges from complete inactivation, as seen in the following memory experiment, to a partial loss of protection against restriction.

Memory and reversibility

To test whether Holloway's observation of iREN's long memory could be replicated in PAO1, I performed a similar experiment. In short, I inactivated restriction in WT PAO1 by growth at 43 °C. I then took several time points in which I measured bacterial replication, restriction of JBD30·PA14, modification of JBD30·PAO1, and prepared dilutions into fresh media. The resulting bacterial dilution was incubated at 37 °C until late log phase, at which point a time point was taken. Once restriction fully recovered, the final incubation was performed at 43 °C.

This experiment revealed that restriction recovers gradually during bacterial replication at 37 °C (Fig. 3.3). The recovery of restriction can be described by the function:

$$log(1/EOP) = 0.03504 \times generations - 0.03504 \qquad (R^2 = 0.9669,\ P = 0.0004)$$

By about 60 generations, JBD30·PA14's EOP decreased to ~10^{-1}, compared to ~10^{-3} in naïve cells. By ~100 generations, restriction had fully recovered. After this complete recovery of restriction, a second round of bacterial growth at 43 °C once again fully inactivated restriction. MTase activity was completely ablated at first (in contrast to other experiments, which only partially inactivated methylation). However, this defect in MTase activity was not inherited very long and MTase activity fully recovered between 14 and 35 generations. The long persistence of iREN demonstrates that it is inherited during bacterial replication.

Induction Kinetics

To determine the requirements for inactivation of restriction, I tested various conditions during growth of PAO1 for an effect on restriction activity. First, I investigated the amount of time and bacterial replication required at 43 °C to fully inactivate restriction. In short, I incubated PAO1 at 43 °C for varying amounts of time, after which I completed their growth to saturation at 37 °C so all cultures were tested by phage at the same MOI. Saturated cultures were used in a plaque assay to determine restriction strength. This experiment demonstrated that restriction activity remained active even when incubated at 43 °C until PAO1 reached early log phase (Fig. 3.4).

Once at early log phase, PAO1's restriction decreased rapidly, but with intermediate states of activity. The optical density at which inactivation was complete suggests that at least 5 doublings had elapsed. This corresponds to ~5 hours at 43 °C.

An inverse induction time course experiment was conducted in which cultures were first grown at 37 °C and then shifted to 43 °C and allowed to grow to saturation. As seen in the previous experiment, cultures that are grown at 43 °C during lag and early log phase fully inactivate restriction. Surprisingly, cultures grown at 43 °C starting during mid-log only partially inactivated restriction (Fig. 3.5). This suggests that restriction can only be fully inactivated during a particular window of bacterial physiological states during bacterial replication.

Induction Temperature

Additionally, I tested the temperatures at which iREN is induced by growing PAO1 in liquid culture at various temperatures and testing restriction activity by plaque assay. I noted that 42 and 43 °C grown cultures were indistinguishable in their level of restriction (Fig. 3.6). I again saw intermediate phenotypes for certain temperatures. A large inflection point was noted at 40.5 °C.

Induction Growth Conditions

An interesting feature of iREN is that restriction is only inactivated when PAO1 is grown in liquid culture. Streaking PAO1 on nutrient agar plates and then incubating the plates at 43 °C overnight does not yield iREN colonies (data not shown). However, static cultures incubated long enough to reach high optical density do inactivate restriction completely (data not shown).

Inducing stresses and stimuli

Considering that RA in *E. coli* is activated by DNA damage, I tested other stressful stimuli in bacterial growth to test whether they would also inhibit restriction in PAO1. PAO1 was treated with 10,000 J of UV irradiation, which did not inactivate restriction (data not shown). However,

this dose of radiation did not lead to a decrease in the viability of cells (data not shown). Additionally, I tested up to 0.2 ug/mL mitomycin C, which did not inhibit restriction (data not shown). This result suggests a difference between RA, which is caused by DNA damage and iREN, which requires bacterial growth during early log phase at 42 °C or above in a liquid culture (Fig. 3.4, Fig. 3.6).

Comparative Genomics

Different *P. aeruginosa* strains were tested for the iREN phenomenon. Best understood are the PAK and PA14 strains. PAK encodes 2 type I R-M systems, which are each different from PAO1's, in its genome and exhibits a strong restriction phenotype against phages. When grown in liquid culture at 43 °C with shaking overnight, PAK loses this restriction activity, as measured by plaque assays (Fig. 3.7). The induction requirements and memory were not tested in this strain. Another well-known strain is PA14. This strain does not encode a type I R-M system, but it does encode a type II R-M system. When tested for iREN, as PAK and PAO1 have been, this strain did not lose immune activity against the tested phages (Fig. 3.7). A long list of other *P. aeruginosa* strains was tested, predominantly including clinical and environmental isolates. Many of these strains were not sequenced beforehand, so no prediction for immunity genes could be made. The ability of phage JBD30 propagated strains PAO1, PA14, and PAK to plaque on these strains was measured and the differential between EOP after growth at 43 and 37 °C was determined. In total, including PAO1 and PAK, ~50 % of tested *P. aeruginosa* strains exhibit greater plaquing efficiency of phages after growth at 43 °C rather than 37 °C (Table 3.1).

Some of these strains were subsequently sequenced. BLAST searches of the strains' contigs using different *hsd* genes from *E. coli* K-12, PAO1, and PAK revealed that most strains with immune activity encode a type I R-M system. Of the strains that encode type I R-M most exhibit iREN. Interestingly, one strain, A7, featured an improvement in phage plaquing after growth at 43 °C, even though no type I R-M system was detected by BLAST (Table 3.1).

Electroporation Efficiency

The electrocompetence of PAO1 is notably improved after growth at 43 °C. To determine whether this was due to inactivation of type I restriction, I quantified electrocompetence of the PAO1 *ΔhsdR* strain using a pHERD30T plasmid with 1 GATCN$_6$GTC site (Fig. 3.8). This strain had about 2-fold higher electroporation efficiency in comparison to the WT strain. When the same strain was grown at 43 °C instead of 37 °C, its electrocompetence improved much further, at least by a factor of 10. This demonstrates that the improvement of electrocompetence after growth at 43 °C only is only partially accounted for by the inactivation of type I restriction.

***hsdR* knockout**

Preliminary bioinformatic analyses of PAO1's genome identified only the type I R-M system encoded by genes PA2732, PA2734, and PA2735 as an immune system. Doberenz *et al.* first discovered this immune system[6]. By a gene knockout, they tested the *hsdM* gene's effect on methylation globally across the PAO1 genome. However, they did not demonstrate nuclease activity by *hsdR*. In order to test whether the *hsdR* gene imparts restriction activity to PAO1 and whether this restriction activity is the target of iREN, I deleted the gene using CRISPR-Cas9 and I deleted the *hsd* locus CRISPR-Cas3 (Fig. 3.9).

PAO1 *ΔhsdR* made using CRISPR-Cas9 completely lost restriction activity against phage JBD30·PA14 (Fig. 3.1). Restriction activity was complemented by expression of either HsdR or HsdSMR from a plasmid (Fig. 3.10). Expression of the Hsd proteins from either of these plasmids led to stronger restriction than WT PAO1 and even enabled restriction against JBD30·PAO1, which is protectively methylated. These results demonstrate that PAO1's *hsdR* imparts restriction activity against phages. The EOP of JBD30·PA14 on PAO1 *ΔhsdR* was identical to that on iREN WT PAO1. This demonstrates that during iREN, PAO1's *hsdR*-dependent restriction activity is completely ablated. Attempts to complement restriction during iREN by plasmid-based of

expression of the HsdR protein yielded unexpected results. When HsdR was overexpressed during iREN, PAO1 experienced high toxicity but this was not the case for naïve PAO1 (Fig. 3.10). This toxicity caused by HsdR's overexpression during iREN was not only true for PAO1 *ΔhsdR* but also for WT PAO1. Toxicity was not seen when HsdSMR were overexpressed in iREN cells (data not shown).

Deletion of the entire *hsd* locus was done using the type I-C CRISPR-Cas3 system instead because Cas3's processivity enables large deletions[17]. The resulting strain, named PAO1 *ΔhsdSMR* was confirmed to have lost all restriction activity by plaque assay (data not shown). Additionally, modification activity was tested by propagating JBD30·PAO1 on PAO1 *ΔhsdSMR* and then testing whether the JBD30·PAO1 *ΔhsdSMR* phage was resistant or sensitive to restriction by naïve, WT PAO1. JBD30·PAO1 *ΔhsdSMR* was completely sensitive to restriction and was therefore unmodified, confirming that PAO1 *ΔhsdSMR* had also lost its *hsd* MTase activity (data not shown).

RT-qPCR

In order to determine whether the *hsd* transcripts are present during iREN, a quantitative reverse transcription PCR (RT-qPCR) experiment was performed using primers against the *hsdSM* transcript and the *hsdR* transcript. This experiment revealed that the *hsdR* transcript is less abundant than the *hsdSM* transcript. Both transcripts were equally abundant during naïve and iREN states (Fig. 3.11). Therefore, iREN is not mediated by transcriptional repression of any of the *hsd* genes or by post-transcriptional degradation of the *hsd* transcripts.

RNA-Seq

To test for any transcriptional shifts globally, which may reveal upstream effectors of iREN, I performed an RNA sequencing (RNA-Seq) experiment using the same DNA-free total RNA as was used in the RT-qPCR experiment. The RNA-Seq experiment did not identify any statistically

significant changes in transcript levels between iREN and naïve samples (Fig. 3.12). A small list of genes was compiled that did not have statistically significant fold-changes but had the largest differential between conditions (Table 3.2). Depleted transcripts included the pyochelin operon and the rRNA loci's spacer tRNAs. Enriched transcripts included several different genes with no consistent pattern such as genomic location or predicted function.

Spacer tRNAs that decode rare alanine and isoleucine codons were found in all 4 of PAO1's rRNA-encoding loci between the 16S and 23S genes. All 4 of these spacer tRNAs were depleted during iREN. I hypothesized that their depletion may lead to a global translational change that causes loss of restriction. To test this, I generated PAO1 strains that express these spacer tRNAs from an inducible promoter. These strains were incubated at 37 and 43 °C with induction and their restriction activity was measured by plaque assay. This experiment revealed that restriction was fully inactivated at 43 °C even with overexpression of the spacer tRNAs, which rules out depletion of these tRNAs as a necessary factor for inactivation of restriction (Fig. 3.12).

All transcripts from the pyochelin operon were depleted in the iREN state. A previously engineered CRISPR-Cas3 large deletion strain of PAO1 had a partial deletion of the pyochelin operon. To test whether inhibition of this pathway can cause iREN, this strain was grown in LB at 37 and 43 °C and their restriction was then tested by plaque assay. Restriction was still inactivated by growth at 43 °C, ruling out the pyochelin operon as being involved in iREN (data not shown).

Western Blots

Custom antibodies against the Hsd proteins HsdS (2), HsdM (2), and HsdR (3) were ordered from GenScript®. GenScript® identified several polypeptides as candidate antigens to raise antibodies in rabbits (Table 3.6). I used these antibodies to perform Western blots of PAO1 strains of varying genetic backgrounds and iREN states.

Using antibodies against HsdS and HsdM, I identified bands of the expected migration for HsdS and HsdM in PAO1, though the antibodies varied in specificity, and some blots showed

nonspecific bands (Fig. 3.13). Using antibodies against HsdR, no bands of the expected migration were detected and all visible bands were also detected in the PAO1 *ΔhsdR* genetic background. To test whether this was due to HsdR's low expression, I performed Western blots using PAO1 *ΔhsdR* containing either an empty vector or a plasmid expressing HsdR. These strains were grown only at 37 °C, as overexpression of HsdR during iREN is toxic. Antibiotic selection and maximal induction were maintained throughout the entire experiment. This Western blot revealed strong, crisp bands of the expected migration in the total lysate and the pellet fractions but not in the soluble lysate fraction. This suggests that HsdR may be expressed at very low levels in its native context and that it is not soluble in the lysis conditions used here.

Cherry Fusions

To test whether the HsdR protein is translated during iREN, the HsdR protein was tagged with the fluorescent protein sfCherry2 (Fig. 3.9). First, sfCherry2 was fused to either the N-terminus or the C-terminus of the HsdR protein by by PCR and Gibson assembly into an inducible expression vector. These plasmids were electroporated into PAO1 *ΔhsdR*. Though p30T::sfCherry2-*hsdR* and p30T::*hsdR* were efficiently electroporated, p30T::*hsdR*-sfCherry2 was not electroporated at all (data not shown). This toxicity suggests that the C-terminal fusion protein is lethal in PAO1, though it was not lethal in the *E. coli* strain used for cloning. The sfCherry2-*hsdR* fusion protein enabled potent restriction activity and was toxic to PAO1 during iREN when overexpressed, as seen before with overexpression of HsdR during iREN (Fig. 3.10). Because this fusion protein retained restriction activity, I prepared an N-terminal fusion of sfCherry2 to *hsdR* in the genomic locus of PAO1.

To tag the genomic copy of *hsdR* with sfCherry in PAO1, I used the type I-C CRISPR-Cas3 system along with a recombination template. The resulting PAO1 sfCherry2-*hsdR* strain was used in perform plaque assays, which revealed that it retained restriction activity after growth at 37 °C (Fig. 3.14). When grown at 43 °C, the culture fully lost restriction activity, as WT PAO1.

Additionally, the culture was washed once in minimal media to reduce background fluorescence and the fluorescence was quantified and normalized by the optical density of the strain. Normalized fluorescence revealed that despite PAO1 sfCherry2-*hsdR* grown at 43 °C losing restriction activity, it was equally fluorescent to the naïve PAO1 sfCherry2-*hsdR*. This result suggests that the HsdR protein is translated during iREN.

Microscopy

The PAO1 sfCherry2-*hsdR* strain grown at both 37 and 43 °C was prepared in fresh media and imaged by fluorescence microscopy. This strain, when grown at 37 °C, exhibited diffuse fluorescence in sfCherry's corresponding fluorescence channel (Fig. 3.15). However, PAO1 sfCherry2-*hsdR* grown at 43 °C commonly displayed puncta of red fluorescence. This result suggests that iREN may occur by aggregation of the HsdR protein. Because this experiment was performed few times, it must be replicated.

Discussion

The **i**nactivation of **R**estriction **EN**donuclease in *P. aeruginosa* is a fascinating phenomenon due to its long memory and the question of what advantage inactivating a potent immune system could serve. In addition, investigating its mechanism may reveal novel means of genetic regulation. To deepen our understanding of iREN, I have characterized the requirements for inactivation of restriction. Additionally, I have systematically probed the different stages of the central dogma to identify the stage at which HsdR's restriction activity is ablated (Fig. 3.16).

iREN presents an exciting opportunity to test an uncharacterized regulatory pathway that may feature a novel molecular mechanism. Based solely on the observation that PAO1 grown at 43 °C loses restriction activity, it appears possible that heat simply leads to denaturing of the Hsd proteins (Figure 3.1). However, as seen in the induction time course, heat alone is insufficient to inactivate restriction (Figure 3.4). This strongly argues against denaturation as the means of inhibition. Additionally, iREN's long memory suggests that restriction-inactivation is an actively regulated process rather than a transient consequence of protein denaturation (Figure 3.3).

The experiments testing the requirements for inactivation of restriction demonstrate that iREN requires a relatively long incubation at ≥ 42 °C for complete inactivation of restriction (Fig. 3.4, Fig. 3.6), in comparison to the brief heat shocks that inactivate restriction in other organisms[2,3,5]. Heat shock treatments, comprising 43 °C incubation for up to 30 minutes, are insufficient for inactivation of restriction in PAO1 (data not shown), differentiating this phenomenon from the heat shock response. The inactivation time course suggests that inactivation may require bacterial replication, as restriction only decreased after the onset of log phase (Fig. 3.4). Though the experiment probing different incubation temperatures was only performed with n = 1 and was performed across multiple days in different incubators, the result suggests that iREN depends on a sensitive molecular thermometer (Fig. 3.6). Incubation at 43 °C on solid media did not inactivation restriction, despite many rounds of bacterial replication being necessary to form a macroscopic colony (data not shown). A static, liquid culture at 43 °C did

inactivate restriction after two days of incubation (data not shown). Interestingly, Holloway's original experiments were all performed using static, liquid cultures[1]. All of these results demonstrate that liquid growth is necessary, but aeration is not for inactivation of restriction.

Interestingly, intermediate phenotypes were noted (Fig. 3.3, Fig. 3.4, Fig. 3.5, Fig. 3.6), which suggests that either 1) iREN is neither binary at the cellular level or population level, allowing intermediate amounts of active endonuclease in a given cell or 2) iREN is not binary at the population level but is binary at the cellular level, with a population composed of cells that have either full or no restriction activity but no intermediate levels.

The fact that restriction activity recovers gradually further begs the question of whether iREN is binary at the cellular level or gradual at both the cellular and population levels. Importantly, the ability to inactivate restriction again after full recovery demonstrates that iREN is a fully reversible state (Fig. 3.3). This suggests against mechanisms based on irreversible processes such as large deletion mutations. Though this may at first appear to argue against mutations generally, some type I R-M systems control expression of different *hsdS* genes by reversible, recombination-based inversions of promoters between two genes[18,19].

Deletion and complementation of the *hsdR* satisfactorily demonstrates that it imparts restriction activity to PAO1 and that HsdR is the target of iREN (Fig. 3.1, Fig. 3.10). Interestingly, overexpression of HsdR is only nontoxic during iREN when the HsdS and HsdM proteins are also expressed (Fig. 3.10). This likely reflects a balance of MTase and REase activities against the bacterial chromosome. These results could explain the necessity of evolving the iREN phenomenon: because HsdR overexpression is toxic during iREN but not in the naïve state, it may be that iREN cells become sensitized to nuclease-based autoimmunity. This may be due to a defect in the MTase activity at high temperatures. Additionally, this toxicity may result from the iREN mechanism being overwhelmed and unable to inactivate all the HsdR proteins during this iREN. Alternatively, this may signify that HsdR can only be inactivated in its native genetic context

and that plasmid-expressed HsdR with a different promoter, untranslated regions (UTRs), and intergenic contexts cannot be inactivated by the iREN mechanism.

Having ruled out transcriptional regulation globally and translation of HsdR as causative of iREN, a few possible regulatory means remain. Firstly, it may be that HsdR is in fact translated, per the fluorescent tagging of the native *hsdR* gene (Fig. 3.14). However, it remains possible that HsdR is post-translationally degraded during iREN and that the mechanism that performs this spares the sfCherry2 portion of the fusion protein. Alternatively, the HsdR polypeptide may remain efficiently translated and maintained cellularly, but it may fail to fold appropriately. Often, misfolded proteins form aggregates. This is a particularly exciting hypothesis, partly encouraged by preliminary observation of fluorescent puncta in the PAO1 sfCherry2-*hsdR* strain during iREN (Fig. 3.15). Computational searches for prion domains (PrD) in the HsdR ORF did not identify the well-known domain necessary for formation of prions (data not shown). However, proteins may form aggregates even in the absence of the typical amyloid fold[20,21]. The long memory of iREN is compatible with prions, some of which are noted to be inherited in bacteria for ~100 generations[10].

An alternative hypothesis, ignoring the preliminary microscopy data, proposes that the HsdR protein is translated and maintained efficiently and that it is localized as the HsdR protein is in naïve cells. To inactivate its restriction activity, the HsdR protein can be the recipient of a post-translation modification (PTM), which inhibits the nucleolytic activity of the HsdR protein. The long memory of iREN in this case could occur by varied means. First, the PTM-depositing enzyme may be the factor that features memory directly and HsdR is only a downstream recipient of this memory. Alternatively, the HsdR protein may be inactivated by a protein inhibitor. Phage-encoded nuclease inhibitors have been discovered for type I R-M systems, including Ocr, which bind to type I R-M proteins to inactivate both restriction and methylation[22]. ArdB proteins, which are nonhomologous to Ocr also inhibit restriction but do not inhibit methylation[23,24]. ArdB and their homologous KlcA proteins have been identified in pathogenicity islands in uropathogenic *E. coli*[25]. Though no homologs of known anti-restriction proteins were detected by BLAST in the PAO1

genome (data not shown), it is conceivable that a novel restriction inhibitor may be encode in the PAO1 genome. Because type I R-M is active in many conditions in PAO1, this hypothetical inhibitor would be inactive in most circumstances and would only be activated in response to particular signals, such as bacterial growth at elevated temperatures. The memory of this regulatory scheme could be entirely contained in the expression or activation of the inhibitor molecule. Further experiments are necessary to distinguish between these hypotheses, but all possibilities present the opportunity for discovery and elucidation of a novel regulatory strategy.

In studying the prevalence of iREN, I have found that about half of the tested *P. aeruginosa* strains become more permissive of phage JBD30 when grown at 43 °C (Table 3.1). Of the sequenced strains that feature iREN, homologous *hsd* genes are sometimes shared between strains, but iREN is not limited to a single type I R-M system. Instead, iREN appears to regulate type I R-M genes of diverse subtypes and phylogenies. Along with the observation that so many strains feature temperature-dependent improvements in phage plaquing, these suggest that iREN is a commonplace means of regulating diverse type I R-M systems in *P. aeruginosa*. This suggests an adaptive advantage to inactivation of restriction during bacterial growth at high temperatures. When considering the broader literature on heat-inactivated R-M, which appears to occur via different means, an underlying benefit or necessity of regulation of R-M is expected[2,3,5].

None of my experiments directly address the adaptive advantage of inactivating restriction, though some of my observations form a basis for speculation. The widespread occurrence of iREN in *P. aeruginosa* strains suggests it is an adaptive process. When HsdR alone is overexpressed from a plasmid in iREN PAO1, the cells experience great toxicity (Fig. 3.10). This suggests that iREN serves to protect cells that have, after growth at 43 °C, become sensitive to nucleolytic cleavage by the HsdR protein. The main means by which PAO1 can become sensitive to this nuclease is by loss of its chromosome's protective methylation. I've determined that PAO1 loses methylation activity during growth at 43 °C, though this phenomenon does not

appear to be inherited very long (Fig. 3.2, Fig. 3.3). This observation suggests that PAO1's HsdM may fail to fully methylate every restriction site during bacterial incubation at 43 °C. Therefore, PAO1 may have evolved a means to inactivate the HsdR restriction endonuclease during this unprotected state to prevent autoimmunity. This hypothesis is corroborated by the finding that overexpression of HsdS and HsdM along with HsdR does not cause any toxicity, even during iREN (Fig. 3.10). This hypothesis is less apt to explain the long-lived inheritance of the iREN state: methylation fully recovered between 14 and 35 generations, but restriction remained inhibited to some degree for at least 60 generations (Fig. 3.3). Considering the immense adaptive benefit of an antiphage immune system, it is unlikely that the brief inactivation of methylation during 43 °C is the main driver of such long memory. This is especially true when considering other R-M-inactivating phenomena which recover restriction activity far more quickly.

An especially exciting hypothesis to account for the inactivation of restriction and for its long inheritance is that the PAO1 cells improve their ability to take up foreign DNA during growth at 43 °C. In addition to the kinetics of inactivating and inheriting restriction (Fig. 3.3, Fig. 3.4), the finding that PAO1's electrocompetence improves after growth at 43 °C supports this hypothesis (Fig. 3.8). Interestingly, this improvement of competence at uptake of plasmid DNA after growth at 43 °C is independent of type I restriction, as this electrocompetence is improved even in strains deleted for *hsdR* and deletion of *hsdR* does not fully recapitulate the improvement of competence. This phenomenon, however, did not have memory. Together, these overlapping but distinct phenomena suggest that at elevated temperatures, bacteria may enact a regulatory program to improve horizontal gene transfer (HGT). An intriguing hypothesis is that this improvement of HGT is enacted in this case of high temperature because it may represent a stress to the bacterial cells, therefore uptake of foreign genes may enable the bacterial cells to better survive a less hospitable environment.

Aside from the immense reward of discovering novel biological processes for its own sake, greater understanding of the regulation of antiphage bacterial immune systems also offers useful

benefits. The rise of antibiotic resistance in pathogenic bacteria has created a great need for alternative treatments for bacterial infections[26,27]. Phage therapy has emerged as a viable option for certain bacterial infections[28,29]. However, a major barrier for phage infection of bacteria is the long and diverse list of bacterial immune systems[30]. Type I R-M is the most common bacterial immune system and discovering novel means of inhibiting this significant barrier to phage infection could facilitate phage therapies.

Type I R-M also poses a significant barrier to HGT and genetic editing in prokaryotes[31]. Inhibition of type I R-M by heat treatment has previously been suggested in articles discussing heat-induced inactivation of R-M[4]. Greater understanding of the mechanisms underlying inactivation of restriction by heat treatment could further improve competence of cells and may even reveal ways to inactivate restriction without heat treatment, which triggers the heat shock response and may otherwise impact downstream experiments.

References:

1. Holloway, B. W. Variations in Restriction and Modification of Bacteriophage Following Increase of Growth Temperature of Pseudomonas aeruginosa. *Virology* **25**, 634–642 (1965).
2. Schell, J. & Glover, S. The Effect of Heat on Host-controlled Restriction of Phage lambda in Escherichia coli K (P1). *J. Gen. Microbiol.* **45**, 61–72 (1966).
3. Uetake, H., Toyama, S. & Hagiwara, S. On the Mechanism of Host-Induced Modification Multiplicity Activation and Thermolabile Factor Responsible for Phage Growth Restriction. *Virology* **22**, 202–213 (1964).
4. Edwards, R. A., Helm, R. A. & Maloy, S. R. Increasing DNA Transfer Efficiency by Temporary Inactivation of Host Restriction. *BioTechniques* **26**, 892–900 (1999).
5. Sanders, M. E. & Klaenhammer, T. R. Restriction and Modification in Group N Streptococci: Effect of Heat on Development of Modified Lytic Bacteriophage. *Appl. Environ. Microbiol.* **40**, 500–506 (1980).
6. Doberenz, S. *et al.* Identification of a *Pseudomonas aeruginosa* PAO1 DNA Methyltransferase, Its Targets, and Physiological Roles. *mBio* **8**, (2017).
7. Bickle, T. A. Restricting restriction: Restriction alleviation. *Mol. Microbiol.* **51**, 3–5 (2003).
8. Simons, M., Diffin, F. M. & Szczelkun, M. D. ClpXP protease targets long-lived DNA translocation states of a helicase-like motor to cause restriction alleviation. *Nucleic Acids Res.* **42**, 12082–12091 (2014).
9. Guisbert, E., Yura, T., Rhodius, V. A. & Gross, C. A. Convergence of Molecular, Modeling, and Systems Approaches for an Understanding of the *Escherichia coli* Heat Shock Response. *Microbiol. Mol. Biol. Rev.* **72**, 545–554 (2008).
10. Yuan, A. H. & Hochschild, A. A bacterial global regulator forms a prion. *Science* **355**, 198–201 (2017).
11. Tuite, M. F. & Serio, T. R. The prion hypothesis: from biological anomaly to basic regulatory mechanism. *Nat. Rev. Mol. Cell Biol.* **11**, 823–833 (2010).

12. Halfmann, R., Wright, J. R., Alberti, S., Lindquist, S. & Rexach, M. Prion formation by a yeast GLFG nucleoporin. *Prion* **6**, 391–399 (2012).

13. Halfmann, R. *et al.* Prions are a common mechanism for phenotypic inheritance in wild yeasts. *Nature* **482**, 363–368 (2012).

14. Franzmann, T. M. *et al.* Phase separation of a yeast prion protein promotes cellular fitness. *Science* **359**, eaao5654 (2018).

15. Newby, G. A. & Lindquist, S. Blessings in disguise: biological benefits of prion-like mechanisms. *Trends Cell Biol.* **23**, 251–259 (2013).

16. Fleming, E., Yuan, A. H., Heller, D. M. & Hochschild, A. A bacteria-based genetic assay detects prion formation. *Proc. Natl. Acad. Sci.* **116**, 4605–4610 (2019).

17. Csörgő, B. *et al.* A compact Cascade–Cas3 system for targeted genome engineering. *Nat. Methods* **17**, 1183–1190 (2020).

18. Dybvig, K., Sitaraman, R. & French, C. T. A family of phase-variable restriction enzymes with differing specificities generated by high-frequency gene rearrangements. *Proc. Natl. Acad. Sci.* **95**, 13923–13928 (1998).

19. Zamora, M., Ziegler, C. A., Freddolino, P. L. & Wolfe, A. J. A Thermosensitive, Phase-Variable Epigenetic Switch: *pap* Revisited. *Microbiol. Mol. Biol. Rev.* **84**, e00030-17, /mmbr/84/3/MMBR.00030-17.atom (2020).

20. Mortier, J., Tadesse, W., Govers, S. K. & Aertsen, A. Stress-induced protein aggregates shape population heterogeneity in bacteria. *Curr. Genet.* **65**, 865–869 (2019).

21. Govers, S. K., Mortier, J., Adam, A. & Aertsen, A. Protein aggregates encode epigenetic memory of stressful encounters in individual Escherichia coli cells. *PLOS Biol.* **16**, e2003853 (2018).

22. Walkinshaw, M. D. *et al.* Structure of Ocr from Bacteriophage T7, a Protein that Mimics B-Form DNA. *Mol. Cell* **9**, 187–194 (2002).

23. Balabanov, V. P. *et al.* ArdB Protective Activity for Unmodified λ Phage Against EcoKI Restriction Decreases in UV-Treated Escherichia coli. *Curr. Microbiol.* **76**, 1374–1378 (2019).

24. Kudryavtseva, A. A., Okhrimenko, I. S., Didina, V. S., Zavilgelsky, G. B. & Manukhov, I. V. Antirestriction Protein ArdB (R64) Interacts with DNA. *Biochem. Mosc.* **85**, 318–325 (2020).

25. Serfiotis-Mitsa, D. *et al.* The structure of the KlcA and ArdB proteins reveals a novel fold and antirestriction activity against Type I DNA restriction systems in vivo but not in vitro. *Nucleic Acids Res.* **38**, 1723–1737 (2010).

26. Skandalis, N. *et al.* Environmental Spread of Antibiotic Resistance. *Antibiotics* **10**, 640 (2021).

27. Varela, M. F. *et al.* Bacterial Resistance to Antimicrobial Agents. *Antibiotics* **10**, 593 (2021).

28. Walsh, L., Johnson, C. N., Hill, C. & Ross, R. P. Efficacy of Phage- and Bacteriocin-Based Therapies in Combatting Nosocomial MRSA Infections. *Front. Mol. Biosci.* **8**, 654038 (2021).

29. Yang, B., Fang, D., Lv, Q., Wang, Z. & Liu, Y. Targeted Therapeutic Strategies in the Battle Against Pathogenic Bacteria. *Front. Pharmacol.* **12**, 673239 (2021).

30. Koonin, E. V., Makarova, K. S. & Wolf, Y. I. Evolutionary Genomics of Defense Systems in Archaea and Bacteria. *Annu. Rev. Microbiol.* **71**, 233–261 (2017).

31. Roer, L., Aarestrup, F. M. & Hasman, H. The EcoKI Type I Restriction-Modification System in Escherichia coli Affects but Is Not an Absolute Barrier for Conjugation. *J. Bacteriol.* **197**, 337–342 (2015).

32. Bondy-Denomy, J. *et al.* Prophages mediate defense against phage infection through diverse mechanisms. *ISME J.* **10**, 2854–2866 (2016).

33. Mendoza, S. D. *et al.* A bacteriophage nucleus-like compartment shields DNA from CRISPR nucleases. *Nature* **577**, 244–248 (2020).

34. Marino, N. D. *et al.* Discovery of widespread type I and type V CRISPR-Cas inhibitors. *Science* **362**, 240–242 (2018).

35. Qiu, D., Damron, F. H., Mima, T., Schweizer, H. P. & Yu, H. D. P_{BAD} -Based Shuttle Vectors for Functional Analysis of Toxic and Highly Regulated Genes in *Pseudomonas* and *Burkholderia* spp. and Other Bacteria. *Appl. Environ. Microbiol.* **74**, 7422–7426 (2008).

Methods

iREN Measurements

Restriction activity and its inactivation were measured by resuspending bacterial colonies in lysogeny broth (LB), splitting the inoculum into 2 tubes, and incubating one of each at 37 and 43 °C. Once saturated, plaque assays were performed to quantify EOP. EOP was calculated by quantifying the apparent titer of the particular phage on the particular strain in question and dividing by the apparent titer of the particular phage on the strain that originally produced it. “Relative Restriction Activity” is then calculated by the following formula:

$$\textit{Relative Restriction Activity} = log_{10}(EOP^{-1})$$

By measuring the Relative Restriction Activity against phage produced on a different strain, the restriction activity of a particular culture is quantified.

Plaque Assays

Plaque assays were performed by mixing 100 µL of saturated bacterial culture with 3 mL molten 10 mM $MgSO_4$ 0.7% top agar and spreading on 10 mM $MgSO_4$ LB agar plates containing any additional antibiotics or inducers. Once set, 2.5 µL of 10-fold serial dilutions of a phage preparation were spotted on the plate and allowed to dry. Once dry, plates were incubated at 37 °C overnight.

Phage Propagation

To propagate phage, 100 µL of this bacterial culture were mixed with ~10,000 PFUs of bacteriophage in 10 mM $MgSO_4$, incubated at room temperature for 15 minutes, and spread on a 10 mM $MgSO_4$ LB agar plate using 10 mM $MgSO_4$, 0.7% top agar. Once set, plates were incubated at 37 °C overnight. Once grown, plates were flooded with 3 mL SM phage buffer and incubated at room temperature for 15 – 30 minutes with slow shaking. SM phage buffer was then removed from the plate and transferred to a fresh 2.0 mL tube. The phage lysate was centrifugated at 16,000 × g for 2 minutes. The supernatant was transferred to a fresh tube and

centrifugation was repeated until no cellular debris was visible in the pellet. Phage lysate was then treated with 40 µL chloroform, mixed briefly, and centrifugated at 21,130 × g for 2 minutes. The aqueous phase was transferred to a fresh 2.0 mL tube and chloroform treatment was repeated until no cellular debris was visible at the interface of the organic and aqueous phases. Phage stock was stored with chloroform at 4 °C.

Induction Kinetics Experiments

I prepared a 1:1000 dilution of a saturated PAO1 culture grown at 37 °C. This large inoculum was split into several different tubes, all of which were incubated at 43 °C. Starting at time = 0, I took time points in which I measure the optical density of the cultures and move them to 37 °C to grow to saturation. This exploited the memory of iREN and ensured that all cultures were tested at the same cellular density, which can affect EOP measurements. Once saturated, cultures were used to perform plaque assays. Relative Restriction Activity was calculated and graphed with OD_{600} as a function of time.

Induction Temperature Experiment

I prepared inocula of PAO1 and incubated them at various temperatures between 37 and 43 °C to saturation. Saturated cultures were used to perform plaque assays. Relative Restriction Activity was calculated and graphed by incubation temperature.

Memory Measurement

I grew PAO1 in 6 mLs of LB at 37 °C with shaking to saturation. This culture was then used to inoculate 6 mL of fresh LB using a $1:10^3$ dilution and incubated at 43 °C overnight. Serial dilutions of this culture were prepared in fresh LB and spotted on LB agar plates. Additionally, this culture was tested by plaque assay to measure restriction activity. JBD30·PAO1 was propagated with this culture by full plate lysate. Lastly, this culture was diluted $1:10^6$ in 1000 mL fresh LB, which

was then incubated at 37 °C for ~12 hours. Plates for measurement of bacterial CFUs, plaque assays, and full plate infections were incubated at 37 °C overnight. At each time point, this procedure was repeated. Once plates were ready (~16-20 hours), CFUs from the bacterial dilution and PFUs from the plaque assay were quantified. Progeny phage were harvested. This experiment was repeated until restriction activity had fully recovered, (~ 100 generations), at which point the cells were diluted $1:10^6$ as before, but were instead grown at 43 °C. All progeny phage from each time point were tested by plaque assay all at once on PAO1 37 °C at the end of the experiment.

Cas9-mediated deletions

I designed a type II-A SpyCas9 spacer against the 5' end of *hsdR*. I introduced this spacer into a sgRNA expression vector. I then designed a repair template that deleted all of the *hsdR*-coding base pairs, including the stop codon. This repair template was cloned into the sgRNA-expression vector and introduced into a PAO1 strain that expressed SpyCas9 from its tn7 site. Clones of this strain were grown in 50 µg/mL gentamicin LB at 37 °C overnight. Once saturated, they were diluted 1:1000 in 50 µg/mL gentamicin, 0.1 % (L)-arabinose LB at 37 °C and their growth was measured by optical density. In comparison to a nontargeting control, the targeting strains had a prolonged lag phase (data not shown). The template-containing version of this experiment had a mild benefit to this lag phase (data not shown). Once the cells had grown to saturation, a sample of the culture was spotted on a 50 µg/mL gentamicin, 0.1 % (L)-arabinose LB agar plate and struck for single colonies. Once colonies had grown, 20 colonies were screened by PCR using primers that flank the *hsdR* gene. PCRs were then analyzed by gel electrophoresis: full length amplicons hypothetically represented wild type (WT) or indel clones, whereas amplicons of the 500 bp expected length suggested successful deletion of *hsdR*. These amplicons were then cleaned using a PCR clean up kit and sequenced. Correct deletion of the *hsdR* gene was confirmed by sequence alignments. Verified *ΔhsdR* clones were passaged in nonselective and

noninducing LB with patching on 50 µg/mL gentamicin and nonselective LB agar plates to test for loss of gentamicin resistance. The clones that lost gentamicin resistance were understood to have lost the sgRNA expression vector. These strains were then used for downstream experiments.

Cas3-mediated deletions

As before, a spacer against *hsdR* was designed and introduced into a I-C crRNA expression vector. Because Cas3 is a processive enzyme that yields large deletions and a large deletion of the *hsd* locus was desired, no repair template was designed. This expression vector was electroporated into a PAO1 strain encoding the necessary *cas* genes in the tn7 site. The targeting and the screening of clones was done as with Cas9, with a difference in the PCR screening approach: PCRs were performed using primers that amplify part of the *hsdR* gene. Full length amplicons were hypothesized to be WT, while no amplicon at all was hypothesized to signify a deletion in the region. Sequencing was not performed in this strain. Candidate mutants were tested for restriction and modification activities *in vivo*.

Complementation

hsdSM and *hsdR* were amplified by PCR with primers that introduce overhangs for Gibson assemblies. *hsdSM* and *hsdR* fragments were cloned into the rhamnose-inducible version of pHERD30T, p30Rha, by Gibson assembly. Plasmids were verified by sequencing and introduced into PAO1 and PAO1 Δ*hsdR*. Strains were grown in LB with 50 µg/mL gentamicin as appropriate and with and without 0.2 % rhamnose at 37 and 43 °C to saturation. Cultures were tested by plaque assay with JBD30 on 10 mM $MgSO_4$ LB agar plates with 50 µg/mL gentamicin as appropriate and with and without 0.2 % rhamnose.

hsdR was amplified by PCR with primers that introduce overhangs for Gibson assembly. *hsdR* fragment was cloned into pHERD30T. Plasmid was verified by sequencing and introduced into PAO1 and PAO1 Δ*hsdR*. Strains were grown in 50 µg/mL gentamicin, 0.1 % arabinose LB at

37 and 43 °C overnight. Cultures were tested by plaque assay with JBD30 on 10 mM $MgSO_4$, 50 µg/mL gentamicin, 0.1 % arabinose LB agar plates.

RT-qPCR

Primers were designed against the *hsdR*, *hsdS*, and *hsdM* coding-regions, with primers against *rpoD* as a housekeeping gene for nomalization. I performed this experiment in biological triplicate by streaking PAO1 to single colonies and resuspending 3 colonies in LB. This inoculum was then split into 2 equal volumes, one of which was incubated at 37 °C and the other at 43 °C with shaking overnight. Saturated cultures were diluted 1:1000 and grown at 37 °C with shaking to midlog, at which point they were harvested. Plaque assays were performed using both saturated cultures and harvested cultures. The saturated and harvested cultures were also serially diluted 10-fold in LB and spotted on LB agar plates. These plaque assays and CFU counts were measured to determine restriction activity and the generations elapsed between saturated cultures and harvested cells. Restriction was fully inactivated by bacterial growth at 43 °C and remained inactive even after bacterial growth at 37 °C to the harvesting point (data not shown). At the harvest point, RNA was extracted from cells and by phenol:chloroform precipitation and was treated with DNase. Total RNA was then used in an RT-qPCR experiment using a Luna® RT-qPCR kit. ΔCt was calculated by comparison to *rpoD*.

RNA-Seq

The same DNA-free total RNA prepared during the RT-qPCR experiment was submitted to GENEWIZ, Inc. for paired-end RNA-sequencing (RNA-Seq). GENEWIZ, Inc. depleted ribosomal RNAs, prepared libraries, and sequenced the libraries. They returned raw reads, which were of excellent quality. I then removed adapter sequences and any reads shorter than 20 nt. I aligned the resulting reads to a reference genome and outputted raw read counts for every annotated gene in the PAO1 reference genome. I calculated reads per kilobase of transcript, per million

(RPKM) and measured the fold-change (iREN RPKM / naïve RPKM) and log 2-fold change of transcripts globally. Using Prism 9 software, I performed an unpaired t-test to identify any significant changes in RPKM between iREN cultures and naïve cultures.

To test the spacer tRNA candidates, I cloned the entire intergenic region between 16S and 23S from PA5369 into pHERD30T under transcriptional control of P_{BAD}, an arabinose-inducible promoter. I introduced this tRNA-expression vector into WT PAO1, along with an empty vector control. Each of these strains were grown in 50 µg/mL gentamicin, 0.3 % (L)-arabinose LB at both 37 °C and 43 °C with shaking overnight and were then tested by plaque assay.

Western Blot

Strains were grown in LB at 37 °C and 43 °C overnight. The cultures were diluted 1:100 in 50 mL LB and grown at 37 °C. At OD_{600} = 0.8 – 1.0, the cultures were centrifugated at 4 °C at 6,000 × g for 10 minutes. The supernatant was discarded and the pellet was frozen in liquid nitrogen. The pellet was resuspended in 1 mL of lysis buffer, 50 mM Tris-Cl pH 7.4, 150 mM NaCl, 20 mM MgCl2, 0.5% NP40, 5% glycerol [v/v], 5 mM DTT and 1 mM PMSF. Cells were lysed by boiling at 98 °C for 10 minutes. A portion of the boiled lysate was reserved as “Total Lysate”. The remainder was centrifugated at 21,130 × g at 4 °C for 10 minutes. The supernatant was reserved as “Lysate” and the pellet was resuspended in lysis buffer and reserved as “Pellet”. Samples were mixed with 4× Laemmli buffer to a total of 1× and were loaded into a 4 – 20% SDS PAGE gel. The gel was run at 100 V for 60 minutes. Once run, a gel was reserved for Coomassie staining and others were used for transferring.

The gel was Coomassie stained by incubating gel in ddH_2O at room temperature for 5 minutes with shaking three times. The gel was then incubated in Bio-Rad’s Bio-Safe™ Coomassie Stain at room temperature for 30 minutes with shaking. The gel was then destained by incubating in ddH_2O at RT with shaking for 30 minutes. Coomassie stained gels were imaged for analysis.

To transfer, gels were assembled into transfer cassettes with equilibrated PVDF membranes, flanked by filter paper and sponges. Cassettes were inserted into transfer boxes and filled with 10 % ethanol tris-glycine transfer buffer. Proteins were transferred at 100 V at 4 °C for 60 minutes. Membranes were blocked using 5 % nonfat dry milk (NFDM) at room temperature with shaking for 60 minutes. Membranes were then incubated in primary antibodies diluted in 10 mL 5% NFDM 1× TBS-T at 4 °C with shaking overnight. The membrane was then incubated in TBS-T at room temperature with shaking for 5 minutes three times. The membrane was then incubated in secondary Cell Signaling α-rabbit IgG, HRP-linked antibody diluted 1:1000 in 10 mL 5% NFDM 1× TBS-T at room temperature with shaking for 60 minutes. The membrane was then incubated in TBS-T at room temperature with shaking for 5 minutes three times. The membrane was developed using ECL Clarity substrate by mixing the two solutions, adding to the membrane, and incubating for 5 minutes. The membrane was then imaged using a chemiluminescent imager.

Cherry Fusions

A type I-C spacer against PAO1's *hsdR* gene was designed to target the 5' end of the gene. I then designed a repair template that includes 500 bp upstream of the spacer, the sfCherry2 gene, and 500 bp downstream of the spacer in that order. The region that encodes the protospacer was designed such that the sfCherry2 gene separated the PAM and the spacer, therefore making targeting impossible in the sfCherry2 mutant. Additionally, I took care to ensure that the overlapping upstream gene did not have its last few amino acids disrupted and that the *hsdR* fusion retained a ribosome binding site (RBS), as in WT PAO1. I performed the mutation steps as done previously in the deletion of *hsdR*. In brief, the crRNA and repair template- encoding plasmid was electroporated into PAO1 encoding the type I-C *cas* genes in the tn7 site. This strain was grown to saturation, diluted into 50 µg/mL gentamicin, 0.3 % (L)-arabinose, 1 mM IPTG LB, and incubated at 37 °C with measurements of OD_{600}. A prolonged lag phase indicated toxicity of the crRNA. Once the culture recovered and grew to saturation, it was plated for single colonies

on 50 μg/mL gentamicin, 0.3 % (L)-arabinose, 1 mM IPTG LB agar plates and incubated at 37 °C. Individual colonies were screened by PCR for the insertion of sfCherry2 at the 5' end of *hsdR*. PCRs which produced a larger amplicon, by gel electrophoresis, were purified and submitted for Sanger sequencing. This sequencing confirmed clones with the appropriate tag of *hsdR*. These strains were serially passaged with patching on 50 μg/mL gentamicin and nonselective LB agar plates at each dilution until antibiotic sensitive clones were identified. These clones were used for downstream experiments. PAO1 sfCherry2-*hsdR* was resuspended in fresh LB and incubated at both 37 and 43 °C with shaking overnight to saturation. These cultures were centrifugated at 8,000 × g for 2 minutes. The pellet was resuspended in M9 minimal media and its fluorescence and OD_{600} were measured. The fluorescence was normalized by dividing by optical density. To test restriction activity, the cultures were tested by plaque assay.

Microscopy

PAO1 and PAO1 sfCherry2-*hsdR* were grown in LB at 37 and 43 °C with shaking to saturation. Cultures were diluted 1:100 in 1:4 LB and treated with DAPI. Diluted cells were then spotted on a 1:4 LB, 0.85 % agarose pad on a concave glass microscopy slide. Slide was covered with a coverslip and imaged by fluorescence microscopy with recording of transmitted light, red fluorescence, and blue fluorescence. Images were taken at the same exposure, but brightness and contrast were adjusted to reduce background fluorescence signal. Images were cropped to show specific cells. Representative images are shown.

Figures:

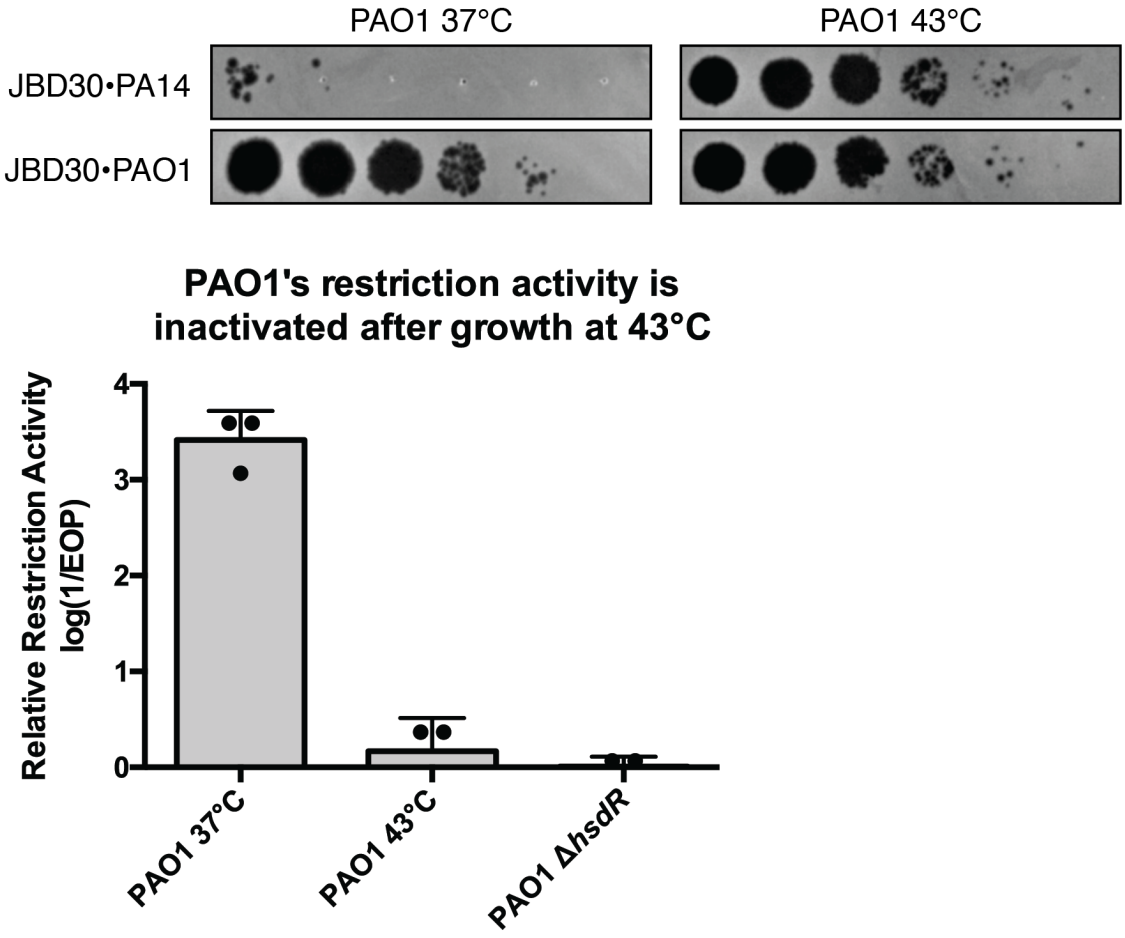

Figure 3.1: PAO1's restriction against phage JBD30 is ablated after growth at 43 °C.
a, Plaque assay with the indicated phage spotted in ten-fold serial dilutions on a lawn of *P. aeruginosa* strain PAO1 grown at either 37 or 43 °C, dark clearings in the lawn represent phage replication. **b,** Relative Restriction Activity (log(1/EOP)) of JBD30·PA14 on PAO1 strains as indicated. Mean values are plotted as bars with error bars representing standard deviation (n = 3).

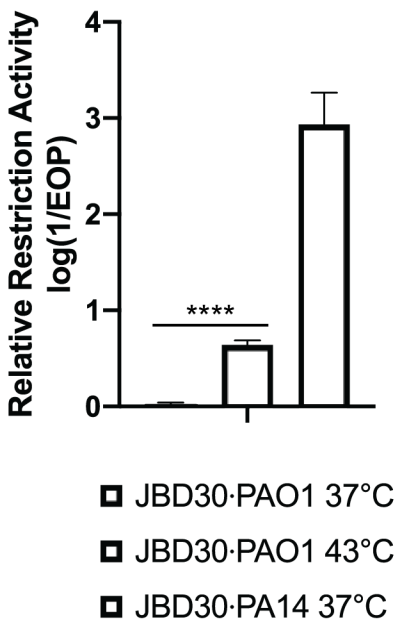

Figure 3.2: PAO1's HsdM's methylation activity is partially inhibited after bacterial growth at 43 °C. JBD30·PAO1 was propagated on different P. aeruginosa strains, as labelled (top to bottom = left to right). Relative Restriction Activity (log(1/EOP)) by naïve PAO1 was measured by plaque assay (n = 3). Mean values are plotted as bars with error bars representing standard deviation. A t-test comparing JBD30·PAO1 37 °C to JBD30·PAO1 43 °C yielded a p-value of 2.5×10^{-5}.

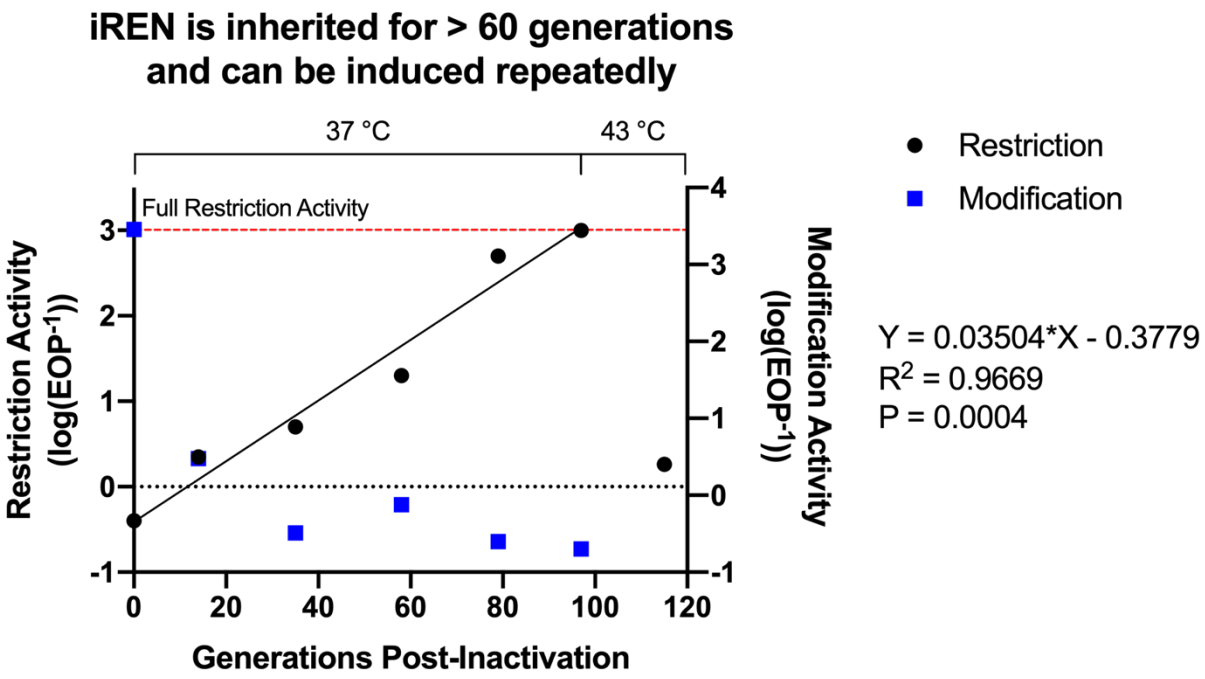

Figure 3.3: iREN is inherited for > 60 generations, while inactivation of methylation recovers much more quickly. PAO1 was grown at 43 °C to inactivate restriction and then cultured at 37 °C. At the final time point, PAO1 was grown again at 43 °C. At each time point, restriction (left y-axis), modification (right y-axis), and bacterial replication (x-axis) were quantified. Restriction Activity (log(EOP^{-1})) was analyzed by a simple linear regression. Restriction recovered by a rate described by Y = 0.03504*X – 0.3779, the fit of which had an R^2 = 0.9669; P = 0.0004.

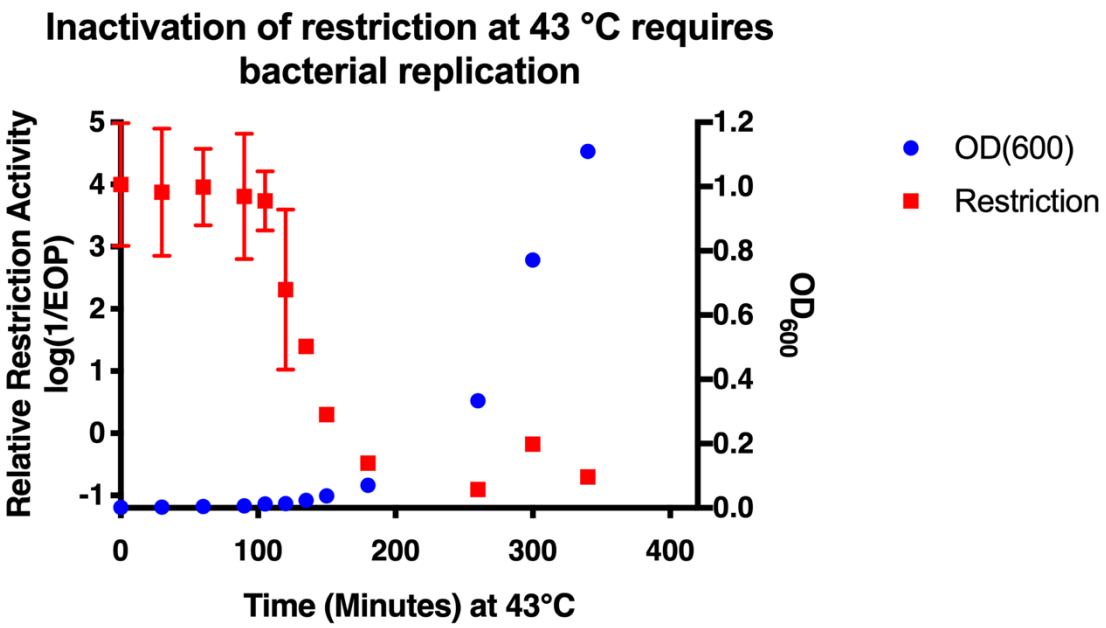

Figure 3.4: Restriction is inactivated during early log-phase at 43 °C. PAO1 was grown at 43 °C for varying amounts of time to inactivate restriction. At specific time points (x-axis), OD_{600} (right y-axis) was measured and the culture was incubated at 37 °C. Once saturated, plaque assays measured restriction activity (left y-axis). For time points 1-6, restriction n = 2, subsequent time points and OD_{600}, n = 1.

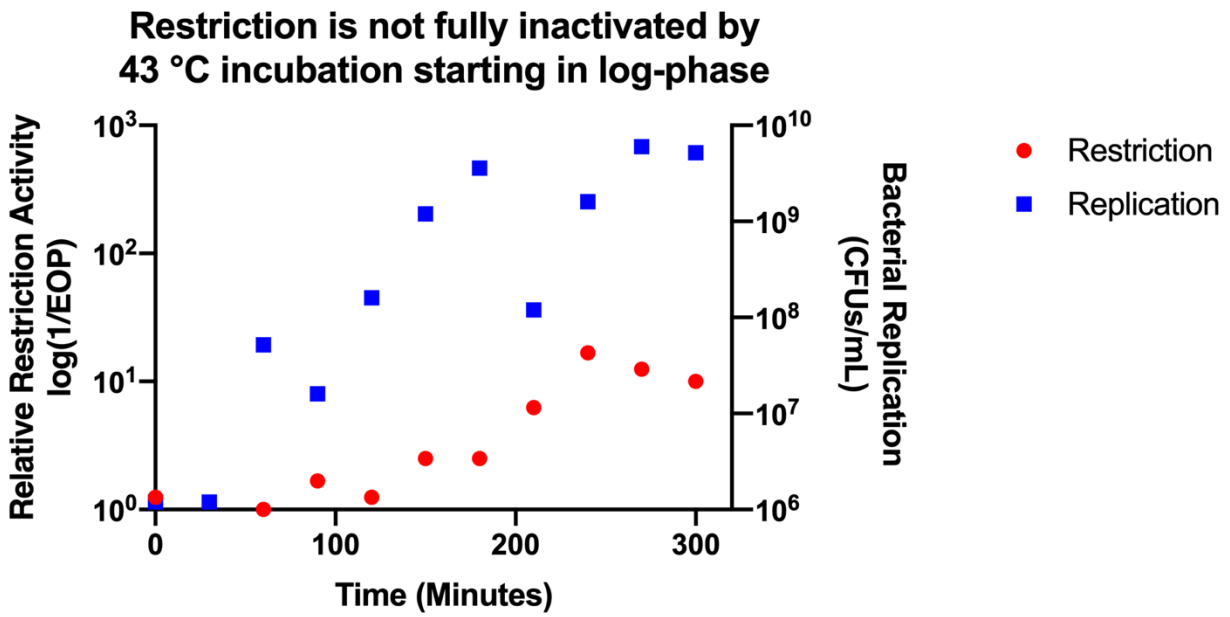

Figure 3.5: Incubation at 43 °C during mid-log is insufficient for full inactivation of restriction. PAO1 was grown at 37 °C for varying amounts of time. At specific time points (x-axis), CFUs/mL were measured (right y-axis) and the culture was incubated at 43 °C. Once saturated, plaque assays measured restriction activity (left y-axis).

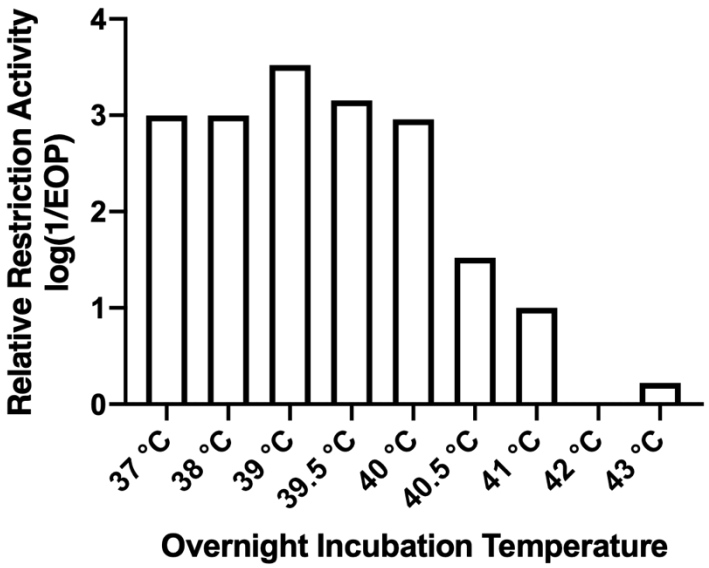

Figure 3.6: Restriction activity is inactivated partially at 40.5 °C and fully at 42 °C. WT PAO1 cultures were incubated at varying temperatures and their restriction activity was measured by plaque assay using JBD30·PA14 (n = 1).

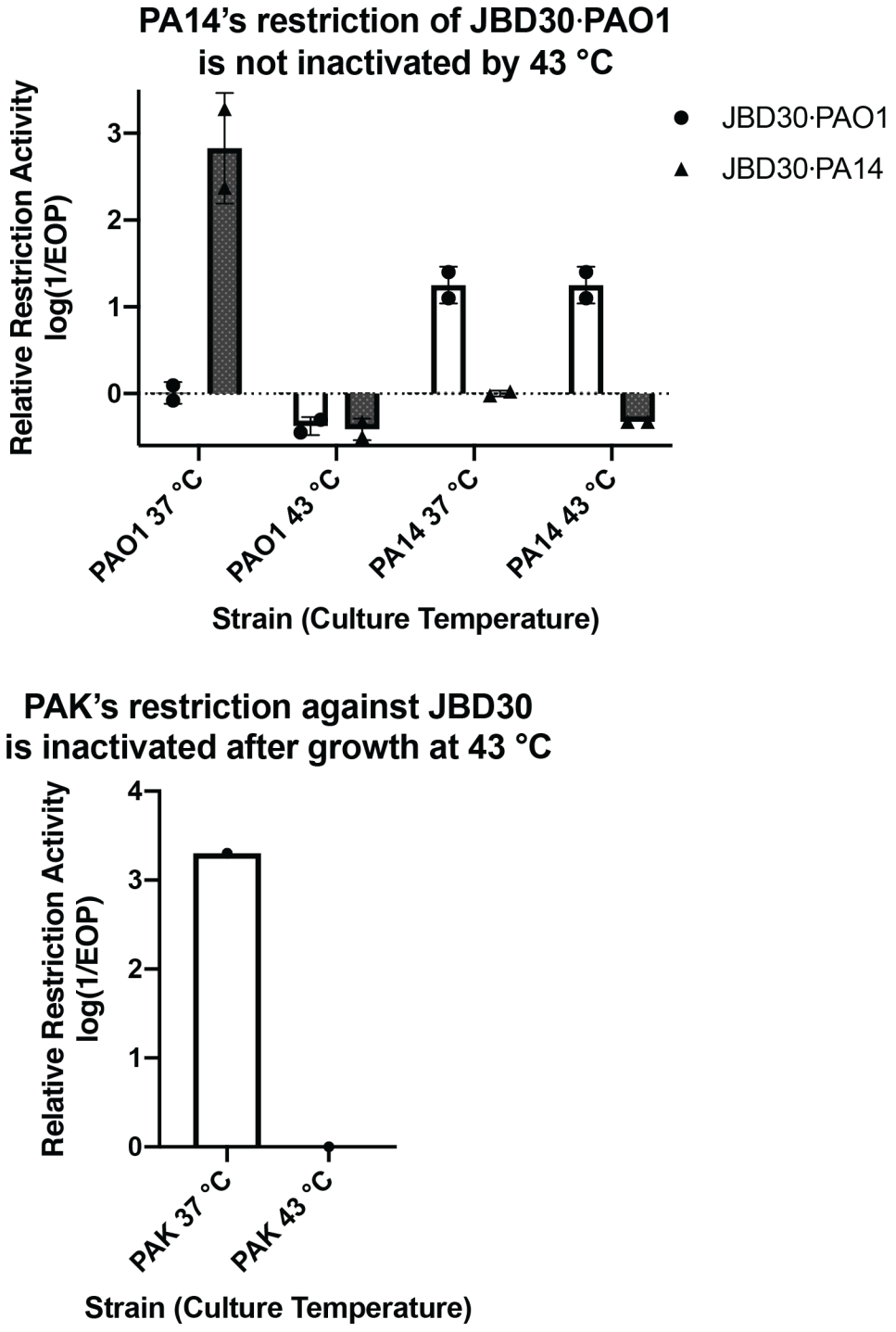

Figure 3.7: *P. aeruginosa* strain PA14 has temperature-insensitive restriction while PAK's restriction is inactivated at 43 °C. a, PA14 was incubated at 37 and 43 °C and infected with JBD30·PAO1 and JBD30·PA14 in a plaque assay, with PAO1 as a control. Restriction activity was calculated from EOP and plotted (n = 2). **b,** PAK was incubated at 37 and 43 °C and infected

with JBD30·PAO1 in a plaque assay, with PAO1 as the indicator strain. Restriction activity was calculated from EOP and plotted (n = 1).

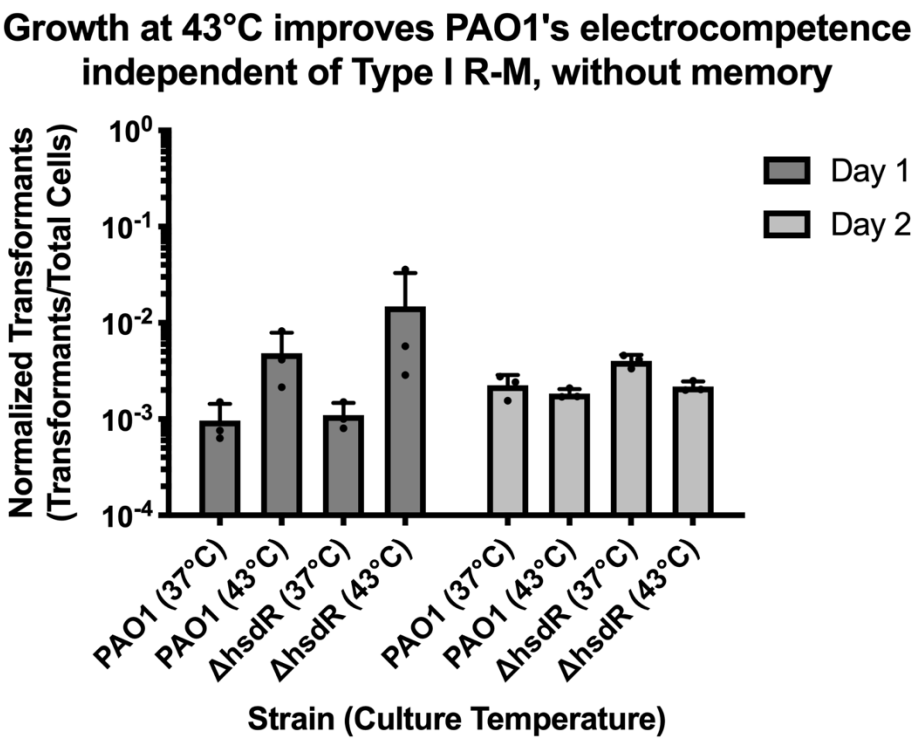

Figure 3.8: PAO1's electrocompetence improves after incubation at 43 °C independent of *hsdR*, but this improvement is not inherited. PAO1 and PAO1 ΔhsdR were grown at 37 and 43 C to saturation and electoporated with a plasmid. Antibiotic-resistant transformants were quantified and normalized to total cells input into the electroporation experiment (Day 1). Cultures were diluted and grown at 37 C to saturation. Electroporations and quantifications were repeated (Day 2).

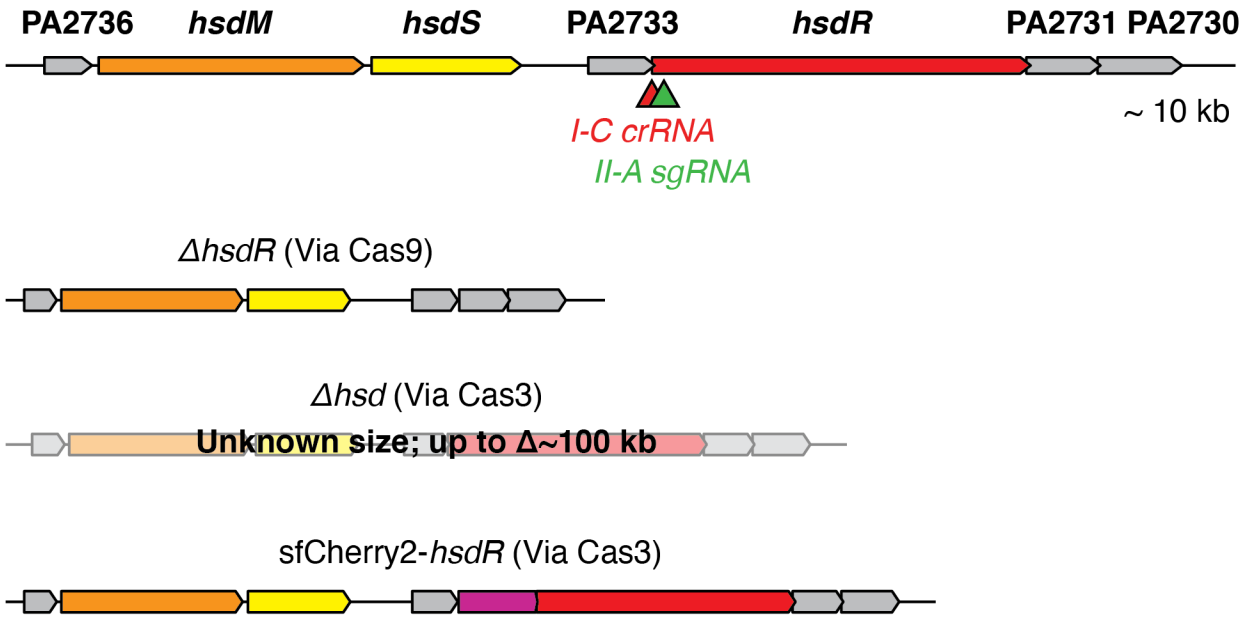

Figure 3.9: PAO1's *hsdSMR* locus and mutants used in this study. a, PAO1's WT *hsd* locus with spacer targets for I-C and II-A-mediated mutagenesis labeled. **b,** PAO1 Δ*hsdR*'s *hsd* locus as created by Cas9-mediated targeting with a repair template; confirmed by PCR and Sanger sequencing. **c,** PAO1 Δ*hsd* has not been sequenced, but restriction and modification activity are lost. Type I-C CRISPR-Cas3 can generate large deletions in excess of 100 kb. **d,** PAO1 sfCherry2-*hsdR*'s *hsd* locus as generated by type I-C CRISPR-Cas targeting with a repair template; confirmed by PCR and Sanger sequencing.

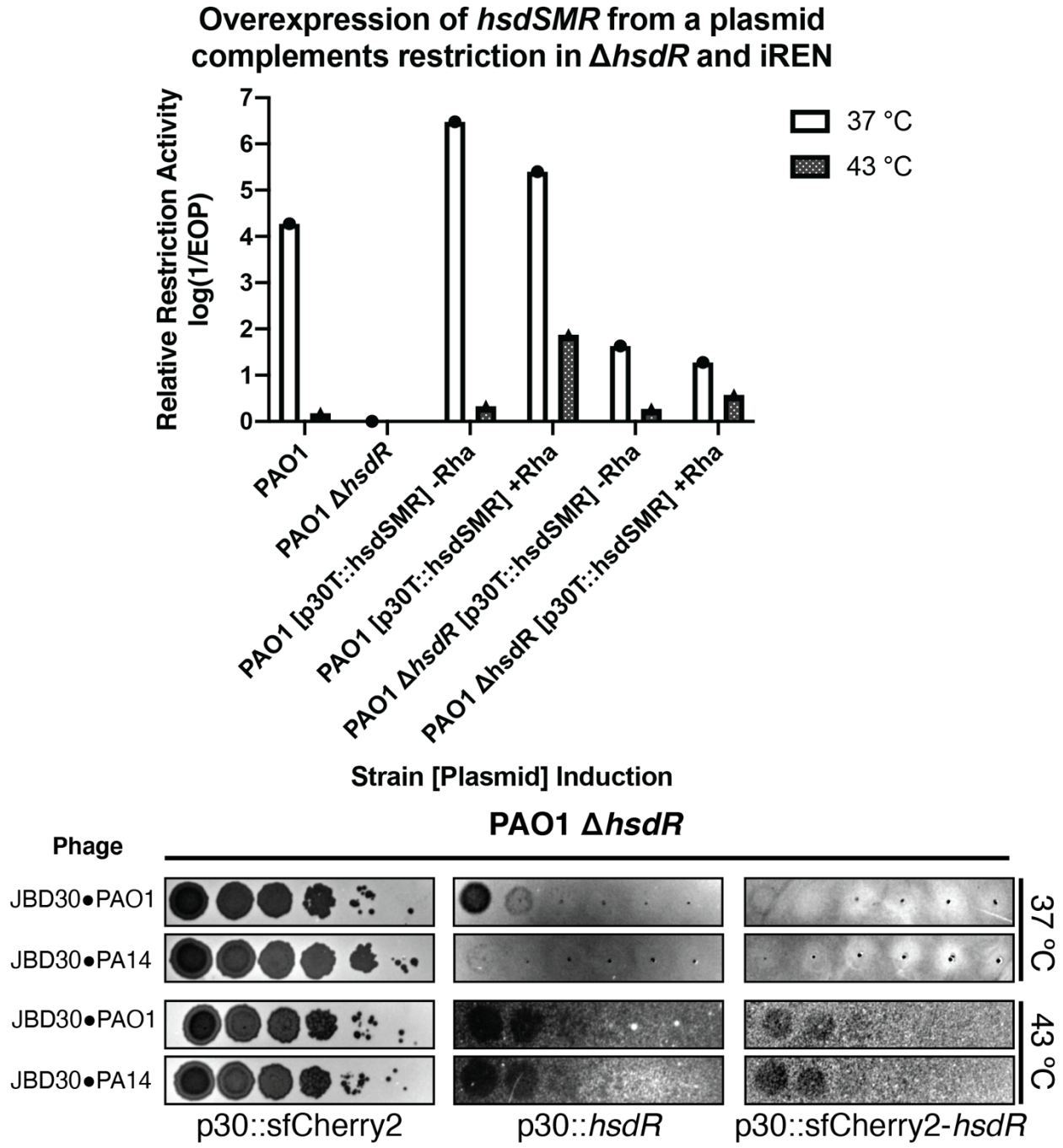

Figure 3.10: PAO1 Δ*hsdR*'s loss of restriction can be complemented by overexpression of HsdR from a plasmid, but this is toxic during iREN. a, Basal and induced expression of HsdSMR from rhamnose-inducible pHERD30T in PAO1 and PAO1 Δ*hsdR* grown at 37 and 43 °C improved restriction against JBD30·PA14 (n = 1). **b,** Overexpression of HsdR and sfCherry2-HsdR (without overexpression of HsdSM) complemented restriction in PAO1 Δ*hsdR* grown at 37 °C. When overexpressed in PAO1 Δ*hsdR* grown at 43 °C, lawns were not confluent, indicating toxicity.

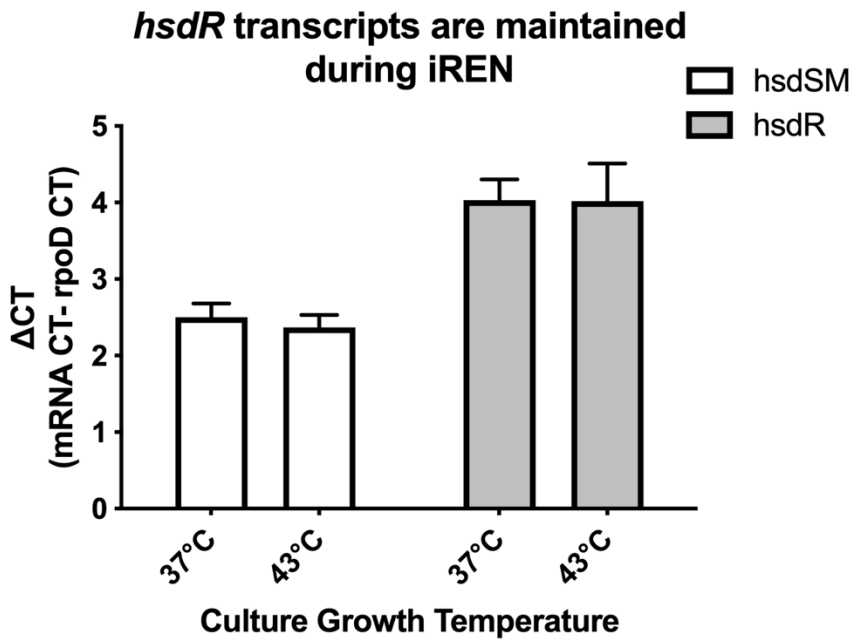

Figure 3.11: hsdSM and hsdR transcripts are present during iREN. RT-qPCR using primers against the hsdSM and the hsdR transcripts was performed on DNA-free total RNA from naïve and iREN PAO1. Cycle threshold (Ct.) values were normalized to the rpoD transcript. (n = 3).

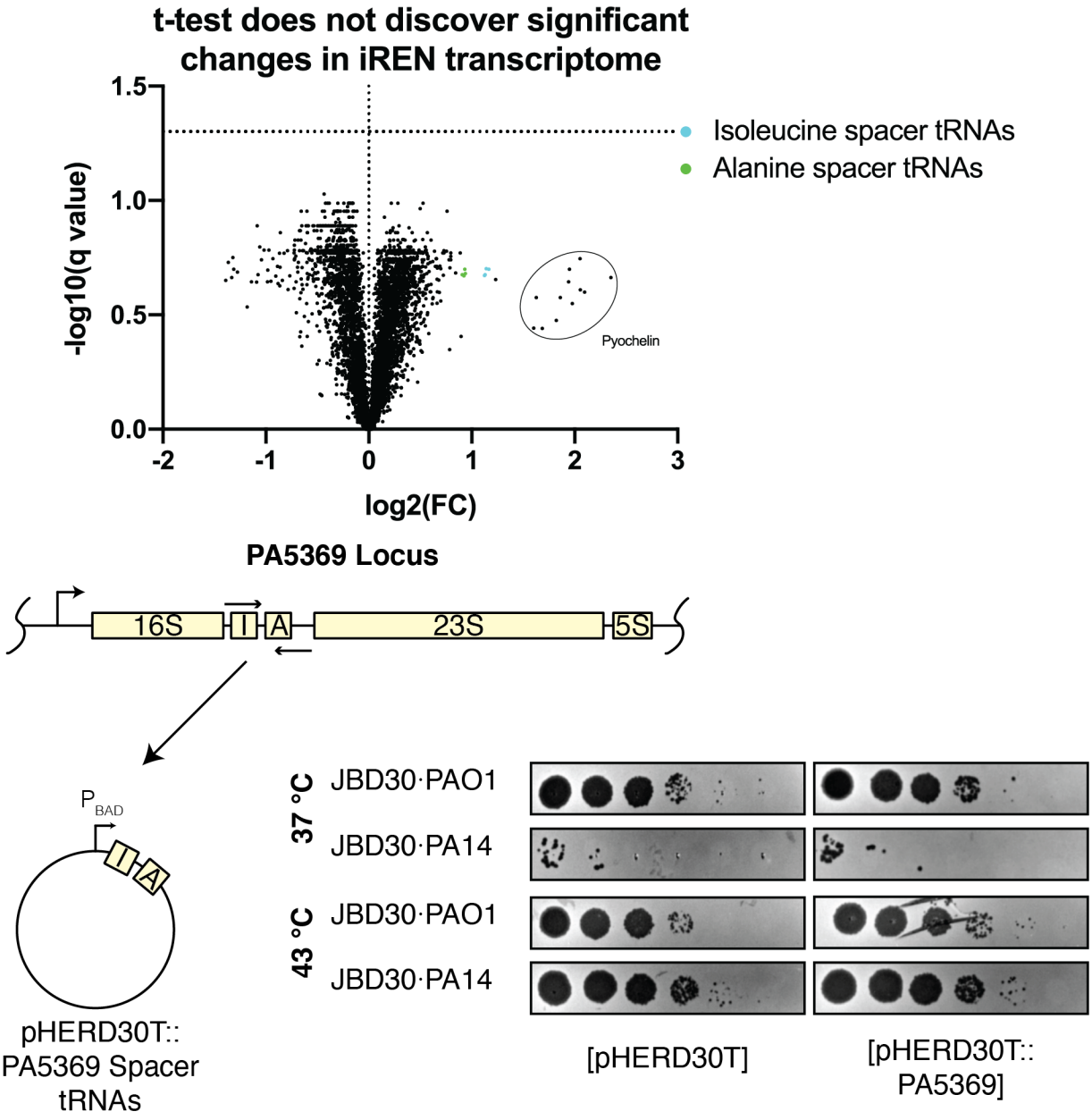

Figure 3.12: RNA-Seq does not identify any statistically significant changes to PAO1's transcriptome during iREN. a, Total DNA-free RNA was submitted to and sequenced by GENEWIZ, Inc., which returned raw reads. Reads were analyzed for quality, trimmed of adapter sequences, aligned to a reference PAO1 genome, and RPKMs were determined for each gene. Unpaired t-test with desired FDR (Q) = 5.00 % was performed and -$\log_{10}$(q value) of naïve vs. iREN RPKMs was plotted for each gene. Isoleucine and alanine spacer tRNAs are labeled in cyan and green, respectively as they were half as abundant in the iREN sample (not statistically significant). Pyochelin biosynthesis pathway transcripts are circled, as they were less abundant in the iREN sample (not statistically significant). **b,** Spacer tRNAs from the PA5369 rRNA locus were introduced into pHERD30T and overexpressed in PAO1 during growth at 37 and 43 °C, which did not affect inactivation of restriction.

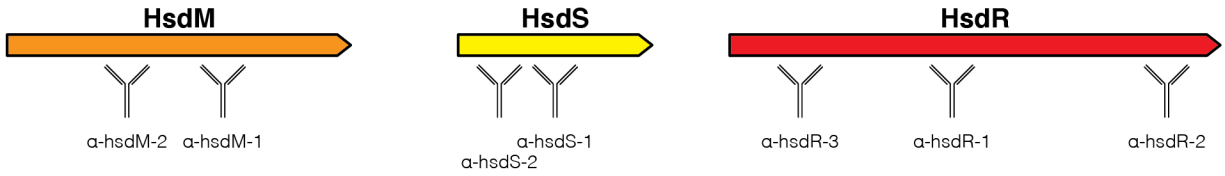
HsdM
HsdS
HsdR
α-hsdM-2
α-hsdM-1
α-hsdS-1
α-hsdS-2
α-hsdR-3
α-hsdR-1
α-hsdR-2

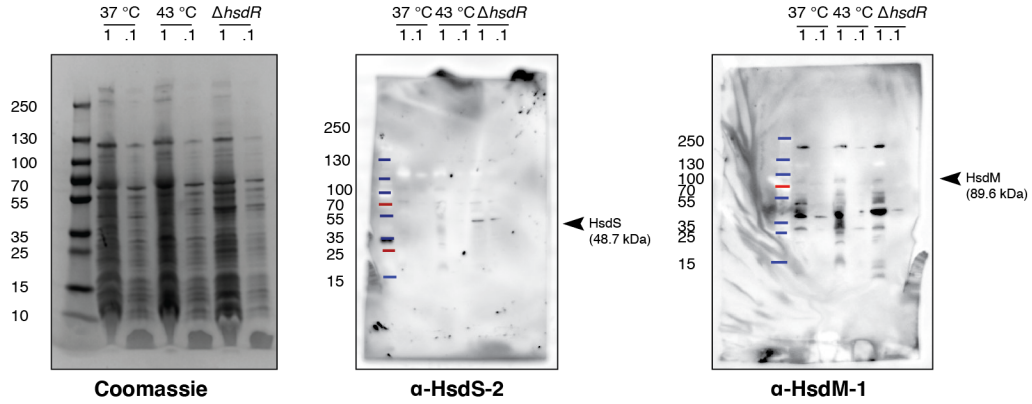
37 °C
43 °C
ΔhsdR
1
.1
250
130
100
70
55
35
25
15
10
HsdS
(48.7 kDa)
HsdM
(89.6 kDa)
Coomassie
α-HsdS-2
α-HsdM-1

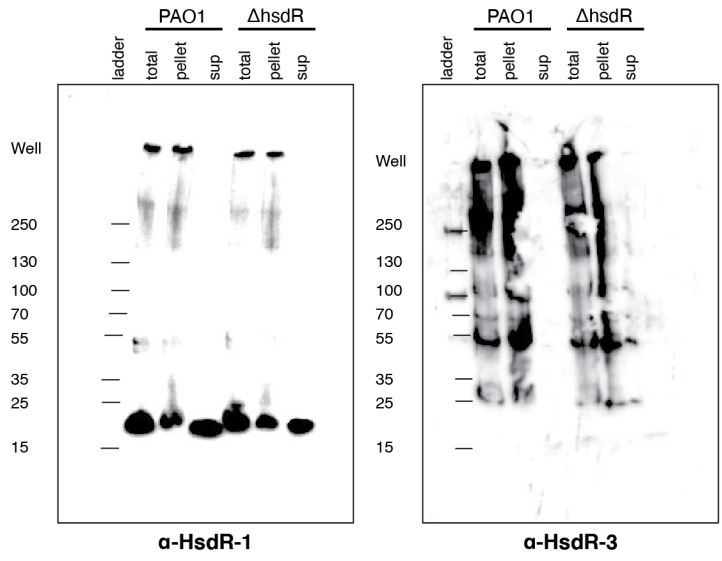
PAO1
ΔhsdR
ladder
total
pellet
sup
Well
250
130
100
70
55
35
25
15
α-HsdR-1
α-HsdR-3

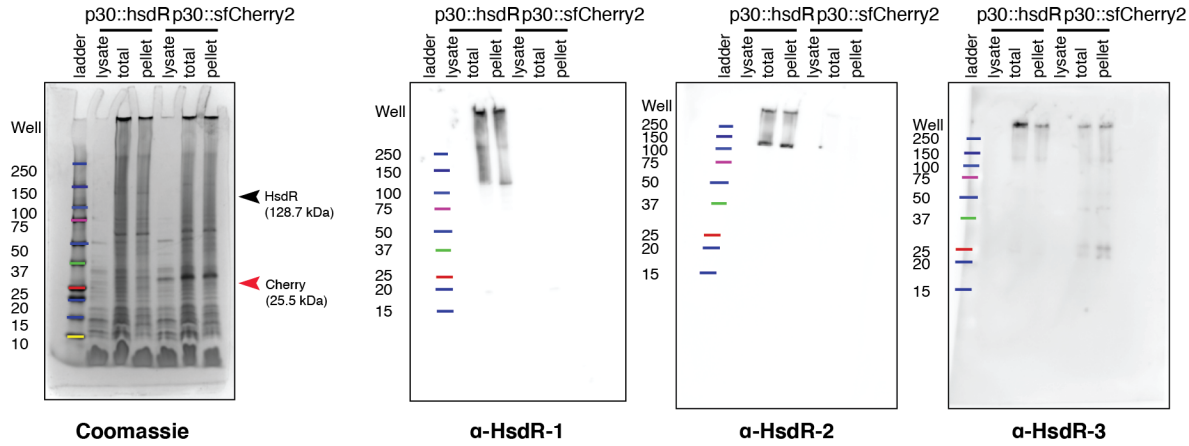
p30::hsdR
p30::sfCherry2
ladder
lysate
total
pellet
Well
250
150
100
75
50
37
25
20
15
10
HsdR
(128.7 kDa)
Cherry
(25.5 kDa)
Coomassie
α-HsdR-1
α-HsdR-2
α-HsdR-3

Figure 3.13 (Previous Page): Western blots using custom antibodies reveal that HsdR is lowly expressed and insoluble in its native context. a, Custom antibodies were purchased from Genscript®, who identified antigens and produced antibodies against the Hsd proteins as shown. **b,** Western blots against HsdS and HsdM reveal a specific band against HsdS that is only present in the PAO1 Δ*hsdR* background. HsdM antibody shows poor specificity and may demonstrate a band of the appropriate size in all conditions. 1 and .1 refer to dilution factors of lysate analyzed by Western blot. **c,** Western blots against HsdR using lysates from WT PAO1 do not reveal specific bands of the expected size (HsdR = 128.7 kDa). **d,** Western blots against HsdR using lysates from PAO1 overexpressing either sfCherry2 or HsdR from a plasmid reveal specific bands at the expected migration and at the well in the total and pellet fractions.

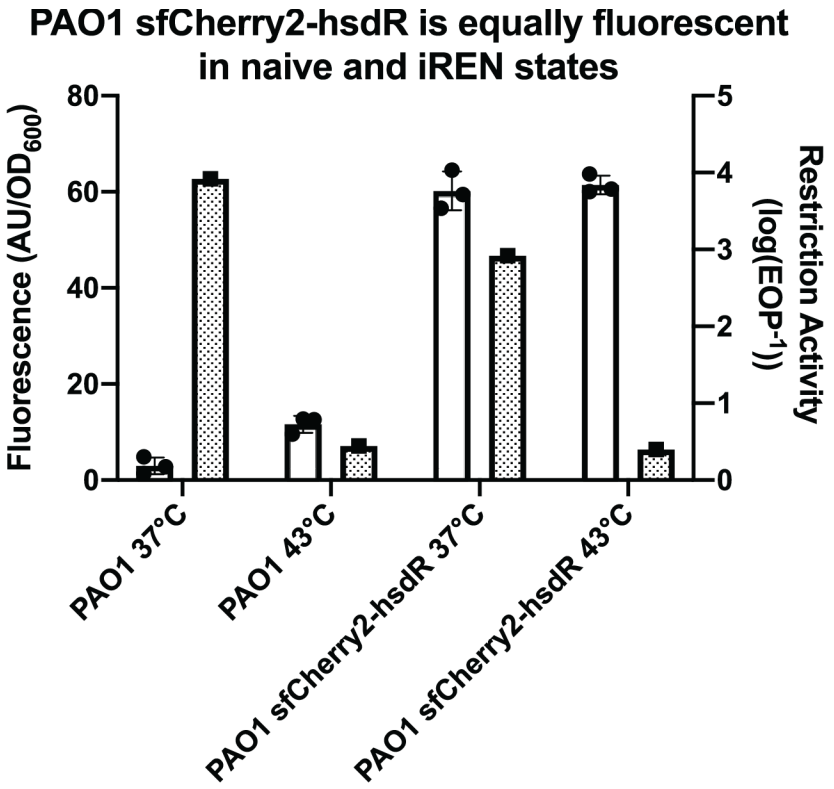

Figure 3.14: PAO1 sfCherry2-*hsdR* grown at 43 °C retains fluorescence despite losing restriction activity. PAO1 sfCherry2-*hsdR* was grown at 37 and 43 °C and was used in a plaque assay with JBD30·PA14. Additionally, the cells were washed in minimal media and fluorescence and optical density were measured. Fluorescence (arbitrary units) was normalized by OD_{600}.

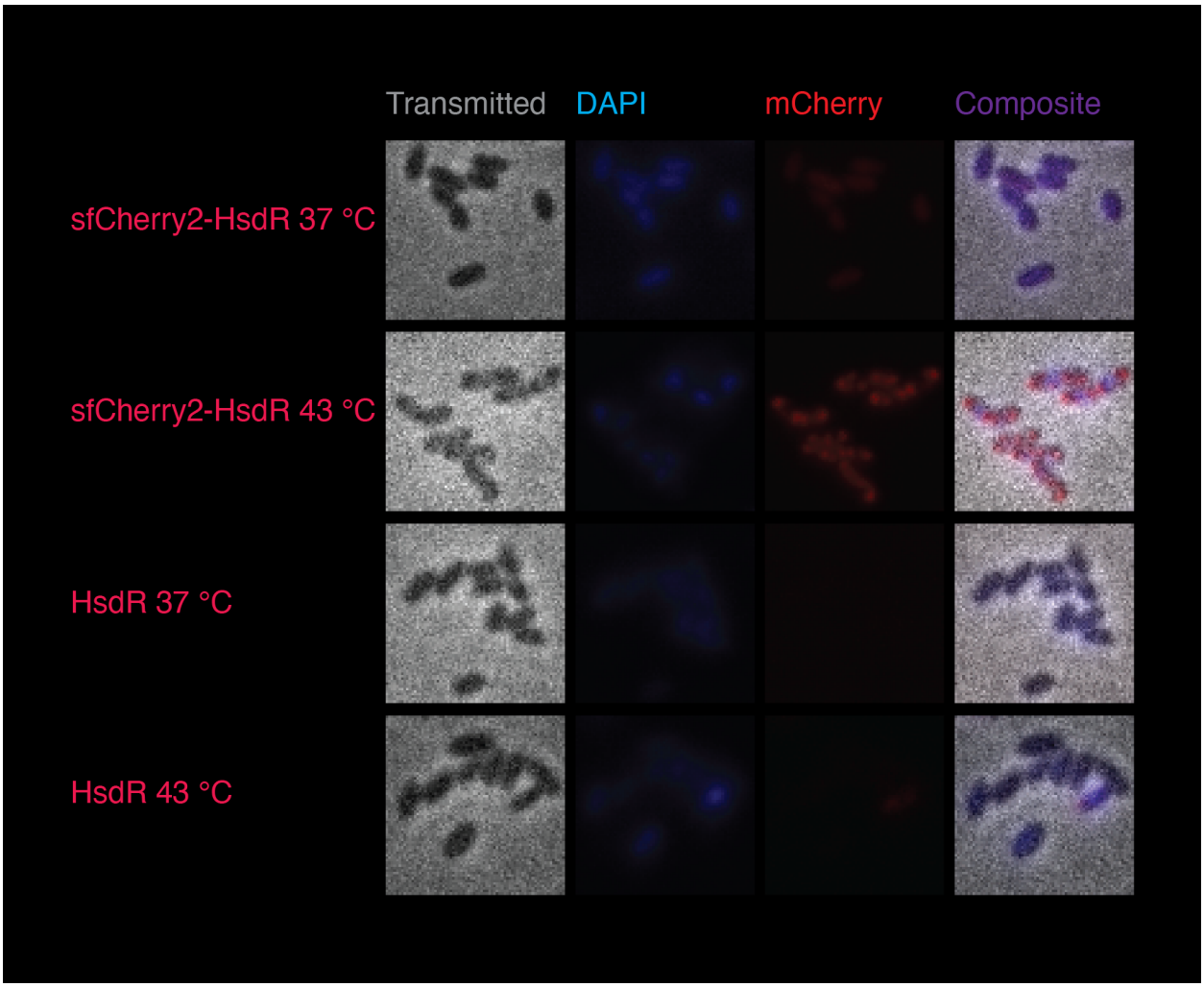

Figure 3.15: sfCherry2-HsdR forms red puncta during iREN but is diffuse in naïve cells. PAO1 and PAO1 sfCherry2-*hsdR* were incubated at 37 and 43 °C in liquid culture with shaking. Saturated cultures were diluted into 1:4 LB, treated with DAPI, and spotted on a 1:4 LB, 0.85 % agarose pad. Cells were imaged by fluorescence microscopy.

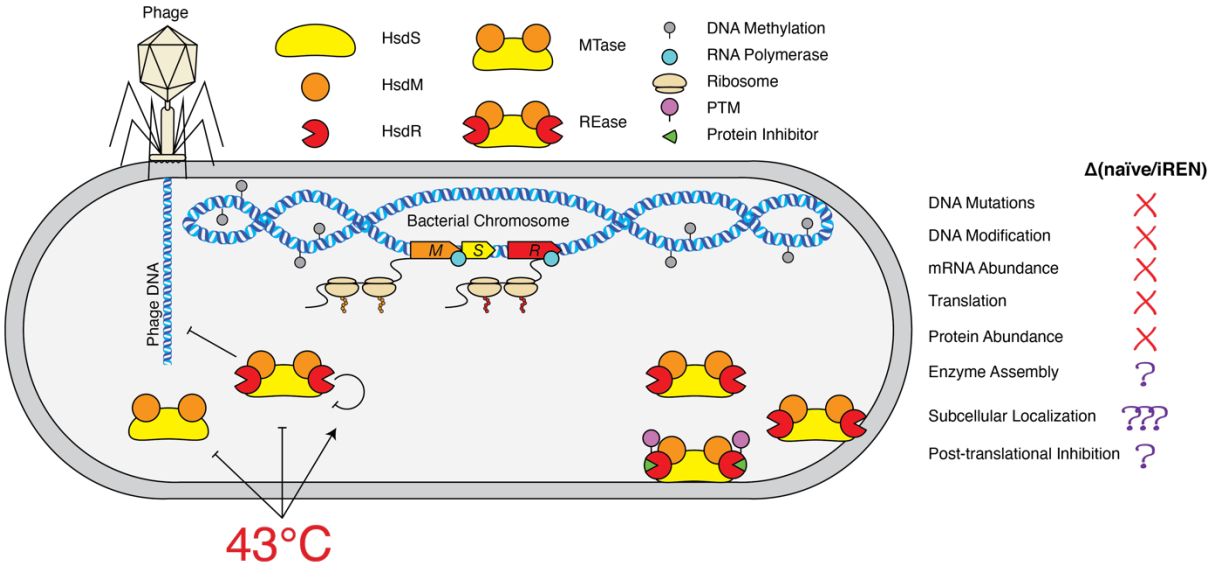

Figure 3.16: *P.aeruginosa's* restriction activity is inhibited post-translationally. Bacterial growth at ≥ 42 °C in liquid culture briefly impacts HsdM's MTase activity (Fig. 3.2) and inactivates HsdR's REase activity (Fig. 3.1), with memory (Fig. 3.3). The inactivation of restriction is not due to changes in DNA sequence globally (data not shown), DNA modification globally (data not shown), mRNA abundance at the *hsd* locus (Fig. 3.11) or globally (Fig. 3.12), or translation of HsdR (Fig. 3.14). Microscopy (Fig. 3.15) suggests that HsdR may aggregate during the iREN state. Alternative hypotheses propose that HsdR may be post-translationally degraded, post-translationally modified, or inhibited by a novel HsdR inhibitor.

Tables:

Table 3.1: iREN in *P. aeruginosa*: Sequenced *P. aeruginosa* isolates were tested for immune activities against JDB30 from different strains and were tested for iREN. Their genomes were searched for *hsd* genes, which were counted (e.g., A7 has 2 type I R-M systems). A9 sequencing quality was poor, but at least one of each *hsd* gene can be detected. C6 could not be tested for iREN because it formed a sick lawn after growth at 43 °C. B1 appeared to be come less phage sensitive after growth at 43 °C. E1 became more permissive of phage at 43 °C despite no type I R-M genes being detected.

		Total Gene Counts		
Strain	iREN	HsdS	HsdM	HsdR
A7	Yes	2	2	2
A8	Yes	1	1	1
A9	Yes	Yes	Yes	Yes
A31	Untested	2	2	2
B1	Inverse	1	1	1
B2	Yes	1	1	2
B7	Yes	1	1	2
B10	Yes	1	1	2
C2	Yes	1	1	1
C6	Bad lawn (43°C)	2	2	2
C9	Yes	1	1	1
C35	Untested	0	0	0
D7	Unsure	0	0	0
E1	Yes	0	0	0
E5	Untested	0	0	0
E16	Untested	0	0	0

Table 3.2: RNA-Seq Hits

Type	Gene	Mean FC (43°C/37°C)	Function
tRNA	PA3133.2	1.109691721	tRNA-Ala
tRNA	PA3133.4	1.044586752	tRNA-Ala
Depleted during iREN			
tRNA	PA0668.3	0.531212553	tRNA-Ala
tRNA	PA4280.3	0.53476708	tRNA-Ala
tRNA	PA4690.3	0.540352653	tRNA-Ala
tRNA	PA5369.3	0.530398659	tRNA-Ala
tRNA	PA0668.2	0.454325848	tRNA-Ile
tRNA	PA4280.4	0.46670463	tRNA-Ile
tRNA	PA4690.4	0.468289193	tRNA-Ile
tRNA	PA5369.4	0.464525091	tRNA-Ile
CDS	PA4224	0.227240299	pyochelin biosynthetic protein PchG
CDS	PA4220	0.249451116	
CDS	PA4219	0.267859845	
CDS	PA4226	0.27066082	dihydroaeruginoic acid synthetase
CDS	PA4222	0.276105406	
CDS	PA4223	0.284007973	
CDS	PA4218	0.298725327	
CDS	PA4225	0.318951038	pyochelin synthetase
CDS	PA4229	0.334739161	pyochelin biosynthetic protein PchC
CDS	PA4221	0.341983234	Fe(III)-pyochelin outer membrane receptor
CDS	PA4230	0.363212021	isochorismate-pyruvate lyase
CDS	PA4228	0.374994818	2C3-dihydroxybenzoate-AMP ligase
CDS	PA4231	0.431684991	salicylate biosynthesis isochorismate synthase
Enriched during iREN			
Type	**Gene**	**Mean FC**	**Function**
CDS	PA0447	1.524147551	glutaryl-CoA dehydrogenase
CDS	PA0511	2.142900604	heme d1 biosynthesis protein NirJ
CDS	PA1655	1.837979483	glutathione S-transferase
CDS	PA2047	1.521294106	transcriptional regulator
CDS	PA2125	2.088423097	aldehyde dehydrogenase
CDS	PA2259	1.578027068	transcriptional regulator PtxS
CDS	PA2260	2.139276685	hypothetical protein
CDS	PA2263	1.574670376	2-hydroxyacid dehydrogenase
CDS	PA4465	1.520803935	hypothetical protein
CDS	PA5172	2.6865089	ornithine carbamoyltransferase

Table 3.3: Phages and Strains

Name	**Source**	**Reference**
JBD30	Davidson Lab	[32]
	Genotype	**Reference**
JB10	PAO1 tn7::Cas9^{Spy}	[33]
LL7	PAO1 tn7::I-C/Cas3^{PA}	[34]
SDM020	PAO1 Δ*hsdR*	[33]
SDM273	PAO1 Δ*hsdSMR*	This study
SDM276	PAO1 sfCherry2-hsdR	This study
A7-E5	Wild-type isolates	Unpublished (Davidson Lab)
A31, C35, E16	Wild-type isolates	Courtesy of Steve Miller, MD, PhD

Table 3.4: Plasmids

Name	Information	Ref.
pHERD30T	Arabinose inducible, gentamicin resistant shuttle vector	[35]
pJW1	pHERD30T with BsaI site at pos. 235 GAGACC mutated to GTGACC	[33]
pJW13	pJW1 with Type I-C pseudo-CRISPR array for spacer cloning	[33]
pJB1	pJW1 with Type II-A sgRNA backbone at the +1 TSS of pBAD	[33]
pSDM020	p30 plasmid, (L)-Rhamnose-inducible promoter	This study
pSDM013	Rhamnose-inducible expression vector for HsdSMR	This study
pSDM009	HsdR spacer: GCCCTCATCGAAGAAACCAG	This study
pSDM018	Repair Template for deletion of HsdR, spacer against HsdR	This study
pSDM153	hsdR under pBAD	This study
pSDM154	sfCherry2 under pBAD	This study
pSDM155	hsdR-sfCherry2 under pBAD	This study
pSDM156	sfCherry2-hsdR under pBAD	This study
pSDM182	pHERD30T with Type I-C crRNA with a spacer against hsdR for deletion repair template	This study
pSDM183	pHERD30T with Type I-C crRNA with a spacer against hsdR for sfCherry2 tagging repair template	This study
pSDM188	pHERD30T with Type I-C crRNA with a spacer against hsdR for sfCherry tagging repair template; sfCherry2-hsdR RT in NheI site	This study
pSDM189	pHERD30T with Type I-C crRNA with a spacer against hsdR for sfCherry tagging repair template; hsdR::sfCherry2 RT in NheI site	This study
pSDM190	pHERD30T with PA5369 Spacer tRNAs at the +1 TSS	This study

Table 3.5: Oligonucleotides

Name	Sequence	Notes
oSDM019	gcccatttcatcgggtga	Test HsdR Deletion
oSDM020	ttcttcgccacggtgc	Test HsdR Deletion
oSDM021	CCATGCCCTCATCGAAGAAACCAG	spacer for deletion of HsdR
oSDM022	AAACCTGGTTTCTTCGATGAGGGC	spacer for deletion of HsdR
oSDM035	TGGCGATGGACGATACC	Test HsdR Deletion; Formerly "HsdR 5' Deletion R"
oSDM036	GAAGATCACCAGGTCGAG	Test HsdR Deletion; Formerly "HsdR 3' Deletion F"
oSDM037	CTAGGCCAGATCCAGCGG	Amplify pHERD30T Backbone (deleting araC, pBADF, MCS, and lacZ)
oSDM038	GGGGATTCCTTAAGGTATACTTTCCG	Amplify pHERD30T Backbone (deleting araC, pBADF, MCS, and lacZ)
oSDM039	ctggatctggcctagTTAATCTTTCTGCGAATTG	Amplify MCS, pRhaBAD, and RhaSR from pJM231)
oSDM040	accttaaggaatccccGTCGACGGTATCGATAAG	Amplify MCS, pRhaBAD, and RhaSR from pJM231)
oSDM045	tcaactagtgctctgcaggaattccATGCAGAAACGACAGCAAG	Amplify HsdSM for GA into p30Rha
oSDM046	ctgccaaccttcgggTCAGTCTTCAGCATCGGC	Amplify HsdSM for GA into p30Rha
oSDM047	tgctgaagactgacccgaaggttggcagATGAAACCCACCGATACCAGCG	Amplify HsdR for GA into p30Rha
oSDM048	tcgacggtatcgataagcttcctaatggtggtggtggtgatgTCGCCCATGCGCAATCCT	Amplify HsdR for GA into p30Rha
oSDM050	gtgttttcagaGCGTCGTCTCCCTTCTTCTTG	Amplify 500 bp upstream of HsdR for recombination template
oSDM051	gacgacgcTCTGAAAACACTGTTGGGC	Amplify 500 bp downstream of HsdR for recombination template
oSDM053	ccatgggatctgataagTTCTTCGCCACGGTGCAG	Amplify 500 bp upstream of HsdR for recombination template
oSDM054	cgggtaccgagctcgCCCATTTCATCGGGTGATC	Amplify 500 bp downstream of HsdR for recombination template
oSDM055	gcaagccaccaaacgc	Amplify equence outside of pSDM016-pSDM019 repair template to test HsdR deletion

Name	Sequence	Notes
oSDM283	AGA GCT CGA ATT CTT ATC AGA TCC	Primers for linearization of pHERD30T
oSDM284	TGC AGG CAT GCA AGC TTG	Primers for linearization of pHERD30T
oSDM357	atgggatctgataagaattcgagctCTatgaaacccaccgataccag	Primers for amplification of HsdR fusion fragments for Gibson assembly into p30
oSDM358	CGAGCCACCGCCACCtcgcccatgcgcaatc	Primers for amplification of HsdR fusion fragments for Gibson assembly into p30
oSDM359	atgggatctgataagaattcgagctCTATGGAGGAGGACAACATG	Primers for amplification of sfCherry2 Fusion Fragments
oSDM360	GGTGGCGGTGGCTCGatgaaacccaccgataccag	Primers for amplification of HsdR fusion fragments for Gibson assembly into p30
oSDM361	ccagtgccaagcttgcatgcCTGCActatcgcccatgcgcaatc	Primers for amplification of HsdR fusion fragments for Gibson assembly into p30
oSDM346	CGAGCCACCGCCACCgccgccggtgc	Primers for amplification of sfCherry2 Fusion Fragments
oSDM347	GGTGGCGGTGGCTCGatggaggaggacaacatg	Primers for amplification of sfCherry2 Fusion Fragments
oSDM394	AGCTGTCCTCCTCTTATCAGATCCCATGGGTATG	pHERD30T_rev
oSDM395	CCATGGGATCTGATAAGAGGAGGACAGCTATGAAACCCACCGATACCA GCG	p30-HsdR_fwd
oSDM396	CGACGGCCAGTGCCATTATCGCCCATGCGCAATC	HsdR-p30_rev
oSDM397	TGGCACTGGCCGTCGTTT	pHERD30T_fwd
oSDM398	GAG CCA CCG CCA CCT CGC CCA TGC GCA ATC CT	HsdR-GS_rev
oSDM399	ATG GGC GAG GTG GCG GTG GCT CGA TGG AGG AGG ACA ACA TGG C	GS-sfCherry2_fwd
oSDM400	CGA CGG CCA GTG CCA TTA GCC GCC GGT GCT GTG	sfCherry2-p30_rev
oSDM401	CCA TGG GAT CTG ATA AGA GGA GGA CAG CTA TGG AGG AGG ACA ACA TGG CC	p30-sfCherry2_fwd
oSDM402	GAG CCA CCG CCA CCG CCG CCG GTG CTG TGT CT	sfCherry2-GS_rev
oSDM403	CCG GCG GCG GTG GCG GTG GCT CGA TGA AAC CCA CCG ATA CCA GC	GS-HsdR_fwd
oSDM437	ATG GAG GAG GAC AAC ATG	sfCherry2_seq_fwd
oSDM438	GCC GCC GGT GCT GTG	sfCherry2_seq_rev

Name	Sequence	Notes
oSDM457	ATG GAG AAA CAG TAG AGA GTT G	Gibson assembly primer for linearizing pHERD30T with insert at +1 TSS
oSDM458	GAA TTC GAG CTC GGT ACC	Gibson assembly primer for linearizing pHERD30T with insert at +1 TSS
oSDM463	GAA ACA TGC GTC GTC TCC CTT CTT CTT GCC CGG CTT ATT G	Type I-C crRNA against PAO1's PA2732 for N-terminal tagging with sfCherry2
oSDM464	GCG ACA ATA AGC CGG GCA AGA AGA AGG GAG ACG ACG CAT AG	Type I-C crRNA against PAO1's PA2732 for N-terminal tagging with sfCherry2
oSDM483	GAA ACC TGC GCG TTG TCG GAA TGG CCG AAA ATC GAA GCC G	Spacer against hsdR for deletion
oSDM484	GCG ACG GCT TCG ATT TTC GGC CAT TCC GAC AAC GCG CAG G	Spacer against hsdR for deletion
oSDM491	ACTCTCTACTGTTTCTCCATtcgaagatctcagcttcttcataagc	PA5369 Fwd
oSDM492	CGGGTACCGAGCTCGAATTCcatataaccccaagcaatctggttatactg	PA5369 Rev
oSDM493	gctgagcatcgcaagg	Primers for screening hsdM mutants
oSDM494	gatatctgctcgtggctgtc	Primers for screening hsdM mutants
rpoD (PA0576) FWD	GGGCGAAGAAGGAAATGGTC	Primers for RT-qPCR
rpoD (PA0576) REV	CAGGTGGCGTAGGTGGAGAA	Primers for RT-qPCR
hsdR FWD Set 1	GACGATGCCGAGGTGTATTT	Primers for RT-qPCR
hsdR REV Set 1	CTTCCACAGGTAATCGGTCTTC	Primers for RT-qPCR
hsdR FWD Set 2	GGAAGGAACAGTCTGGGTATTG	Primers for RT-qPCR
hsdR REV Set 2	GTGGGCCGATAACAGATTCA	Primers for RT-qPCR
hsdSM FWD Set 2	AGGGTGACATTGCCTACAAC	Primers for RT-qPCR
hsdSM REV Set 2	CTTCTGCATAGGGCTTGACTAC	Primers for RT-qPCR
hsdSM FWD Set 5	CGATGTGATCCTGCCCTTTA	Primers for RT-qPCR
hsdSM REV Set 5	CGTTCTGATTCGCCACTTTG	Primers for RT-qPCR

Table 3.6: Antigens

Protein-#	Antigen
2732-1	CGEKKTEADLNDFPS
2732-2	CRLLAQKDPEGDDWA
2732-3	RQVRYSHDSGNELDC
2734-1	CTRGLDASVKLKPSD
2734-2	CHIGRETKDLDETIA
2735-1	CAQETDSSTDQSKWF
27535-2	CEGAEAENIVGGADK

Publishing Agreement

It is the policy of the University to encourage open access and broad distribution of all theses, dissertations, and manuscripts. The Graduate Division will facilitate the distribution of UCSF theses, dissertations, and manuscripts to the UCSF Library for open access and distribution. UCSF will make such theses, dissertations, and manuscripts accessible to the public and will take reasonable steps to preserve these works in perpetuity.

I hereby grant the non-exclusive, perpetual right to The Regents of the University of California to reproduce, publicly display, distribute, preserve, and publish copies of my thesis, dissertation, or manuscript in any form or media, now existing or later derived, including access online for teaching, research, and public service purposes.

Senen Mendoza
Author Signature

6/8/2021
Date